Damage Prognosis of Aging Reinforced Concrete Structures through Visual Screening and Rebound Hammer Test

A Thesis

Submitted to the Department of Disaster Engineering and Management,
Chittagong University of Engineering and Technology, Chittagong
in partial fulfilment for the degree
of

Master of Science in

Disaster and Environmental Engineering

Submitted By
Mohammed Mahmudur Rahman Patwary
Student ID: 14MSDEE005P

Supervised by
Prof. Dr. Maruful Hasan Mazumder

Department of Disaster Engineering and Management
CHITTAGONG UNIVERSITY OF ENGINEERING AND TECHNOLOGY
Chattogram-4349

March, 2024

CERTIFICATION

The thesis titled **"Damage Prognosis of Aging Reinforced Concrete Structures through Visual Screening and Rebound Hammer Test"** submitted by Mohammed Mahmudur Rahman Patwary, Roll No:14MSDEE005P, Session-2014-2015 has been accepted as satisfactory in partial fulfilment of the requirements for the degree of Master of Science in Disaster and Environmental Engineering on 28th March 2024.

BOARD OF EXAMINERS

Dr. Maruful Hasan Mazumder Professor Department of Disaster Engineering and Management, CUET	Chairmen (Supervisor)
Head Department of Disaster Engineering and Management, CUET	Member (Ex-Officio)
Dr. Md. Moinul Islam Professor Department of Civil Engineering, CUET	Member
Dr. Md. Abul Hasan Professor Department of Disaster Engineering and Management, CUET	Member
Dr. Syed Ishtiaq Ahmad Professor Department of Civil Engineering, BUET	Member (External)

Declaration

I hereby affirm that the content of this thesis has not been submitted previously to fulfil the requirements for any degree at this or any other institution of higher education. To the best of my knowledge, this thesis does not include any material that has been published or authored by others, except where proper citations are provided. Additionally, this thesis adheres to the PLAGIARISM and ACADEMIC INTEGRITY policies of CUET.

Mohammed Mahmudur Rahman Patwary
Student ID: 14MSDEE005P
Department of Disaster Engineering and Management (DEM)
Chittagong University of Engineering & Technology (CUET)

Dedication

To

My Parents

Approval/Declaration by the Supervisor

This is to certify that **Mohammed Mahmudur Rahman Patwary** has carried out this research work under my supervision, and he has fulfilled the relevant Academic Ordinance of the Chittagong University of Engineering and Technology, so he is qualified to submit the following Thesis in the application for the degree of MASTER OF SCIENCE IN DISASTER AND ENVIRONMENTAL ENGINEERING (M.Sc. in DEE)**.** Furthermore, the thesis complies with the PLAGIARISM and ACADEMIC INTEGRITY regulations of CUET.

Prof. Dr. Maruful Hasan Mazumder
Department of Disaster Engineering and Management
Chittagong University of Engineering & Technology

Acknowledgement

The author would like to express heartfelt gratitude to the gracious Almighty Allah for His boundless kindness and blessings which have made the successful completion of this thesis possible. Special thanks are extended to Prof. Dr. Maruful Hasan Mazumder of the Department of Disaster Engineering and Management at Chittagong University of Engineering & Technology (CUET), for his invaluable guidance, insightful suggestions, and unwavering support throughout this research journey. The author is deeply appreciative of his encouragement and contributions of new ideas which were instrumental in shaping this work.

Additionally, the author acknowledges the support provided by Professor Dr. Md. Abul Hasan from the same department at CUET, whose assistance was crucial during the research process. The author also wishes to convey profound thanks to other course teachers, laboratory staffs, friends and family members for their unwavering support, love, encouragement and patience, which served as a continuous source of inspiration. Finally, the author expresses gratitude to all who contributed to the successful and productive completion of this thesis.

Abstract

Periodic monitoring of concrete quality of Reinforced Concrete (RC) structure is essential for maintaining structural performance, ensuring regulatory compliance and continuously tracking many different causes of quality deterioration processes to ensure serviceability of aging RC structures. In this research, visual inspection of an aging RC building of Chattogram is performed according to an ACI protocol. The findings of visual screening are indicative of significant deterioration of concrete strength over the period of 40 years' service life of the building. A non-destructive rebound hammer test (RHT) is conducted on different RC elements and results of in-situ concrete strength of the building indicates an average 13% reduction from reference strength. Current concrete compressive strengths of two other selected buildings of Chattogram are also indicative of high inconsistency between their field test results and audit records of strength. One of the major objectives of this research is, therefore, aimed at establishing reliable basis of RHT data for estimating in-situ concrete strength of RC structures. A comparative analysis of time variable strengths is performed for three laboratory scale RC beam specimens cast with two concrete strengths, 20 MPa and 22 MPa. The concrete compressive strengths determined by RHT tests of the beams is well correlated by empirical expressions of time variation of strength, and the empirical laws can be used to provide a reliable estimate of strength by 3% to 4% less than reference strengths.

A selected RC structure is modelled for 3D pushover analysis considering design strength of concrete of 4 ksi and also with a randomly chosen 30% reduction of concrete strength. A comparative evaluation of their capacity curve shows that the maximum capacity of RC structure with concrete strength of 2.5 ksi is substantially low as compared to the same structure modelled with baseline strength of 4.0 ksi. The degradation of concrete strength is shown to have significantly reduced global capacity of the structure. There is also increased numbers of plastic hinges formed in the structure modeled with concrete of 2.5 ksi, particularly beyond the Collapse Prevention (CP) state of the capacity curve. A simply supported RC beam is also modelled to assess other associated effects of concrete strength degradation on crack formation and propagation. The accumulation of fracture strain and formation of cracks are more concentrated near the failure zone of the RC beam modelled with lower strength of concrete.

বিমূর্ত

রিইনফোর্সড কংক্রিট (আর.সি) ভবনের কর্মক্ষমতা নিশ্চিতকরণ, নিয়ন্ত্রক সংস্থার বিধি-বিধানের কমপ্লায়ান্স এবং নানাবিধ কারণে কংক্রিটের ক্ষতি তদারকিপূর্বক ভবনের সেবাসক্ষমতা নিশ্চিতকরণের জন্য নিয়মিত বিরতিতে পুরনো আর.সি ভবনের কংক্রিটের গুণগত মানপর্যবেক্ষণ করা প্রয়োজন। এ গবেষণায় এ.সি.আই-এর (আমেরিকান কংক্রিট কাউন্সিলের) একটি প্রটোকল অনুসরণ করে চট্টগ্রামের পুরনো একটি আর.সি ভবনের ভিজ্যুয়াল পর্যবেক্ষণ করা হয়েছে। ভিজ্যুয়াল পরিদর্শনে দেখা গেছে যে, ৪০ বছরের পুরনো ভবনটির জীবনচক্রে কংক্রিট উপাদানের শক্তিমাত্রার উল্লেখযোগ্য অবনতি হয়েছে। ভবনটির বিভিন্ন কংক্রিটের কাঠামো উপাদানের উপর অ-ধ্বংসাত্মক (এন.ডি.টি) পদ্ধতির রিবাউণ্ড হাতুড়ি পরীক্ষা চালানো হয়, এবং পরীক্ষার ফলাফল অনুযায়ী ভবনের কংক্রিটের রেফারেন্স শক্তিমাত্রার চেয়ে বর্তমান শক্তিমাত্রার গড়ে ১৩% অবনতি হয়েছে। চট্টগ্রামের অন্য আরও দুইটি নির্বাচিত ভবনের ক্ষেত্রেও মাঠ পরীক্ষার মাধ্যমে নির্ণীত কংক্রিটের বর্তমান শক্তি ও অডিট রেকর্ডের রেফারেন্স শক্তিমাত্রার মধ্যে বড় ধরনের অসামঞ্জস্যতা পরিলক্ষিত হয়। তাই, এন.ডি.টি পদ্ধতির হাতুড়ি পরীক্ষার মাধ্যমে নির্ণীত আর.সি কংক্রিট ভবনের শক্তিমাত্রার পরিমাপকে শক্তিমাত্রা পরিমাপের একটি নির্ভরযোগ্য ভিত্তি হিসাবে প্রতিষ্ঠা করা এ গবেষণার অন্যতম একটি লক্ষ্য হিসাবে স্থির করা হয়। এলক্ষ্যে ২০ এবং ২২ এমপিএ শক্তিমাত্রার কংক্রিটে নির্মিত তিনটি ল্যাব স্কেল আর.সি বিমের সময়ের সাথে পরিবর্তনশীল শক্তিমাত্রার তুলনামূলক পর্যালোচনা করা হয়। রিবাউণ্ড হাতুড়ি পরীক্ষার ফলাফল অনুযায়ী নির্ণীত কংক্রিটের (সংকোচন) শক্তিমাত্রাকে সময়ের সাথে শক্তিমাত্রার পরিবর্তনের এমপিরিক্যাল গাণিতিক সুত্রের মাধ্যমে সন্তোষজনকভাবে সম্পর্কিত করা যায়, এবং এমপিরিক্যাল গাণিতিক নিয়মকে রেফারেন্স শক্তিমাত্রার চেয়ে গড়ে ৩% হতে ৪% কম ধরে শক্তিমাত্রা পরিমাপের একটি নির্ভরযোগ্য ভিত্তি হিসাবে ব্যবহার করা যেতে পারে।

কংক্রিটের রেফারেন্স ডিজাইন শক্তি ৪ কে.এস.আই এবং দৈবচয়নে ৩০% শক্তির অবনতি বিবেচনা করে ত্রিমাত্রিক পুশওভার লোড প্রয়োগে একটি নির্বাচিত আর.সি ভবনের মডেল এনালাইসিস করা হয়েছে। দুটি মডেলের ক্যাপাসিটি কার্ভের তুলনামূলক বিবেচনায় দেখা যায় যে, কংক্রিটের ৪ কে.এস.আই ডিজাইন শক্তিবিশিষ্ট মডেলের তুলনায় কংক্রিটের ২.৫ কে.এস.আই ডিজাইন শক্তিবিশিষ্ট মডেলের সক্ষমতা অনেক কম। কংক্রিটের শক্তিমাত্রার অবনতি উল্লেখযোগ্যভাবে ভবনটির সার্বিক সক্ষমতা কমিয়ে দিয়েছে। কংক্রিটের ২.৫ কে.এস.আই ডিজাইন শক্তিবিশিষ্ট মডেলে লোড প্রয়োগের ফলে, বিশেষত এর ক্যাপাসিটি কার্ভের কলাপ্স প্রিভেনশন (সি.পি) ধাপের পর, সৃষ্ট প্লাস্টিক হিংজ তুলনামূলকভাবে বেশি পরিলক্ষিত হয়। কংক্রিটের শক্তিমাত্রার অবনতির কারণে প্রভাবিত আরও অন্যান্য ফলাফল যেমন ফাটল সৃষ্টি ও এর বিস্তার মূল্যায়নের জন্য একটি সাধারণভাবে স্থাপিত আর.সি বীমের মডেল পর্যালোচনা করা হয়েছে। কংক্রিটের কম শক্তিমাত্রার বীম মডেলে এর ব্যর্থ এলাকার কাছাকাছি ভাঙ্গন বিকৃতির মান ও ফাটল সৃষ্টির ঘনত্ব বেশি পরিলক্ষিত হয়।

Table of Contents

List of Figures

List of Tables

Nomenclature

DT	Destructive Test
G (Δ)	Function describes the Shape of the capacity curve.
k*	Generalized stiffness.
ksi	Kip per square inches.
m*	Generalized mass
mm	Millimeters
MPa	Mega Pascale
N/mm^2	Newton per millimeter square
psi	Pound per square inches
NDT	Non-Destructive Test
RHT	Rebound Hammer Test
V	Base shear
V{f}	Normalized load vector
Φ	Deformation profile for the building
ξ	Damping ratio
Δ	Centre of mass (CM) displacement
2-D	Two-dimension
3-D	Three dimension
°	Degree
′	Feet
″	Inch
°C	Degree Celsius

Acronyms and Abbreviations

ACI	American Concrete Institute
ASTM	American Standard Testing Materials
BS	British Standard
BNBC	Bangladesh National Building Code
CM	Centre of Mass
CTM	Concrete Testing Machine
CR	Centre of Rigidity
RC	Reinforced Concrete
RCC	Rebound Hammer Test
RHT	Rebound Hammer Test
US	United States

Copyright Declaration

I hereby declare that I am the sole author of the thesis titled “Damage Prognosis of Aging Reinforced Concrete Structures through Visual Screening and Rebound Hammer Test”. Along with this, submitted a soft copy is true copy of my final hard copy thesis including any required final revisions, as accepted by the board of examination.

I hereby release my copyright to **Chittagong University of Engineering and Technology (CUET)** for uploading the electronic version of the same to the ‘**Digital Repository (Institutional Repository)’** of **CUET** after one year from the day of submission. Apart from this, the existing or to be approved **Open Education Resources (OER)** policies and procedures of **Chittagong University of Engineering and Technology (CUET)** shall be applicable to this research work.

I also acknowledge my sincere delivering of copyright to Chittagong University of Engineering and Technology (CUET) to reproduce this thesis reprography or by other means, in total or by part at the necessity of individual for the purpose of scholarly research.

………………………..
Signature of the Author

Chapter 1
Introduction

1.1 Background and Present State of the Problem

Safe and efficient management of a built infrastructure for an expected service life of at least fifty years is a challenging task particularly in the backdrop of its exposure to frequently occurring natural disasters or harsh environmental conditions. To keep a high level of structural safety, durability and performance of infrastructures especially that of critical facilities in each country, an efficient system for early and regular structural assessment is urgently required (ACI Report 228.2R-98, 1998; ACI Report 201.1R-08; Shariati et al., 2011; Bagavathiappan et al., 2013; Gehlot et al., 2016). Over the past few decades, urbanization in Bangladesh has been taking place without proper guidance and many of the urban centers have been developed in a haphazard manner. Structural health monitoring and regular maintenance of built infrastructures of the country are not generally done in an organized way although it should be considered as a mandatory task for ensuring quality of structure for living and serviceability compliance. Many built infrastructures in Bangladesh have already served a service life of more than 30 years and some of them have already started showing signs of very poor structural health conditions. Many of these structures, if properly assessed with a structural health monitoring tool, might not serve the standard living conditions or serviceability compliance.

Infrastructural development in Bangladesh has been progressing at a fast rate during the last few decades. Many built infrastructures such as buildings, bridges etc. have been built in the urban centers all over the county and most of these built infrastructures are Reinforced Concrete (RC) structures. These RC structures deteriorate over their life span as they are exposed to harsh environmental conditions or sustain excessive loads. Some of these RC structures in Bangladesh have already started showing signs of significant damage or deterioration not only due to aging but also due to intermittent exposure to extreme loading conditions arising from man-made causes or natural disasters such as moderate earthquakes, flood, cyclones, etc. (CDMP Report, 2009). These buildings may not perform well under the demand of extreme loading conditions of an earthquake or other disasters. Therefore, the built infrastructures, especially the aging structures, should be monitored for signs of damage or deterioration.

The topic of structural health monitoring has gained significant attention over the past decades, driven by several catastrophic events and a growing awareness of the condition of existing infrastructure. On 24 April 2013, the collapse of Rana Plaza at Savar, Dhaka killed 1134 and injured about 2500 people (ILO Report, 2018). On 11 April 2005, Spectrum Garments building collapsed in Dhaka killing 60 and injuring about 100 people (IEB Investigation Report, 2007). On 21 November 1997, a moderate earthquake damaged a residential building at Hamzarbag Chittagong killing 28 and injuring about 200 people (Mondal et al., 2018).

Figure 1.1: Under construction Garments factory collapsed in 2005 in Dhaka
(IEB invetstigation Report, 2007)

Although aged not more than 15 years, these three buildings collapsed due to avoidance of the building code regulations, use of poor construction materials, lack of construction quality control management and lack of follow-up activities for ensuring building serviceability compliance (CDMP Report, 2009; ILO Report, 2018; IEB Investigation Report, 2007). This growing problem of poor infrastructural condition and also ensuring serviceability compliance of aging infrastructures need to be addressed as important issues of public safety concerns.

One effective approach engineers can employ is structural health monitoring which involves systematically tracking the condition of a structure to assess the nature and extent of any existing damage and its impact on structure's integrity. By obtaining this crucial information, engineers can significantly enhance the maintenance process, potentially preventing future damage or even catastrophic failures of civil infrastructures due to earthquakes (Plankias, 2012; Storchak et al., 2013).

Figure1.2: Rana Plaza factory building collapse in 2013 at Savar, Dhaka

In RC structures, the strength and properties of concrete significantly influence the overall structural behavior. Traditional methods for determining concrete strength often rely on destructive testing methods which necessitate loading concrete specimens to failure. This process requires the extraction, shipping, and laboratory testing of special specimens, potentially leading to delays in evaluating existing structures. Due to these limitations, non-destructive testing (NDT) techniques have been developed to assess material properties other than strength and correlate them with strength, durability and other characteristic parameters. The term "non-destructive" describes testing methods that do not damage or alter the structural integrity of components, allowing the structure to remain in acceptable condition for the client. NDT methods allow engineers to evaluate the condition of RC structures without causing damage, providing timely insights into their integrity and facilitating better maintenance decisions. However, a persistent challenge in the concrete industry is that the true properties of in-place specimens have never been evaluated without inflicting some level of damage.

For most cast-in-place concrete structures, construction specifications mandate that test cylinders to be cast to determine their strength at 28 days. Unfortunately, these test specimens do not accurately represent the in-situ concrete strength due to variations in specimen type, size, and curing processes. This discrepancy can lead to challenges in evaluating the actual strength and performance of existing structures, highlighting the need for more reliable assessment methods (Plankias, 2012; Doebling et al., 1998).

NDT methods can assess various properties of concrete, including surface hardness properties by rebound number (as determined by the rebound hammer test), resistance to penetration or projectiles, resonance frequency, the ability to transmit ultrasonic pulses through the material etc. Furthermore, concrete's electrical properties along with its capacity to absorb, scatter and transmit x-rays and gamma rays, estimations of moisture content, density, thickness and cement content are also conventionally measured by different NDT methods. The results of many non-destructive tests primarily serve as indirect indicators of strength. These results can be correlated with strength data through calibration charts and by comparing them with secondary data such as design strength or information from specimens obtained during initial casting. This methodology enables a more comprehensive assessment of the concrete's condition without damaging the structure.

In recent years, structural health monitoring (SHM) has gained significant attraction among engineers and professionals in this field. The primary objective of SHM is to identify damage within a structure which is assessed through four distinct levels. The first level establishes the presence of damage while the second level focuses on locating the specific area affected. The third level evaluates the extent of the damage, and finally, the fourth level utilizes the information gathered from the previous steps to predict the remaining service life of the structure. This systematic approach allows for a comprehensive understanding of a structure's condition, enabling timely maintenance and intervention to ensure safety and longevity (Doebling et al., 1998). The first three levels can be efficiently addressed through visual screening methods by following appropriate engineering protocol for those tests. However, the fourth and final level needs to be done using test results of destructive or non-destructive testing of structures or specimens.

Structural health monitoring techniques encompass two main categories of methods for identifying levels of damage. The first category includes global monitoring methods which provide insights into the overall behavior of the structure and its response to loads. The second category consists of local health monitoring methods focusing on specific critical points within the structure. These local methods allow for the identification of areas likely to sustain damage ensuring that the analysis yields relevant data. Depending on the information engineers seek regarding a structure, various destructive and non-destructive testing systems as well as sensor-based monitoring techniques can be employed to collect necessary data (Plankias, 2012; Doebling et al., 1998).

Structural modeling and analysis for performance evaluation and damage prognosis give an aid to understand the capacity of the structure. Recent interest in developing performance based codes for designing or rehabilitating buildings in seismically active areas indicates that pushover analysis, an inelastic procedure, is a viable method for assessing the damage vulnerability of buildings (ATC-33, 1997; Fajfar and Fischinger, 1988; Fajfar and Gasperisic, 1996; Lawson et al., 1994). In summary, pushover analysis consists of a series of incremental static analyses aimed at developing a capacity curve for a building. This capacity curve allows for the determination of a target displacement, which represents the estimated displacement that the design earthquake would impose on the structure. The level of damage observed in the building at this target displacement is considered representative of the damage that would occur during design-level ground shaking. This method has been successfully employed by various researchers (Fajfar and Fischinger, 1988; Fajfar and Gasperisic, 1996; Qi and Moehle, 1991; Saidii and Sozen, 1981) with minor variations in computational procedures. Most studies have focused on symmetrical structures assuming that the floors act as rigid diaphragms allowing for damage assessment through two-dimensional pushover analysis. If all lateral load-resisting elements are similar, the analysis can be further simplified by evaluating a typical element of the building. Lawson et al. (1994) describe both the advantages and limitations of 2D and 3D pushover analyses for damage assessment, noting that one significant limitation is the method's failure to account for three-dimensional effects (Vision 2000-1995).

In this work, the basic concepts behind the first and second level activities of structural health monitoring are implemented with a view to feasibly consider or utilize an appropriate visual screening protocol to perform the ultimate task of damage prognosis of a selected aging RC structure of Chattogram city. Apart from observations of local or global damage conditions by a visual screening protocol, the NDT method of Rebound Hammer Test (RHT) is used for surface hardness measurement that would yield indirect but rapid indication of in-situ strength of concrete in different RC structural members. Structural model analysis for performance evaluation has been used in conjunction with results of NDT to assess global capacity and damages of RC structures in relation to possible concrete strength deterioration over time.

1.2 Objectives of the Research

This work is intended for collecting data of a selected aging RC structure through visual screening and an appropriate structural modelling method that can be feasibly used by an appropriate authority to monitor damage status and serviceability compliance of any aging RC structure. For this purpose, a few selected RC structures of Bangladesh Railway infrastructural zone at Halishahar region of Chattogram city were studied. The damage prognosis of one of the selected aging RC structures of the study area was performed through visual screening methods, and also through structural modeling and analysis using variable concrete strength data that could be indirectly derived from NDT testing methods such as the RHT test. The major objective of the work is to use test data of RHT test as an effective and useful indicator of in-situ or in-place strength of concrete. The calibration graph for the RHT test is to be verified using secondary test results such as that of core cutting concrete test and/or by other means to isolate the effect of different internal and external factors that could contribute to the strength development of concrete in both new and aging RC structures. Specific objectives of the research are as follows;

i. Calibrate rebound hammer test data to effectively estimate strength data for concrete.

ii. Determine by visual screening common locations of damage due to aging of RC structures.

iii. Develop a protocol for testing representative locations of different structural elements by rebound hammer test.

iv. Structural modelling and analysis for performance evaluation and damage prognosis.

1.3 Organization of the Report

The findings of the research work including scope of the work, objectives and methodology or assessment methods are reported in several chapters of this report. The first chapter provides a brief introduction given on background and rationale of the work including its specific objectives. The second chapter is written about literature review done on relevant topics, especially on different aspects of deterioration of concrete strength and damage prognosis in RC structures. The third chapter is about the methodology of the work and visual screening procedure. Chapter 4 of this report is written on findings of analysis of results and discussions. The last chapter of this report is about conclusive findings and recommendations of the study.

Chapter 2
Literature Review

2.1 Fundamental Concept of Deterioration of Concrete

Concrete is one of the most versatile and widely used construction materials globally, particularly in the form of reinforced concrete in RC structures, which is globally well regarded for their durability and ability to withstand various environmental conditions throughout their lifespan. When properly prepared and placed, this durability is evidenced by the numerous concrete structures built over the past century in diverse locations. However, the steel embedded within these structures, whether as reinforcement or pre-stressed tendons, is susceptible to corrosion, a challenge that cannot be entirely eliminated. While developed countries have implemented necessary preventive measures and revised concrete codes to incorporate suitable durability practices since the 1970s and 1980s, progress has been much slower in Bangladesh. The country's basic concrete codes, including BDS 243:1963 (BNBC, 2006) and several other BDS and EN standards, have not been fully updated to address durability requirements (BNBC, 2020). Given that steel-reinforced concrete structures constitute a critical component of infrastructure, enhancing their durability is essential for long-term performance and safety.

The combination of concrete's high compressive strength and the required tensile properties of reinforcing steel creates an ideal composite material, making it highly versatile for various applications in structural engineering. However, concrete is prone to deterioration over time which significantly affects its serviceability throughout its life span. The factors contributing to the deterioration of aged concrete can be categorized into four main groups, as outlined below. (MAPEI SpA Manual, 2021; ACI Committee Report 222, 2001; ACI Committee Report 224, 1993; ACI Committee Report 210, 1993; ACI Committee Report 201, 1992; Smith, 1991; Higgins, 1981).

i) Deterioration of concrete by chemical action,

ii) Deterioration of concrete by physical action,

iii) Deterioration of concrete by mechanical action,

iv) Deterioration of concrete by defective construction process.

2.1.1 Deterioration of Concrete by Chemical Action

Aggression caused by the chemicals action on concrete, mainly describe in four types which are as follows;

a) Aggression caused by carbon dioxide
b) Aggression caused by sulfates
c) Aggression caused by chlorides
d) Alkali-Aggregate reaction on concrete

2.1.1.1 Aggression Caused by Carbon Dioxide

Aggression caused by carbon dioxide (CO_2) can occur in two distinct forms based on environmental conditions. In structures exposed to the atmosphere, concrete undergoes carbonation, while hydraulic constructions are impacted by the leaching of the cement paste. Carbonation happens when CO_2 infiltrates the concrete and reacts with calcium hydroxide to produce calcium carbonate. This reaction lowers the pH of the concrete, which typically starts above 13, down to approximately 9. The rate of carbonation is affected by various environmental factors, including industrial pollution levels and relative humidity.

When a structure undergoes carbonation, the pH level of the concrete can drop below 9, resulting in a less alkaline environment for the reinforcement rods. If the pH continues to decline and falls below 11, the protective passivation film on the rods is compromised. This loss of protection makes the reinforcement susceptible to corrosion from atmospheric oxygen and humidity. As corrosion progresses, the reinforcement rods begin to expand, increasing in volume by approximately six times their original size. This significant expansion can lead to the detachment of the surrounding concrete and may even cause the rods to be completely expelled from the structure.

Figure 2.1: Carbon deteriorated concrete (MAPEI SpA Manual, 2021)

Once concrete has deteriorated, the degradation of reinforcement accelerates, which occurs through creation of pathways for oxygen and humidity. CO_2 migrates from the exterior to the interior of the concrete, and the rate of penetration depends significantly on the moisture level. CO_2 travels rapidly in its gaseous state, primarily through air-filled pores, while its movement is slower in pores containing moisture. Thus, in water-saturated pores, the penetration rate approaches zero. However, it is crucial to note that the presence of humidity is essential for carbonation to occur. The graph below illustrates the relationship between CO_2 penetration rate and the relative humidity of concrete. The most critical humidity levels range between 50% and 80% (Figure 2.2). Beyond this range, the penetration rate diminishes, reaching zero in conditions of complete dryness or total saturation.

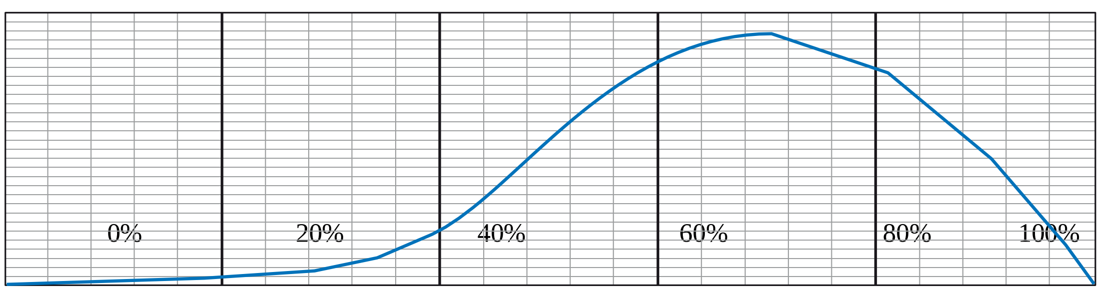

Figure 2.2: Rate of carbonation compared to relative humidity (MAPEI SpA Manual, 2021)

The effects of carbonation are particularly detrimental to reinforced concrete (RC) structures, while they are less significant for unreinforced concrete. In cases where a concrete structure exhibits deterioration similar to that depicted in Figure 2.1, an initial hypothesis can be made regarding the cause. Leaching refers to the process where the cementation matrix is eroded due to the mechanical action of water on the concrete, as illustrated in the figure. This issue is exacerbated when the water is acidic, often due to elevated levels of carbon dioxide, which can be found in pure mountain water, industrial waste products, or organic sulfuric acid present in drainage systems. Such acidic conditions accelerate the leaching process, further compromising the integrity of the concrete structure.

2.1.1.2 Aggression Caused by Sulfates

The most common soluble sulfates found in groundwater, surface water and industrial processes are calcium and sodium sulfates. Magnesium sulfates, while less prevalent, are more damaging. Sulfate ions can infiltrate concrete structures through groundwater or surface water, entering the cement matrix via water transport. Once inside, these sulfate ions react with calcium hydroxide to form gypsum. This gypsum then interacts with hydrated calcium aluminates (C-A-H), leading to the formation of secondary compounds that expand in volume. Such expansion can cause severe issues, including delamination, swelling, cracking, and detachment of the concrete structure.

Primary components in concrete, such as those formed from the bonding of anhydrite aluminates and gypsum (which is added to cement as a setting regulator), are not harmful; rather, they are beneficial. These components create a barrier around the aluminates, effectively slowing the hydration process without causing damage. A key distinction between primary and secondary components is that primary components form almost immediately and uniformly during the casting process. This rapid formation occurs while the concrete is still in its plastic phase, resulting in low expansion stresses that do not pose a risk. In contrast, secondary components develop later, primarily in the outer layers of the concrete where sulfate penetration occurs. This delayed formation leads to high expansion stresses due to the rigidity of the cured concrete, which can result in significant structural problems. Another type of sulfate attack can occur in the presence of calcium carbonate at low temperatures (below 10°C) and high relative humidity (above 95%). Under these conditions, thaumasite forms, leading to decalcification and reducing the concrete to a pulp-like consistency.

Sulfates can also originate from within the concrete itself due to natural impurities in aggregates such as gypsum or anhydrite. The gypsum present in aggregates is typically larger than that added to cement for setting purposes, making it less soluble in water. Consequently, this gypsum is not immediately available to contribute to primary deterioration; instead, it can lead to secondary deterioration within the cured concrete over time, ultimately resulting in cracking.

2.1.1.3 Aggression Caused by Chlorides

Chloride aggression on concrete occurs when it is exposed to environments with high chloride levels, such as seawater or deicing salts, or when contaminated raw materials are used in its preparation. Once chlorides penetrate the concrete and reach the reinforcement bars, they disrupt the protective ferrous oxide film on the rods, exposing them to corrosion. This penetration begins at the surface and progresses deeper into the concrete. The duration of this penetration is influenced by several factors including the following:

i) Concentration of chlorides which come into contact with surface of the concrete
ii) Permeability of the concrete
iii) Percentage of humidity present

Figure 2.3: Typical state of deterioration of concrete by chloride attack
(Part of bridge structure at seawater contact)

Corrosion requires two essential factors, the presence of chlorides which depassivate the reinforcement bars, and humidity that contains oxygen. For instance, a structure fully submerged in seawater will experience a high concentration of chlorides. However, if the concrete's porosity is completely saturated with humidity, oxygen may not penetrate effectively, leading to minimal or negligible corrosion of the reinforcement rods.

Once corrosion initiates, it tends to accelerate regardless of the structure's location, as pathways for corrosive agents become more accessible. The concentration of chlorides required to initiate corrosion of reinforcement bars is directly related to the pH of the concrete; higher alkalinity necessitates a greater concentration of chlorides to start the corrosion process. This relationship underscores a link between deterioration caused by carbonation and that caused by chlorides. Carbonation reduces the pH of concrete, increasing the susceptibility to corrosion even in areas with lower chloride concentrations.

2.1.1.4 Alkali-Aggregates Reaction on Concrete

Alkali-aggregate reaction can lead to significant expansion and deterioration of concrete structures. Certain types of aggregates, particularly those containing reactive silicon, can react with the alkalis in cement, specifically sodium and potassium or with alkalis from external sources such as sodium chloride (NaCl) from deicing salts or seawater. This reaction produces a highly expansive gel when exposed to moisture, exerting pressure that can fracture the surrounding concrete. When concrete begins to deteriorate, increased humidity can accelerate the reaction process posing an additional risk of damage from freeze-thaw cycles.

Figure 2.4 Deterioration due to alkali-aggregates reaction (MAPEI SpA Manual, 2021)

2.1.2 Deterioration of Concrete by Physical Action

Concrete may aggression by physical elements with the following 3(three) ways

i) Freezing and thawing
ii) High temperature
iii) Shrinkage and cracking

i) Freezing and thawing: The impact of ice on concrete is detrimental only when liquid water is present within the material. This does not imply that the concrete must be completely dry; rather the humidity level must remain below a specific threshold known as "critical saturation." This means that the amount of water in the pores should be lower than this critical level to ensure that, even when it expands upon freezing, it can remain contained within the pores without generating excessive stress.

However, if the water nearly fills the entire volume of the pores, freezing will cause significant damage to the concrete due to the pressure exerted by the expanding ice (which increases in volume by approximately 9% when water freezes). In such cases, the pressure can lead to cracking and structural failure.

Damage due to freeze-thaw cycles only occurs when there is a combination of the following conditions are responsible for

i) Low temperatures
ii) Absence of macro-porosity
iii) High Temperature: Reinforcement rods can withstand temperatures of up to 500°C, while concrete itself can endure temperatures as high as 650°C. In this

context, the concrete encasing the reinforcement rods plays a vital role by slowing the transfer of heat. The thicker the concrete layer, the longer it takes for the reinforcement rods to reach their failure temperature of 500°C.

Two primary types of shrinkage that can lead to cracking in concrete are plastic shrinkage and hygrometric shrinkage. Plastic shrinkage occurs during the plastic phase of concrete when it releases moisture into the surrounding environment, causing it to contract. The likelihood of cracking in this phase is influenced by the conditions present when the concrete is cast. For instance, if the concrete is placed in formwork, evaporation is minimized; however, if it is exposed directly to environmental factors such as high temperatures, low humidity, or strong winds, evaporation can occur rapidly. This moisture loss can lead to the formation of micro-cracks on the surface while the concrete is still fresh. Hygrometric shrinkage, on the other hand, results from the continuous release of moisture into an environment with low relative humidity throughout the structure's service life. This type of shrinkage can also contribute to cracking over time as the concrete dries out.

2.1.3 Deterioration of Concrete by Mechanical Action

Deterioration due to external load or pressure refer as mechanical action on concrete. This are mainly 4(four) types: i) Abrasion, ii) Impact, iii) Erosion, iv) Cavitation.

Figure 2.5: RCC bridge girder concrete spalling due to load impact at support zone.

i) Abrasion: Abrasion occurs when a material is repeatedly impacted by particles from a harder body, resulting in wear due to the friction exerted by these harder particles on the surface of the material. Consequently, abrasion is directly influenced by the characteristics of the concrete materials. Strategies to enhance abrasion resistance include reducing the water-to-cement ratio and applying a cement mixture with hard admixtures and aggregates to the concrete surface (MAPEI SpA Manual, 2021; ACI Committee Report 210, 1993).

Factors which influence abrasion resistance:

a) Compressive strength: Higher compressive strength of concrete exhibits less abrasion value.
b) Properties of concrete aggregates: Coarse aggregate sound mechanical properties play an important role in concrete strength and also improve the mechanical properties of concrete.
c) Surface finishing coats: Initially, concrete abrasion starts from the surface, so tough surface finishing coats save the concrete from abrasion.
d) Presence of areas patched up: The weather condition of concrete patched influences its abrasion.
e) Conditions of the surfaces: A smooth and regular surface protects the concrete from friction caused by abrasion by water, air, or other substances through physical contact.

Figure 2.6: Erosion of concrete due to the running water (MAPEI SpA Manual, 2021)

Figure 2.7: Erosion due to high speed of water flow of RCC situ-pile concrete

ii) Impact: Another form of deterioration in concrete structures is caused by impact. Several factors must be considered, as concrete is a brittle material that can suffer damage and lose strength when subjected to impacts of sufficient intensity. Damage from impact may not be immediately apparent, and it often requires multiple cycles of impact to manifest. For example, floor joints experience repeated stress from the movement of mechanical transport vehicles (Figure 2.5). To mitigate the effects of this type of deterioration, it is essential to use concrete that is as strong as possible (ACI Committee Report 210, 1993).

iii) Erosion: Erosion is a specific type of wear caused by wind, water, or ice that leads to the removal of material from the surface of concrete. The extent of erosion is influenced by factors such as the velocity of the erosive agents, the concentration of hard dust particles, and the quality of the concrete itself. To mitigate erosion, it is crucial to exercise special care during the mixing of concrete. The same guidelines that apply to improving abrasion resistance should also be followed in this context.

iv) Cavitation: Cavitation is a significant issue that occurs in environments where water flows at high speeds (greater than 12m/s) (Figures 2.6 and 2.7). The rapid movement of water, combined with irregular surfaces, creates turbulence and areas of low pressure, leading to the formation of vortices that can erode the substrate. Air bubbles generated in the water flow move downstream and, upon encountering regions of higher pressure, implode, producing a powerful impact that results in erosion. When water velocity is particularly high, the erosion caused by cavitation can be severe. To prevent cavitation, it is essential to create smooth surfaces free of obstacles along the watercourse.

2.1.4 Deterioration of Concrete caused due to Defective Construction

Concrete is composed of several key elements, and its preparation is tailored to the specific requirements of each project. The more stringent the project demands, the more precise the mix design must be. The primary components of concrete include cement, aggregates, water, and admixtures. If any of these components are misused, it can lead to weaknesses in the final product. For instance, even if top-quality materials are utilized, improper mixing ratios due to inexperience or other factors can result in a concrete mix that performs poorly, akin to using inferior materials. Therefore, while the quality of the raw materials is crucial, ensuring they are mixed correctly is even more essential for achieving a strong and durable concrete structure (MAPEI SpA Manual, 2021).

Figure 2.8: Segregation of aggregates due to incorrect preparation or casting operations (MAPEI SpA Manual, 2021)

Figure 2.9: Concrete honeycomb in a newly constructed structure

The most crucial component of reinforced concrete is the cement, which must be appropriate for the specific application and exposure class. When considering this "ingredient," several factors must be taken into account. Although cement serves as the binding agent that ensures the required performance levels are achieved, simply increasing the cement quantity does not necessarily enhance performance. In fact, a higher cement content can lead to greater shrinkage during curing. Additionally, the aggregates used must possess an appropriate grain size distribution, with a proper balance between fine and coarse particles. They should also be clean to prevent foreign objects or impurities from affecting their properties or, in some cases, causing deterioration due to contamination, as previously discussed (MAPEI SpA Manual, 2021; Concrete Society Report 22, 1992).

Figure2.10: Segregation of aggregates, a symptom of incorrect casting of the concrete (MAPEI SpA Manual, 2021)

Insufficient protection of the reinforcement rods by the concrete can lead to increased vulnerability to deterioration caused by the penetration of harmful agents. When the concrete cover is inadequate, it allows moisture, chemicals, and other corrosive substances to reach the reinforcement which can accelerate damage and compromise the structural integrity over time. Proper coverage of the reinforcement is essential to enhance durability and prevent these issues. To summarize the defects in concrete, they may be divided into three main categories:

i) Defects due to poor/incorrect design of the mix
ii) Defects due to the wrong composition
iii) Defects due to incorrect/poor quality installation

2.2 Damage Assessment by Testing and Monitoring of RC Structure

There are several test methods available to understand RC structure serviceability and damage assessment. A few of the convenient test methods are as follows (BS EN 12504-2:2001; Bungey and Mandandoust, 1994; ASTM C805, 2019).

a) Non-destructive strength test:

i) Surface hardness methods (Rebound Hammer Test (RHT))

ii) Ultrasonic pulse velocity methods

b) Partially destructive strength tests:

i) Penetration resistance testing:

ii) Pull-out testing,

iii) Pull-off methods,

iv) Break off methods.

v) Core cutting test.

c) Load testing and monitoring:

i) In-situ load testing

ii) Monitoring (visual inspection)

iii) Ultimate load testing

d) Durability tests:

i) Corrosion of reinforcement and pre-stressing steel

ii) Moisture measurement

iii) Absorption and permeability tests

iv) Tests for alkali-aggregate reaction

e) Performance and integrity tests.

A few of the test methods that are relevant and falls within the scope of the work is discussed in the following sections.

2.2.1 Visual Inspection of RC Building

2.2.1.1 General

Completing a visual inspection of concrete immediately after construction, and periodically throughout its service life, is essential for gathering historical data on performance and durability. These inspections facilitate the early identification of distress and deterioration, allowing for timely repairs or rehabilitation before replacement becomes necessary. Inspectors must meticulously document observations related to environmental and loading conditions. Visual inspections are often supplemented by nondestructive tests, destructive tests and further investigations, particularly when signs of distress are present and insights into the internal condition of the concrete are required. While visual inspections are primarily associated with assessing concrete that exhibits defects or distress, they are recommended for all concrete structures. It is crucial for inspectors to record observations concerning environmental exposure, including the effects of physical loads, deformations, defects, imperfections, and overall durability and performance.

To ensure a comprehensive evaluation, concrete material records and construction practices should be gathered and reviewed. The inspection checklist should encompass items that may influence the concrete's durability and performance; however, inspectors should not restrict their investigations to these items alone but consider any additional factors that may contribute to the condition observed. Following established guidelines does not replace the necessity for astute observations and sound judgment.

Inspectors should possess experience and competence in conducting concrete condition surveys. Alongside written descriptions, sketches of relevant features are encouraged as they enhance understanding. Photographs that include a scale for dimensions are invaluable in documenting the concrete's condition. Additionally, video documentation can provide a more dynamic visual perspective than still images alone.

The descriptions and photographs collected during inspections serve to illustrate typical observations and assist in preparing condition survey reports by identifying potential problems and detailing their condition. A checklist was followed to recognize characteristics of potential findings during this assessments.

2.2.1.2 Descriptions of Distress

Defects and distresses in concrete have been systematically classified and illustrated with photographs, allowing for the quantification of their severity and extent when possible. The primary aim of these photographs is to standardize the reporting process regarding the condition of concrete within a structure. Surveyors conducting these assessments should be well-versed in the terminology associated with various types of imperfections and distresses. Accompanying figures depict different defects and distresses, along with known causes of deterioration, enhancing understanding and communication of the observed conditions. (BS EN 12504-2:2001, Bungey and Mandandoust, 1994; Bungey and Grantham, 2018; ASTM C805, 2019; ACI Committee 201, 2008).

2.2.1.3 Different Types of Cracking

i) Definition of Crack**:** Cracking refers to the complete or incomplete separation of concrete into two or more sections, resulting from breaking or fracturing. When documenting cracks, it is important to classify them according to their width and type.

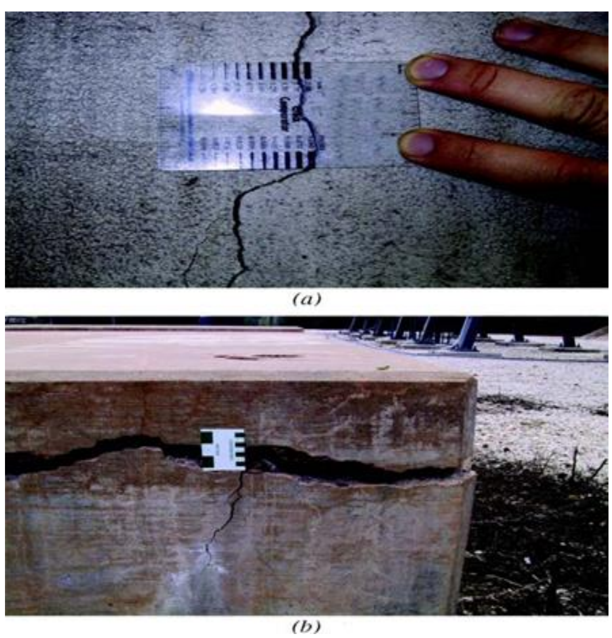

Figure 2.11: Cracks of varying widths (ACI 201.1R-08)

ii) Checking: When concrete shallow cracks development at closely spaced but irregular intervals on the surface of structure.

iii) Craze cracks: Cracks of concrete which are fine and random.

iv) D-cracks: The cracks in concrete that are located near and generally parallel to joints and edges.

v) Diagonal crack: An inclined crack in a flexural member, typically occurring at approximately 45 degrees to the axis, is caused by shear stress. Additionally, it can refer to a crack in a slab that is not aligned with either the lateral or longitudinal directions.

vi) Hairline cracks: Cracks on a visible concrete surface that are so narrow they are barely perceptible.

vii) Longitudinal cracks: A crack that develops longitudinal dimension of the member.

viii) Map cracking: These cracks can vary in width, ranging from fine and barely visible to open and well-defined.

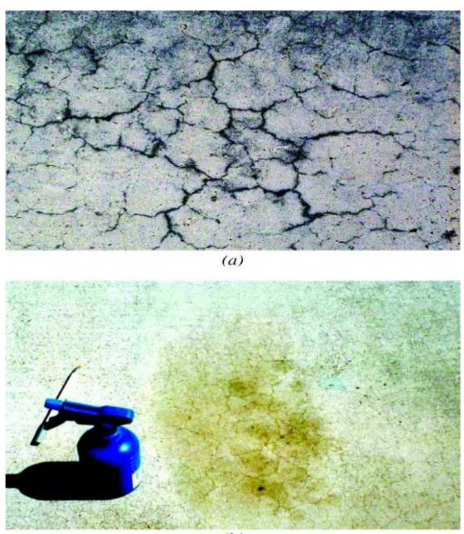

Figure 2.12: (a) Craze cracking; and (b) Craze cracking (ACI 201.1R-08)

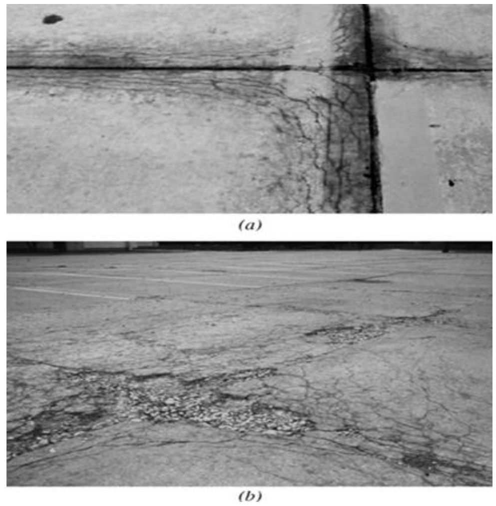

Figure 2.13: Cracks: (a) fine; and (b) severe, with spallation present (ACI 201.1R-08)

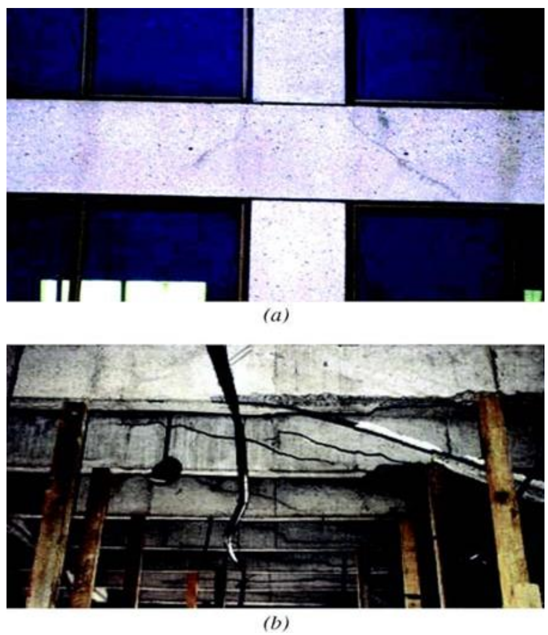

Figure 2.14: Diagonal cracking (ACI 201.1R-08 Report)

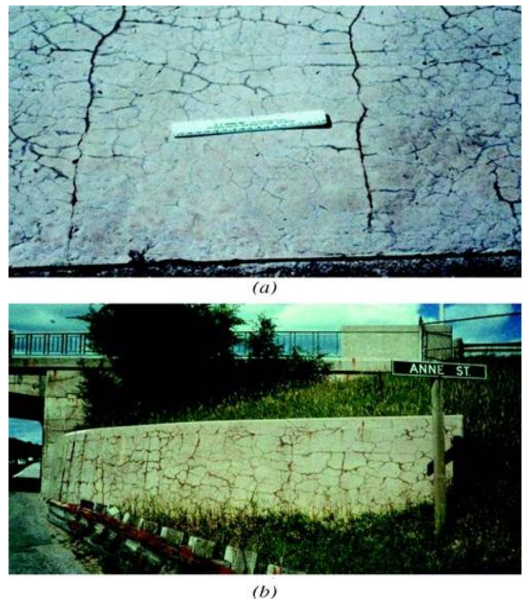

Figure 2.15: Map (pattern) cracking (ACI 201.1R-08)

ix) Pattern cracking: Cracking on concrete surfaces that appears as a repeated pattern results from a decrease in volume near the surface, an increase in volume below the surface, or a combination of both factors.

x) Plastic shrinkage of concrete: Cracking that appears on the surface of freshly poured concrete shortly after it has been placed, while it is still in a plastic state.

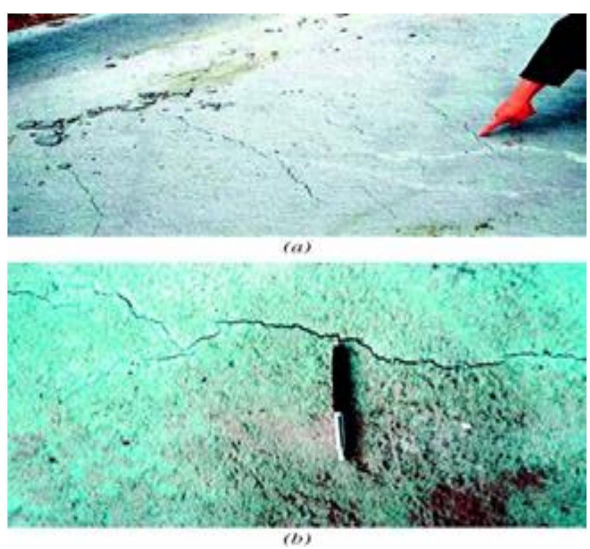

Figure 2.16: Plastic shrinkage cracking (a, b) (ACI 201.1R-08)

xi) Random cracks: Cracks that form in an uncontrolled manner, radiating in various directions from the control joints.

xii) Shrinkage cracking: Cracking in a structure or member occurs due to tensile failure caused by external or internal restraints as moisture content decreases, carbonation takes place, or as a result of both factors.

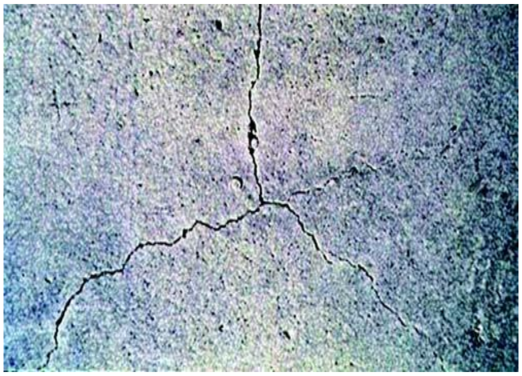

Figure 2.17: Shrinkage cracking (ACI 201.1R-08)

xiii) Temperature cracking: Cracking resulting from tensile failure occurs due to a temperature drop in members that are subjected to external restraints, or from a temperature differential in members that experience internal restraints.

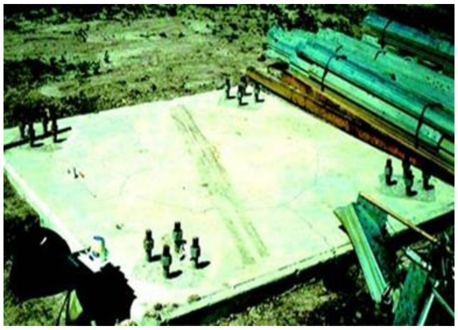

Figure 2.18: Temperature cracking (ACI 201.1R-08)

2.2.1.4 Concrete Distress

Concrete distress should be systematically documented through visual assessments of structural deterioration. This deterioration manifests in various unaesthetic forms, including chalking, curling, deflection, deformation or distortion, delamination, disintegration, dusting, efflorescence, and scaling. The scaling can range from mild to severe, with classifications such as scaling medium, scaling severe, and scaling very severe. Additionally, signs of distress may include spalling and large spalls. Proper documentation of these conditions is essential for assessing the integrity and longevity of concrete structures.

Figure 2.19: Steel industry premises concrete spall by carbon attack.

2.2.1.5 Visual Inspection Report and Documentation

Individuals performing the visual inspection should prioritize items that are relevant to the specific concerns prompting the inspection. It is important not to overlook other items and factors that may not be listed in the checklist but could still play a significant role during the assessment. The Visual Inspection Form provided in the Appendix can be utilized to document the findings of the inspection (ACI Committee Report 201, 2008). A comprehensive final report should be prepared to document results of the completed inspection. This report should include:

i) Names of the individuals conducting the inspection,

ii) Purpose of the inspection,

iii) A list of existing documentation related to the structure,

iv) Type, age, location, and general description of the structure,

v) Inspection techniques employed (e.g., direct visual inspection, chain drag),

vi) Field observations and the extent of the structure inspected,

vii) Field tests conducted and data collected, if applicable,

viii) Conclusions and recommendations,

ix) Annotated photographs and sketches.

This structured approach ensures that all relevant information is captured and presented clearly for future reference and decision-making (ACI Committee Report 201, 2008).

2.3 Time Variation Laws of Concrete Compressive Strength

The analysis of concrete compressive strength as reported in several empirical models of time variation law of concrete compressive strength reveal distinct trends and characteristics of concrete strength variation over time sometimes based on data normalization methods. The long-term time variation law of concrete specimens under the coupling effect of multiple factors was studied by several researchers (Washa et al., 1989; Withey, 1961; Washa and Wendt, 1975; Wood, 1992; Pollock et al., 1981, Chaplin, 1980). Withey proposed empirical expressions for time variation of concrete for two different concrete strengths at low water-cement ratios (Withey, 1961). The expressions were developed based on experimental data of concrete (cylinder) strength of 50 years, which represents development of peak strength at around 25 years with range where the rate of variation of concrete strength different at different ranges of concrete age.

Data normalization is usually processed via division by mean value of the 28 day strength, or of the cubic compressive strength, or of the axial compressive strength (Wang and Yue, 2023). The CEB-FIP Model Code (CEB-FIP Model Code, 1990), as shown by fundamental expression in Eq. 2.1, provides a mathematical framework for predicting concrete strength over time.

$$f_c(t) = f'_c(28).exp[s.[1-28/(t/t_1)]^{1/2}] \quad \text{.................................Eq. 2.1}$$

where $f_c(t)$ is the compressive strength of concrete at time t; $f'_c(28)$ is the 28 days strength of concrete; s is a coefficient which depends on the type of cement; t_1 is the time of 1 day. The normalized compressive strengths collected by Niu (Niu and Wang, 1995) shows progressive increase of concrete strength up to 60 years of service age. The models proposed by Gao (Gao and Ren, 2018) and Wang (Wang, 2022) also shows similar trend over time. The models depicted in Figure 2.20 shows different trends and characteristics based on variable test methods of collecting data or data normalization methods.

Table 2.1: Normalized compressive strengths collected by Niu and Wang (Niu and Wang, 1995)

Service Age (Year)	Normalized compressive strengths	Service Age (Year)	Normalized compressive strengths
0	1.0	12	1.34
1	1.38	17	1.35
2	1.41	20	1.58
2.5	1.35	24	1.40
3	1.41	25	1.56
5	1.5	30	1.35
7	1.34	45	1.21
10	1.53	60	1.16

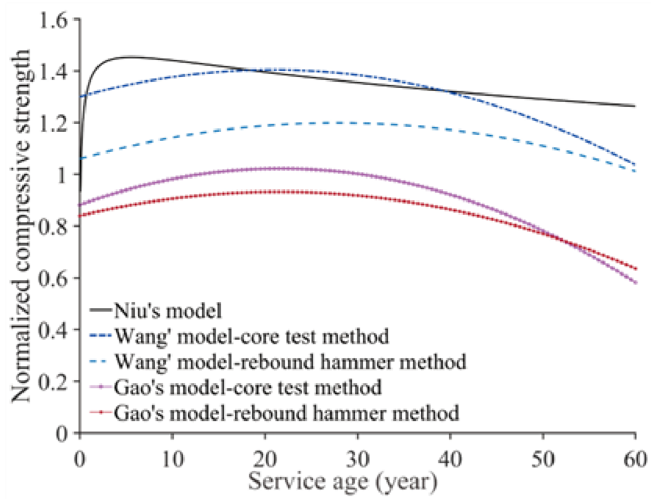

Figure 2.20: Comparison of Niu, Gao and Wang's model of time variation of concrete strength

It can also be seen from Figure 2.20 that the normalized data of strength in Wang's model is always greater than that of Gao's model. Wang's normalized strength was obtained by taking the field test data and dividing the data by the mean value of axial compressive strength, while Gao's model was divided by the mean value of cubic compressive strength. The mean value of the axial compressive strength f_{cm} and the mean value of the cubic compressive strength $f_{cu,m}$can be expressed as follows:

$$f_{cm}= f_{ck}/(1\text{-}1.645\delta_c)\text{.................................Eq. 2.2}$$

$$f_{cm} = f_{cu,k}/(1\text{-}1.645\ \delta c)\ \text{................................Eq. 2.3}$$

where f_{ck} and $f_{cu\,,k}$ is the standard value of the compressive strength of a cube and cuboid, respectively. The relation between f_{ck} and $f_{cu\,,k}$ is expressed as below,

$$f_{ck} = 0.88 * \alpha_1 \alpha_2 f_{cu\,k} \quad \text{Eq. 2.4}$$

where 0.88 is the correction coefficient considering the difference between the structure and the specimen of concrete; α_1 is the ratio of the prism's strength to the cube's strength, $\alpha_1 < 1$; α_2 is the reduced coefficient of concrete considering brittleness, $\alpha_2 \leq 1$.All three models of Niu, Wang, and Gao exhibit a similarity in a trend where compressive strength increases for a considerable time over its service age before declining after a certain time. This pattern is evident in Figure 2.20, which illustrates the normalized compressive strengths across different service ages. Significant differences in the points of inflection in different models arise from the varying data sources (e.g. data collected by core test or RHT).

Niu's model is unique as it is based on an exponential function, with the peak normalized compressive strength occurring around 5 years. Wang's model is developed based on a quadratic function that peaks at approximately 30 years whereas Gao's quadratic model function peaks at about 25 years. The divergence between Niu's model and the others can be attributed to regional data differences; Niu's data primarily comes from international sources, while Wang's and Gao's data are localized within China (in Shandong and Shanghai). Furthermore, Niu's model shows limitations due to its reliance on data predominantly collected within the first 25 years, which skews its long-term predictive capability. Wang's model consistently reports higher normalized strength values compared to Gao's. This discrepancy arises from their respective normalization techniques: Wang uses axial compressive strength as a divisor, while Gao employs cubic compressive strength. Both Wang's and Gao's models demonstrate a consistent finding of the normalized compressive strength from core tests exceeds that from RHT tests. The gap between these two testing methods narrows over time due to the RHT test measuring surface hardness which can degrade with age while core tests assess internal concrete strength. Various other internal factors may also significantly impact concrete strength over time, including cement type, hydration rates and overall strength development. A lower water-cement ratio typically results in higher strength. Moist curing generally yields better results than air curing. Research by Chidiac et al. (Chidiac et al., 2013) and Moutassem and Chidiac (Moutassem and Chidiac, 2015) highlights these relationships, emphasizing that factors such as aggregate type and gradation also play critical roles in determining compressive strength.

In general, understanding the time variation models and their underlying factors is crucial for accurately predicting concrete performance over time which has significant implications for construction practices and material selection. The widely variable finding time variation of concrete compressive strengths may be ascribed to the fact that the effects of concrete strength variation due to aging of concrete could not be clearly excluded from effects from other internal or external factors such as sulfate attacks, carbonization, freeze-thaw cycles etc.

2.4 Non-Destructive Rebound Hammer Test

2.4.1 Rebound Test Equipment and Operation

The Swiss engineer Ernst Schmidt developed a practical rebound test hammer in the late 1940s which has inspired modern versions of the device. A typical Type N hammer, as depicted in Figure 2.21, weighs less than 2 kg and delivers an impact energy of approximately 2.2 Nm. The hammer features a spring-controlled mass that slides on a plunger housed within a tubular casing. When the plunger is pressed against the concrete surface, it compresses the spring, which is then released to allow the hammer mass to strike the concrete. Upon rebounding, a rider attached to the mass moves along a visible scale through a small window in the casing. This rider can be locked in place by pressing a button, facilitating easy reading of results. The equipment is designed for straightforward operation, allowing it to be used both horizontally and vertically, whether upwards or downwards. The schematic diagram in the figure illustrates various components of the rebound hammer, highlighting its user-friendly design.

To perform the test, the plunger of the rebound hammer is pressed firmly and steadily against the concrete surface at a right angle until the spring-loaded mass is released from its locked position. After the impact occurs, the scale index must be read while the hammer remains in place. Alternatively, pressing the locking button can retain the reading, or results can be automatically recorded using an attached paper recorder. The resulting scale reading, referred to as the rebound number, is an arbitrary measure that reflects the energy stored in the spring and the mass utilized. This equipment is typically employed for testing concrete with a strength range of 20–60 N/mm². Additionally, modern versions of this device feature electronic digital readings with automatic data storage and processing capabilities. Specialized rebound hammers are also available for use in impact-sensitive areas and mass concrete applications.

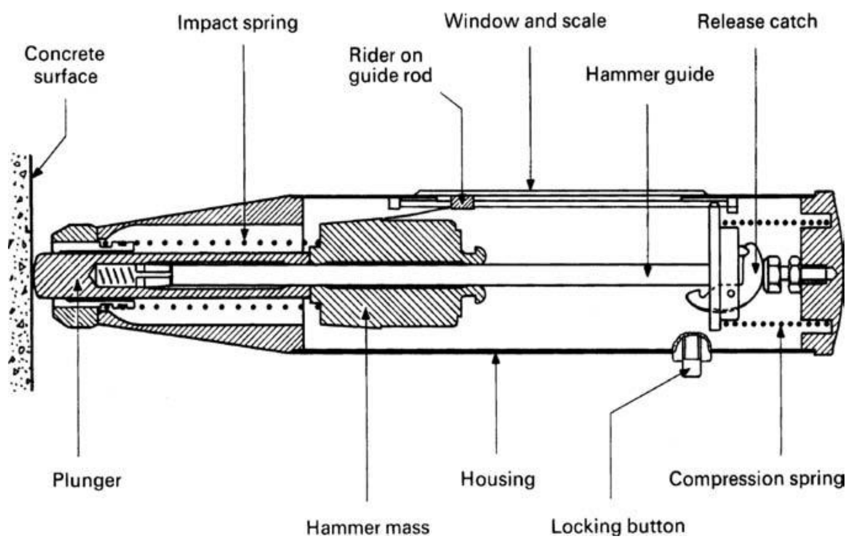

Figure 2.21: Typical Schmidt rebound hammer (Bungey and Mandandoust, 1994)

For low-strength concrete in the 5–25 N/mm² range, a pendulum-type rebound hammer with an enlarged hammer head (Type P) is recommended for optimal results. The rebound hammer method could be used for

a) Assessing the likely compressive strength of concrete with the help of concrete with the help of suitable co-relations between the Rebound index and compressive strength.

b) Assessing the uniformity quality of concrete of one element in relation to another.

c) Assessing the quality of concrete in relation to standard requirements.

2.4.2 Procedure of Rebound Hammer Test

The accuracy of readings is highly influenced by local variations in the concrete, particularly due to the presence of aggregate particles near the surface. To ensure reliable results, it is essential to take multiple readings at each test location and calculate their average. While specific standards may differ, BS EN 12504-2:2001 recommends obtaining at least nine readings from an area not exceeding 300 mm², with impact points spaced no less than 25 mm apart and at least 25 mm from any edge. Utilizing a grid system for locating these points helps minimize operator bias.

Before conducting tests, the rebound hammer should be tested a minimum of three times to verify its functionality and calibrated against a steel reference anvil as needed. The testing environment should maintain a temperature between 10°C and 35°C. Any measurements taken from areas where the surface has crushed or broken due to nearby voids should be disregarded. Additionally, if more than 20% of the results deviate by more than six units from the median, the entire set of readings should be discarded, necessitating the collection of ten new readings. The surface must be smooth, clean, and dry; ideally, it should be formed. If trowelled surfaces are unavoidable, they should be smoothened using the sandstone typically provided with testing equipment. Loose material can be removed, but care must be taken to avoid areas that are rough due to poor compaction, grout loss, spalling or tooling, as these can lead to unreliable results (Bungey and Mandandoust, 1994; Bungey and Grantham, 2018; BS 6089:1981, 2010; ASTM C805, 2019).

2.4.3 Rebound Hammer Test Theory, Calibration and Interpretation

The test operates on the principle that the rebound of an elastic mass is influenced by the hardness of the surface it strikes, providing insights into a surface layer of concrete that is no more than 30 mm deep. The results yield a relative measure of hardness in this zone, although this cannot be directly correlated with other concrete properties. Upon impact, energy is dissipated due to localized crushing of the concrete and internal friction within its structure; it is this internal friction, which relates to the elastic properties of the concrete's components, that complicates theoretical evaluations of test outcomes. Numerous factors can affect the results, and all must be taken into account if the rebound number is to be empirically linked to concrete strength (Akashi and Amasaki, 1984).

2.4.4 Factors Influencing Rebound Hammer Test Results

Rebound hammer tests are influenced by several characteristic features on concrete including its exposure and surrounding environmental factors. However, RHT results are significantly influenced by all of the following major factors:

a) Mix characteristics:

(i) Type of cement

(ii) Content of cement

(iii) Type of coarse aggregate

b) Member characteristics:

(i) Mass

(ii) Compaction

(iii) Type of surface

(iv) Age, rate of hardening and curing type

(v) Carbonation of surface

(vi) Moisture condition

(vii) Stress state and temperature

Given that each of these factors can impact the readings obtained, any efforts to compare or estimate concrete strength will only be valid if all variables are standardized for both the concrete being tested and the correlation specimens. The influences of these factors can vary significantly in magnitude. Additionally, the orientation of the hammer during testing can affect the measured values; however, correction factors can be applied to account for this effect.

2.4.4.1 Mix Characteristics

(i) Cement type: Variations in the fineness of Portland cement are generally not significant, with their impact on strength correlation being less than 10%. In contrast, super-sulfated cement is likely to produce strengths that are 50% lower than those indicated by a Portland cement correlation. Conversely, high alumina cement concrete can exhibit strengths that are up to 100% greater than those suggested by the same correlation.

(ii) Cement content: Different cement content in concrete do not directly correlate with changes in surface hardness. Instead, the interplay of strength, workability, and the proportions of aggregate to cement results in a decrease in hardness relative to strength as the cement content increases. Nevertheless, for most concrete mixes, the error in estimated strength due to this factor is unlikely to exceed 10% (Kolek, 1970).

(iii) Coarse aggregate: The type and proportions of aggregate can significantly influence concrete strength, as both paste and aggregate characteristics play a crucial role. The rebound number is more affected by the hardened paste. For instance, crushed limestone may produce a rebound number that is considerably lower than that of gravel concrete with similar strength, which can correspond to a strength difference of 6–7 N/mm². Additionally, a specific type of aggregate may exhibit varying rebound number/strength correlations based on its source and nature; Figure 2.22 illustrates typical curves for hard and soft gravels. Lightweight aggregates are expected to yield results that differ markedly from those produced with dense aggregates, and substantial variations have also been observed among different types of lightweight aggregates.

However, correlations can be established for specific lightweight aggregates, although the proportion of natural sand used will also affect the results (Bungey and Mandandoust, 1994). Figure 2.21 illustrates the extent of these differences by comparing strength correlations obtained from laboratory specimens that are otherwise 'identical' but vary in age and contain different types of lightweight coarse aggregates.

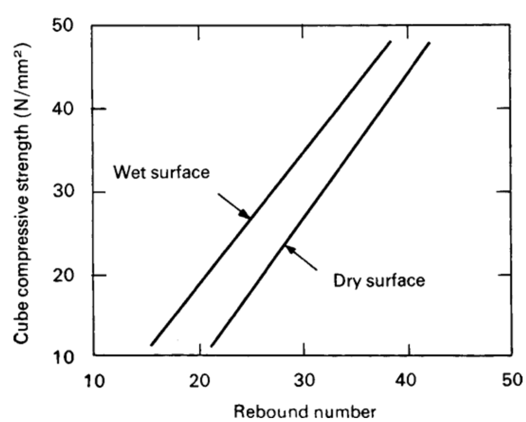

Figure 2.22: Influence of surface moisture condition (Bungey and Mandandoust, 1994)

2.4.4.2 RHT Result Dependency on Member Characteristics

The characteristics of structural members significantly impact the results of the Relative Humidity Test. According to BS EN 12504-2:2001, concrete members must be at least 100mm thicker to ensure accurate readings. Additionally, proper compaction is essential, along with a smooth and level surface. The surface should be texture-free, hardened, and devoid of carbonation to achieve reliable RHT results.

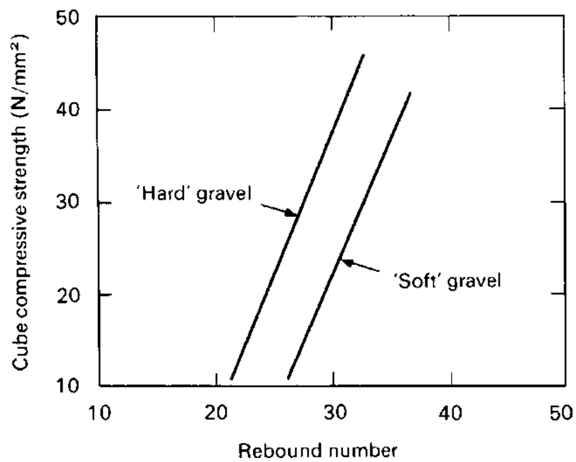

Figure 2.23: Comparison of hard and soft gravels, vertical hammer (Bungey and Mandadoust, 1994)

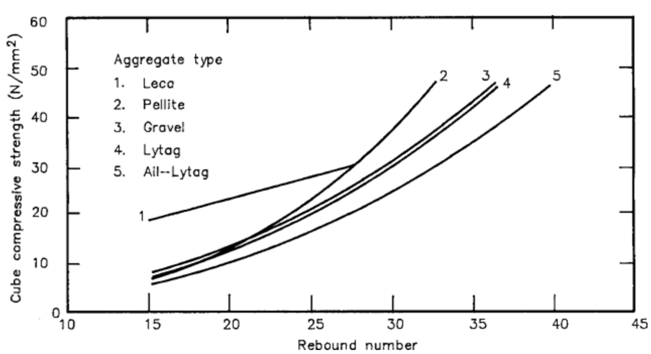

Figure 2.24: Comparison of lightweight aggregates (Bungey and Mandadoust, 1994)

2.4.5 Calibration of Rebound Hammer Test Results

The significance of specimen mass has been previously addressed; it is crucial that test specimens are either firmly clamped in a robust testing machine or placed on a stable, level floor. Specimens should be cubes or cylinders with a minimum size of 150 mm, and it is recommended that a restraining load of at least 15% of the specimen's strength be applied for cylinders, while cubes tested with a type N hammer should have a minimum restraining load of no less than 7 N/mm². Figure 2.25 illustrates typical relationships between rebound number and restraining load, indicating that once an adequate load is applied, the rebound number tends to stabilize (Malhotra, 1976).

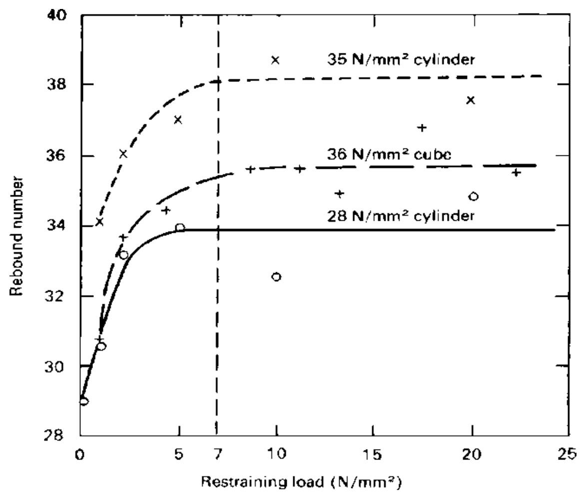

Figure 2.25: Effect of restraining load on calibration specimen (Malhotra, 1976)

2.4.6 Interpretation of Surface Hardness Measurements

The interpretation of surface hardness readings depends on understanding how standardized the factors are between the readings being compared. This is relevant whether the results are used to evaluate relative quality or estimate strength. As illustrated in Figure 2.25, which presents a typical strength calibration chart generated under 'ideal' laboratory conditions, there is a significant scatter in results. The strength range associated with a specific rebound number can vary by approximately ±15%, even for what are considered 'identical' concrete samples. In a practical situation, it is very unlikely that a strength prediction can be made to accuracy better than 25% (Malhotra, 1976). The observed scatter indicates that even when a strength prediction is not necessary, significant variations in rebound numbers can be expected for 'identical' concrete. Therefore, acceptable limits must be established alongside other testing methods. According to BS 6089:1981 (2010), when at least ten readings (n) are taken at a location, the accuracy of the mean rebound number is likely to fall within $\pm 15/\sqrt{n}\%$ with 95% confidence. Presenting the results graphically, as previously described, can be beneficial, and calculating the coefficient of variation may provide insights into concrete uniformity when sufficient data is available.

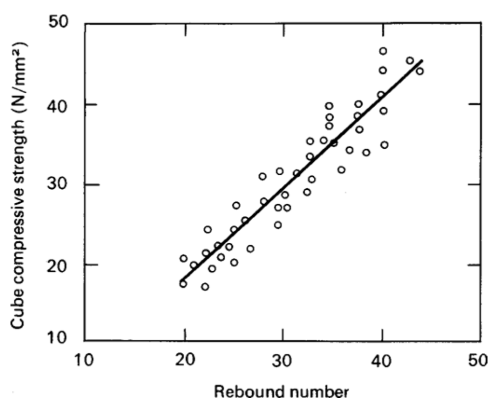

Figure 2.26: Typical rebound number/compressive strength calibration chart (Bungey and Mandandoust, 1994)

While the primary interest often lies in the relationship between rebound number and compressive strength, similar correlations can be established with flexural strength, albeit with even greater variability. Additionally, no general relationship has been found between rebound number and elastic modulus; however, it may be feasible to develop a specific calibration for a particular concrete mix.

2.4.7 RHT Applications and Limitations

Surface hardness measurements can be categorized into four distinct groups:

(i) Uniformity of concrete quality checking

(ii) Specified requirement comparing with a given sample concrete

(iii) Concrete approximate strength estimation

(iv) Classification of abrasion resistance.

Figure 2.27: Surface damage on green concrete (Bungey and Mandandoust, 1994)

Regardless of the application, it is crucial to standardize or account for the factors influencing test results, keeping in mind that the results pertain only to the surface zone of the concrete being tested. An additional significant limitation arises when testing at early ages or low strengths, as rebound numbers may be too low for accurate readings, and the impact can potentially damage the surface. Therefore, it is not advisable to use this method for concrete with a cube strength of less than 10 N/mm^2 or that is less than 7 days old, unless the concrete is of high strength.

2.5 Pushover Analysis for Performance Evaluation and Damage Prognosis

2.5.1 General

Pushover analysis has gained popularity in earthquake engineering, similar to the response spectrum method of analysis. While the response spectrum method serves as an effective equivalent static analysis for the elastic dynamic analysis of structures during an earthquake, pushover analysis acts as a suitable equivalent non-linear static analysis for the inelastic dynamic analysis of structures. This method is particularly beneficial for performance-based design of new buildings that depend on ductility or redundancy to withstand seismic forces.

Pushover analysis generates a load versus deflection curve that illustrates the structural response from its initial state to ultimate failure. In this context, the load represents the equivalent static load associated with a specific mode typically the fundamental mode of the structure, which can be conveniently interpreted as the total base shear. Conversely, the deflection may denote any story's deflection, with the top-story deflection often being selected for analysis. Pushover analysis can be categorized into two types: force-controlled and displacement-controlled.

In the force-controlled approach, the total lateral force is applied in increments, necessitating adjustments to the structure's stiffness matrix for each load increment. Conversely, in displacement-controlled analysis, the top story's displacement is increased incrementally, which requires a corresponding horizontal force that laterally pushes the structure in proportion to its fundamental horizontal translational mode aligned with the lateral load direction. Similar to the force-controlled method, the stiffness matrix may also need to be modified for each increment of displacement in this approach.

Displacement-controlled pushover analysis is generally favored over force-controlled analysis because it allows for evaluation up to a specified level of displacement, providing more flexibility in assessing structural performance under seismic conditions.
Recent interest in developing performance-based codes for designing or rehabilitating buildings in seismically active regions highlights the effectiveness of an inelastic procedure known as pushover analysis for assessing damage vulnerability (Datta, 2010). Essentially, pushover analysis consists of a series of incremental static analyses aimed at generating a capacity curve for the building. From this capacity curve, a target displacement is determined, representing an estimate of the displacement that the design earthquake would impose on the structure. The level of damage sustained by the building at this target

displacement is considered indicative of the damage likely to occur during design-level ground shaking.

This methodology has been refined by various researchers, often with minor variations in computational procedures, and is typically applied to symmetrical structures. By assuming that floors behave as rigid diaphragms, the damage state of the building can be evaluated through a two-dimensional pushover analysis. If all lateral load-resisting elements are uniform, the analysis can be further simplified by conducting pushover analyses on a representative element or on a whole building frame (Lawson et al., 1994; Datta, 2010).

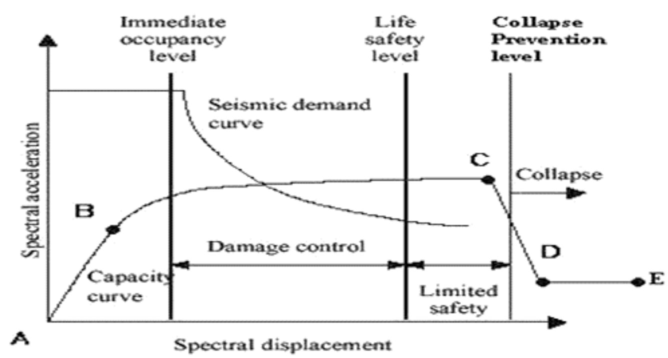

5

Figure 2.28: Structural Performance level and ranges (Datta, 2010; Santosh, 2014)

2.5.2 Force Deformation Behavior and Development of Plastic Hinges

According to Figure 2.28, the different points in the capacity curve can be stated as below (Santosh, 2014)

i) Point “A” unloaded condition of the structural elements.

ii) Point “B” represents yielding of the structural elements.

iv) The ordinate at “C” corresponds to nominal strength

v) The drop from “C” to ”D” means the initial failure of the element and resistance to lateral loads beyond point “C” is usually unreliable.

vi) The residual resistance from “D” to “E” allows the frame elements to sustain gravity loads.

2.5.3 Structural Performance Levels and Ranges

The building performance level is a function of the post event conditions of the structural and non-structural components of the structure (Santosh, 2014). Three steps performance levels are as follows:

i) Immediate Occupancy (IO)

ii) Life Safety (LS)

iii) Collapse Prevention (CP)

As per Figure 2.28, the above three performance level can be briefly described as below, (Chopra, 2007; Santosh, 2014)

a) Immediate Occupancy (S-1)

The Immediate Occupancy state indicates that only minimal structural damage has occurred following an earthquake. In the primary concrete frames, this may manifest as hairline cracking.

b) Damage Control Performance (S-2)

Damage Control refers to a continuous range of damage states that is characterized by less damage than what is defined for the Life Safety level, but more damage than what is specified for the Immediate Occupancy level.

c) Life Safety Performance Level (S-3)

Structural Performance Level S-3, or Life Safety, describes a post-earthquake damage state where the structure has sustained significant damage, yet retains some margin against partial or total collapse; in this condition, the primary concrete frames may exhibit extensive damage in the beams, along with spalling of the concrete cover and shear cracking in the ductile columns.

d) Limited Safety Performance Range (S-4)

Structural Performance Range S-4, or Limited Safety, represents the continuous range of damage states that exist between the Life Safety and Collapse Prevention (CP) levels.

e) Collapse Prevention Performance Level (S-5)

Structural Performance Level S-5, or Collapse Prevention, indicates that the building is on the brink of experiencing partial or total collapse, characterized by extensive cracking and the formation of hinges in the ductile elements of the primary concrete frames.

Chapter 3
Methodology

3.1 Field Investigation

The field investigation of the work was done on selected RC buildings located at Halishahar, Bayezid and Kumira region of Chittagong city. Many of the Bangladesh Railway building infrastructures in Halishahar region were built more than thirty years ago. One of the aging RC structures whose service life has already exceeded thirty years is investigated first by visual screening method and a comparative assessment of the building is done against benchmarks or standards for serviceability compliance. Non-destructive testing instruments such as RHT and ultrasonic pulse velocity tester were used to determine in-situ strength or quality of reinforced concrete at representative locations of columns, beams and slabs of the selected RC building. Locations of testing or sampling are chosen according to a protocol reasonably developed based on visual inspection of the selected RC structure.

A calibration chart is used for indirect measurement of concrete's compressive strength against the rebound numbers (R) recorded during the field tests. Validation of a few selected field test records are also done using core cut samples tested at concrete testing laboratory of CUET. Further validation of the RHT test results of concrete strength is made based on results of RHT tests, cylinders' and cubes' compressive strength tests done for three laboratory scale RC beams tested at CUET.

An outline of the methodology of this work is shown in Figure 3.1 as below

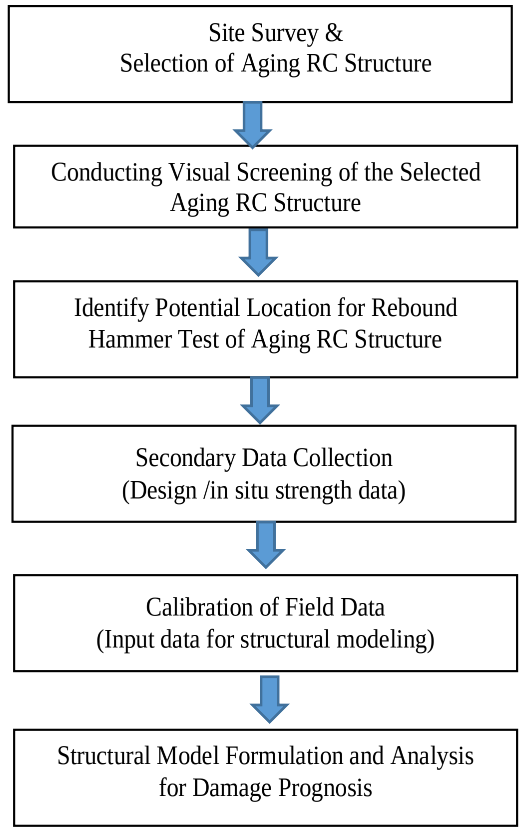

Figure 3.1: Outline of methodology of the research work

The laboratory scale RC beam specimens were constructed conforming to concrete mix design procedure at CUET laboratory to achieve target strengths of 22 MPa and 25 MPa. Each beam was cast in two separate segments where concrete of two target strengths was poured (Figure 3.2 to 3.4). The beams were cast according to laboratory standards to control quality of casting and to avoid typical problems of concrete such as sulfate attack, temperature effect, carbonization etc. that may adversely affect concrete strength development at their early ages. The beams were cast at different times. However, cylinder samples were taken for testing at 7 days, 14 days, 28 days, 45 days, 3 months, 5 months and 8 months for comparison among three beam specimens.

Laboratory-scale beam specimens are subjected to Schmidt RHT test at various ages and indirect measurements of compressive strengths are made from Schmidt RHT calibration charts of correlation between rebound numbers and concrete compressive strength. The strengths read from Schmidt calibration chart are then compared to strengths obtained from respective sample test results of cylinder tests performed at laboratory. Due to the limited scope of this research, this comparative study involving laboratory-scale beam specimens was planned to be conducted over an eight-month period, with the goal of developing an empirical time-variation law for the compressive strength of concrete. The study aims to establish empirical expressions for calibrating RHT test data against beam test data for two target strengths: 22 MPa and 25 MPa.

$$f = ln\,(t) + c \qquad \text{Eq. 3.1}$$

where,

f = compressive strength.

t = age of concrete year

c = constant

Figure 3.2: Laboratory scale RC beam structure sample-1

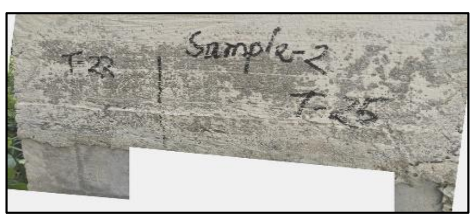

Figure 3.3: Laboratory scale RC beam structure sample-2

Figure 3.4: Laboratory scale RC beam structure sample-3.

3.2 Visual Screening Procedure

Visual characteristics can indicate workmanship quality, structural serviceability and material deterioration. It is essential for engineers to distinguish among different types of cracking that may occur. Figure 3.5 illustrates some common forms of cracks and their typical appearances.

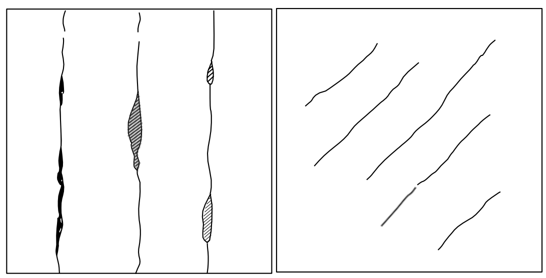

(a) Reinforce corrosion (b) Plastic shrinkage

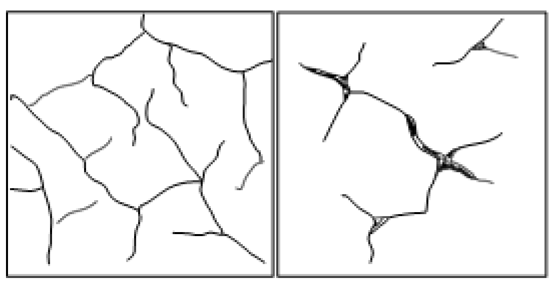

(c) Sulfate attack (d) Alkali/Aggregate reaction

Figure 3.5: Some typical cracks of RC structure (Bungey and Mandandoust, 1994)

The ACI 201.01 report outlines an ideal framework for conducting visual screenings as part of structural health monitoring. This study followed a systematic and step-by-step approach, which included the following components:

i. General Overview: This section provides a description of the structure, including its design and the materials used in its construction.
ii. Environmental and Loading Conditions: An assessment of the environmental factors and loading conditions that may impact the structure's performance.
iii. Distress Indicators: Identification and evaluation of any distress indicators that may suggest deterioration or structural issues.
iv. Current Condition of the Structure: A thorough examination of the present state of the structure to determine its overall health and integrity.

This structured methodology ensures a comprehensive evaluation of the building's condition, facilitating informed decision-making regarding maintenance and repairs.

3.3 Procedure of Rebound Hammer Test

Proceq (Fewtrell, 1993), the original brand name of Schmidt Concrete Test Hammer of Switzerland, provides an operational manual with a brief methodology as follows.

3.3.1 Rebound Hammer Operation and Principle

The operation of the rebound hammer, along with its measuring principle, is summarized below based on the standard manual for Schmidt RHT tests on concrete. This device measures the rebound value (R), which correlates directly with the hardness and strength of the concrete. Consequently, it allows for an indirect assessment of concrete strength using non-destructive RHT methods. This approach provides valuable insights into the concrete's structural integrity without causing damage to the material (Fewtrell, 1993). The following factors must be taken into account when ascertaining rebound values R, as stated in the manufacturer's operation manual-

- Impact direction: horizontal, vertical, downwards or upwards.
- Concrete age.
- Size and shape of the comparison sample (cube, cylinder)

As specified in the manual of Schmidt hammer tests, models N and NR can be used for testing:

- Concrete items which are 100 mm or more in thickness
- Concrete with a maximum particle size ≤ 32 mm

3.3.2 Measuring Procedure

The rebound number R is recorded from impact tests conducted with a concrete test hammer on a smooth, hard surface, which must first be prepared using a grindstone. The concrete test hammer is held perpendicular to the test surface, and the impact plunger (indicated as "1" in Figure 3.7) is activated by pushing the hammer toward the surface until the pushbutton springs out. Each test surface should undergo at least 8 to 10 impacts, with individual impact points spaced a minimum of 20 mm apart. After each impact, the push button is pressed to lock the impact plunger, and the rebound value indicated by the pointer on the scale is recorded. In the NR and LR models of the device, the rebound value R is automatically printed on recording paper, requiring only that the impact plunger be locked after the final impact. Test hammer is pushed against the test surface at a moderate speed until the impact is triggered.

Figure 3.6: Preparing test surface (RHT "Proceq" manufacturer manual; Fewtrell, 1993)

The push button is pressed to lock the impact plunger after each impact, and the rebound value indicated by the pointer on the scale is then read and recorded. In the NR and LR models of the device, the rebound value R is automatically printed on the recording paper. It is only required to lock the impact plunger using the push button after the final impact.

1) Impact plunger
4) Pointer
6) Push-button

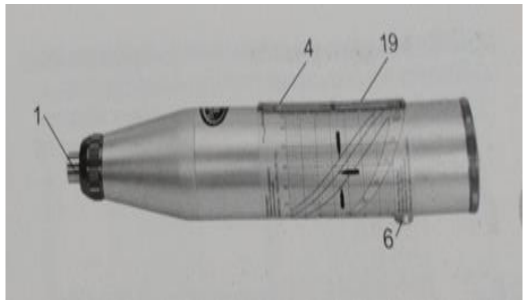

Figure 3.7: Reading the test result from the scale and calibration chart on models N and L (RHT "Proceq" manufacturer manual; Fewtrell, 1993)

3.3.3 Output and Evaluation of Data

3.3.2.1 Output

The rebound value R is displayed by the pointer on the scale of the device. The R value is read and noted down in a manual record entry.

3.3.3.2 Evaluation of Output

Average rebound values R of the 8-10 has to be measured for each test with rebound hammer. Values that are too high or too low (the lowest and highest values) are not included in calculation of average value. Using a conversion curve appropriate for the selected body shape (Models N and L, Proceq), the average rebound value R_m is used on the selected conversion curve to read off the average compressive strength. The average compressive strength is subject to a dispersion (± 4.5 N/mm^2 to ±8 N/mm^2).

3.3.3.3 Median Value

As per Standard BS EN 12504-2:2001 "Test Results", the median value is specified instead of the classic mean value. All measured value must be considered at the time of using this method (no outliers allowed).

For an odd number of impacts, the measured values are arranged in ascending order, and the middle value is taken as the median. For an even number of impacts, the median is calculated as the mean of the two middle values. If more than 20% of the values are spaced more than 6 units apart, the entire measurement series must be rejected, as specified in the standard (Bungey and Mandandoust, 1994).

3.3.3.4 Derivation of the Conversion Curves

The impact value measured by the rebound hammer is represented as the rebound number R, which is plotted on the X-axis of the graph. This value must be converted into the compressive strength of concrete (MPa), which is shown on the Y-axis. The median values are calculated from 10 or more rebound hammer impact values obtained during testing.

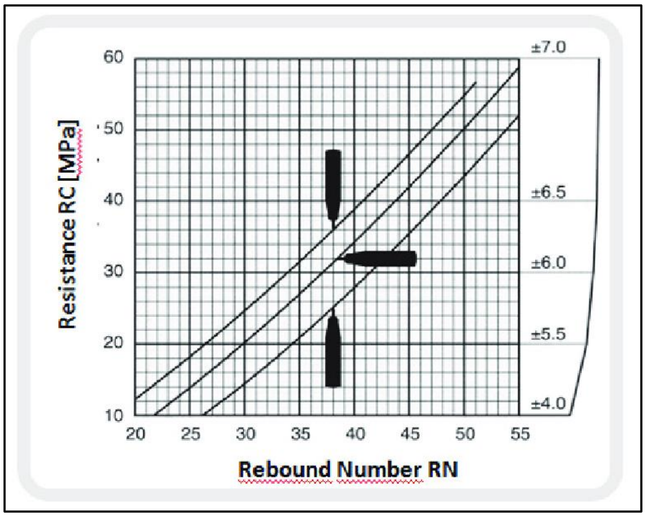

Figure 3.8: Conversion curve for rebound value to compressive strength (RHT "Proceq" manufacturer manual; Fewtrell, 1993)

3.3.3.5 Validity of the Conversion Curves

The conversion curves are valid for any test samples that are made from standard concrete using Portland or blast furnace slag cement with sand gravel (maximum particle size dia. ≤32mm) provided the tests are done on smooth, dry surface aged 14-56 days. The conversion curve is practically independent of the:

a) Cement content of the concrete

b) Particle gradation

c) Diameter of the largest particle in the fine gravel

d) Water/cement ratio.

3.4 Pushover Analysis to Estimate Capacity and Structural Deformations

Pushover analysis is a widely utilized method for assessing the seismic capacity of existing structures, and it features prominently in various recent guidelines for retrofit seismic design. This study employs a static 3-D pushover analysis through a simplified nonlinear technique to estimate seismic deformations in structures. The pushover analysis mimics seismic loading by incrementally applying lateral forces until the weakest link in the structure is identified. Once this weak link is determined, the model is adjusted to reflect the structural changes resulting from this failure. A subsequent iteration of the analysis reveals how loads are redistributed, allowing the structure to be “pushed” again until another weak link is found. This iterative process continues until a comprehensive yield pattern for the entire structure under seismic loading is established. (Khan, 2013).

In procedure of pushover analysis, the capacity curve is obtained by performing a series of three dimensional static analyses on the building when; V$\{f\}$ is applied forces at the center of mass (CM) of the floor building represents as the base shear and $\{f\}$ is the normalized load vector. V-Δrelation obtained from the static analyses of capacity curve where Δ is the CM displacement at the roof. Since the center of mass (CM) of the floors may not align with the centers of rigidity (CR) of the floors, the roof displacement at the CM will reflect both translational and torsional deformations of the building when subjected to seismic lateral loading. The capacity curve has an initial linear range with a slope k and can be expressed in the form V= k x G (Δ) where G (Δ) is a function describing shape of the capacity curve. An equivalent single degree of freedom (SDOF) system can be created to determine target displacement as outlined below; So the equation of motion for an N-story building subjected to horizontal ground motion Üg and in one direction (y-direction) is written as,

$$\begin{bmatrix} [mx] & [0] & [0] \\ [0] & [my] & [0] \\ [0] & [0] & [Im] \end{bmatrix}\{\text{ii}\}+\{R\} = -\begin{bmatrix} [mx] & [0] & [0] \\ [0] & [my] & [0] \\ [0] & [0] & [Im] \end{bmatrix}\ddot{U}(t) \text{ ……………….…………..Eq. 3.2}$$

in which[mx], [my] and [Im]: the mass matrix in x and y-direction and mass moment of inertia matrix about CM (center of mass)

{u}= col ({ ux},{uy} and { θ }),

{ux},{ uy}: x and y-direction displacement vector referred to the CM of the floors.

{ θ }: the floor rotation vector

{R}: the restoring force vector.

Assuming a single-mode response, the displacement vector { u } can be written as

$$\{u\}=\begin{Bmatrix}\{\Phi x\}\\ \{\Phi y\}\\ \{\Phi\theta\}\end{Bmatrix}\Delta t=\{\Phi\}\Delta t \text{……………………………………………………….….Eq. 3.3}$$

where Δ (t) is the generalized coordinate, representing the CM roof displacement, and {φ} is an assumed deformation profile for the building. Further, the restoring force vector {R} is approximately represented by the y-direction pushover analysis and is written as

$$\{R\}= k x G\ (\Delta)\begin{Bmatrix}\{0\}\\ \{f\}\\ \{0\}\end{Bmatrix} \text{………………………………………………………….…..Eq. 3.4}$$

Using relations of Eq. 3.3 and 3.4, the equation of motion for the generalized coordinate Δ (t) can be obtained from Eq. (3.2) as

$$m^*\ddot{\Delta} + k^* G\ \ddot{\Delta}= -L^*\ddot{u}_g(t) \text{ ………………………………...……………………….…..Eq. 3.5}$$

where m*= generalized mass $= \{\Phi\}T\begin{bmatrix}[mx] & [0] & [0]\\ [0] & [my] & [0]\\ [0] & [0] & [Im]\end{bmatrix}\{\Phi\}$

k* = generalized stiffness $=k\{\Phi\}T\begin{bmatrix}\{0\}\\ \{f\}\\ \{0\}\end{bmatrix}$

L*= generalized earthquake excitation factor $=\{\Phi\}T\begin{bmatrix}[mx] & [0] & [0]\\ [0] & [my] & [0]\\ [0] & [0] & [Im]\end{bmatrix}\begin{bmatrix}\{0\}\\ \{I\}\\ \{0\}\end{bmatrix}$

The effect of damping is introduced directly at this stage as a viscous damping term, c* x $\dot{\Delta}$, in which c* = 2ξω m, $(\omega^*)^2$ k* / m *, and ξ = damping ratio; leading to final equation.

$$M^*\ddot{\Delta}+c^*\dot{\Delta}+k^*G(\Delta)= -L^*\ddot{u}_g\Delta\ (t) \text{ ……………………………………….……………..…..Eq. 3.6}$$

For a given excitation $\ddot{u}_g$, the solution of Eq. 3.6 is obtained using a step-by-step integration implemented in successive pushover analysis procedure and the absolute maximum of Δ(t), denoted by Δ_{max} is a predictor of the maximum CM displacement at the roof of the structure. The deformation and damage on elements near the flexible edge of the building is taken as indicative of the deformation and damage of these elements in the building when the building is subjected to earthquake ground shaking (Moghadam and Tso, 2000).

Chapter 4
Results and Discussion

4.1 Results and Discussion on Rebound Hammer Test on RC Structure

Since concrete is one of the two constituent elements of an RC structure, one of the major objectives of the work is to establish the results of RHT for concrete strength as a useful indicator of current structural health conditions. Therefore, the following reported results and discussions establish the basis or the necessity of this non-destructive RHT test for structural health monitoring. The accuracy of RHT results as indicator of concrete strength is also verified within the scope of the work.

4.1.1 Visual Screening of an Aging RC Structure

Damage prognosis for any RC building begins with visual observation, commonly referred to as visual screening, and has been conducted on an aging RC structure located at Halishahar region of Chattogram. This building has been in service for nearly 40 years as one of the Railway Training Academy Hostels in Halishahar, Chattogram. The RC structure was chosen for a thorough evaluation using visual screening procedure according to ACI-201.1R-08 (ACI Committee Report 201, 2008) and its prescribed checklist format suggested in "Guide for Conducting a Visual Inspection of Concrete in Service". The ACI committee describes the inspection to be done in four stages as follows:

i) General
ii) Nature of environmental and loading conditions
iii) Distress indicators or distress mapping and
iv) Present condition of the structure

4.1.1.1 General

The visual screening stages involve gathering structural descriptions and material information from preserved drawing documents, including sketch maps and general as well as detailed photographs taken during inspections. The visual inspection checklist of data included in the Appendix-2 indicates that the building was constructed in 1983 and consists of a four-story RC column-beam framed structure. The foundation of the inspected building features isolated footings on improved soil, supported by wooden piles. Documentation preserved by stakeholders reveals that the concrete utilized 20 mm downgraded stone chips and sand with a fineness modulus (FM) of 2.54. The mix ratio for the concrete materials is specified as 1:1.5:3.

Measurements of the building's length, width, and dimensions, along with the sizes and shapes of structural members and frame types, indicate that the design does not comply with current building codes or even the regulations of BNBC 2006. The physical properties of structural materials, such as aggregates and cement, are at standard levels; however, the mechanical and chemical properties of construction materials are not documented in the preserved stakeholder records. Observations from the inspection also reveal that the selected building is in a state of poor maintenance over the last two decades.

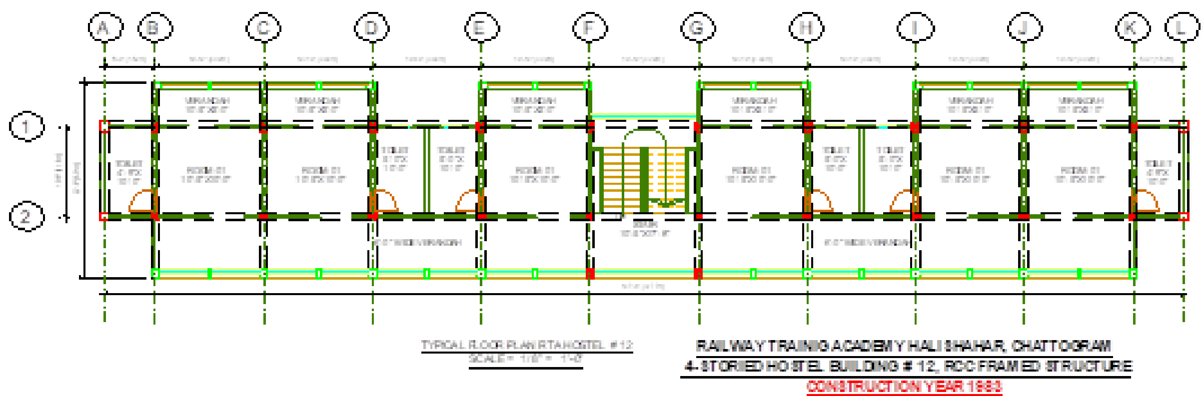

Figure 4.1: Floor plan of selected RC building structure

The sketch map (Figure 4.1) illustrates that the building is framed in the X direction with 12 grids of columns, resulting in a total length of 32.97 meters. In the Y direction, there are only two grids of columns, with a total length of 6.91 meters. Both sides of the Y direction feature heavy overhanging beams and slabs. These heavy overhanging beam slabs present a significant vulnerability to earthquake damage within the structure (CDMP Report, 2009).

4.1.1.2 Nature of Environmental and Loading Conditions

In this section, an inspection of the RC structure is conducted to assess exposure conditions, drainage conditions, loading conditions, and soil or foundation types. The report form attached in Appendix-2 indicates that the building is located in the coastal belt area of Chattogram City Corporation. It has been reported that the structure is exposed to chloride corrosion as well as other factors such as intermittent effects of abrasion, erosion and cavitation impact. The selected building is situated in the Tropic of Cancer, with a recorded average annual rainfall of 200mm.The loading conditions affecting the building include dead loads, live loads, seismic loads and wind loads. The foundation type employed is isolated footings supported by wooden piles on improved soil. However, in the context of harsh environmental loading conditions such as seismic loads, the use of wooden piles is not considered a logical choice in structural design practice. The building's drainage system consists of surface drains operating by gravity flow.

4.1.1.3 Distress of Structure

Distress findings are crucial in the visual screening of RC structures, as they provide insight into the actual damage prognosis of the structure. According to the ACI 201.01-08R checklist, key observations include cracking, staining, surface deposits, exudations and leaking. In the inspected building, three slab hairline cracks, several shear cracks in beams, two cracks in bending zones, and two column cracks were noted. Staining was observed on the rooftop staircase column; however, all structural elements were covered with cement plaster, making it difficult to assess the extent of staining or its prognosis. Additionally, water leakage was detected at the top of the roof slab. Figures 4.2 and 4.3 illustrate the structural distress conditions, highlighting numerous cracks on the surfaces of various structural elements.

Figure 4.2: Cracks seen in RC floor slab bottom

Figure 4.3: Cracks seen in column concrete of the structure

4.1.1.4 Present Condition of the Structure

Upon visual screening inspection of the selected RC structure, the following observations regarding its present condition were noted.

Overall apparent alignment of structure: No settlement, deflection, expansion, and contractions are seen at the time of visual screening inspection of the selected RC structure.

Surface condition of concrete: In general, surface condition of the inspected building is poor having unsmooth with bug holes and few-point staining (Relevant data ACI201.01-8R checklist is shown in Appendix- 2). According to maintenance records, the building has been in service during the last decade with little or no maintenance measures.

Figure 4.4: Spalling and leaching shown in beam and floor slab concrete with corrosion of rebar

As a result, the building is experiencing significant and aggressive damage. Cracking has been observed in various structural elements, including slabs, beams and columns at multiple locations. The selected RC structure exhibits extensive spall at numerous points on the slabs, beams and lintels. The size of the concrete spall ranges from 2 inches by 2 inches to 2 feet by 1 foot. Additionally, corrosion of the mild steel (MS) rods embedded in concrete has been noted on almost every floor of the building, as illustrated in Figure 4.4.

Figure 4.5: Distresses shown in beam and floor slab concrete outside of the structure

Figure 4.6: Weather damp shown in slab, wall, and beam concrete of the structure

The distress features in the aging RC structure are closely linked to exposure of the structure from the following

- Aggressive environmental loading conditions such as salinity intrusion or sulphate attack considering the specific location of the structure near the coastal and industrial zone.
- The exposure of structure from several low to moderate earthquake events during the last three decades.
- The deterioration of steel strength through unrepaired cracks or openings to steel bars.

The selected building has suffered physical deterioration of concrete revealed in various forms of distress including cracks, spalls, staining and corrosions of reinforcement. Common locations of concrete damage or distress are seen to be in the mid zone of slabs and beams, column bottom zone. Cracks are seen to appear in 10 slabs, 5 beams and 2 columns along with staining and leaking across openings of cracks. Additionally, 62 concrete surfaces show signs of severe spalling with corroded reinforcement. Staining of concrete are seen to appear at rooftop stair columns and leaking of concrete found at beam and slab outside of the selected building.

The identified issues underscore the necessity for comprehensive maintenance and repair measures to address the observed distress indicators and to ensure the structural integrity and safety of the RC building. Therefore, the findings from this visual assessment is indicative of required detailed evaluation of concrete's residual strength and steel strength in order to assess building's current overall capacity to withstand environmental and overload conditions. Without timely intervention, these existing problems may exacerbate posing significant risks to both occupants and the long-term stability of the structure.

4.1.2 Rebound Hammer Test on Selected RC Structures

The visual screening data provides a preliminary idea of the likely damage intensity of the aged RC structure that it may experience when subjected to accidental overload conditions such as that may act on the structure during an earthquake. Considering the indicative findings of the distress conditions of the building according to ACI-201.1R-08 checklist, a non-destructive RHT test was done on assess current in-situ strength of concrete in several structural elements of the building. Based on visual screening, a drawing was prepared to execute planned RHT tests on the selected RC building. The RHT measurement of in-situ strength of concrete were taken at different locations of randomly selected RC structural elements of the building. Test locations of the hammer test were chosen avoiding spalled, cracked and damped surfaces. The following Tables 4.1-4.8 present data of RHT measurements of concrete strength at different locations or structural elements of the building, where the element IDs are given according to the floor plan of the building shown in Figure 1. Figure 4.7 presents a summary of concrete strength results determined by RHT.

Table 4.1: Results of rebound test on selected building at Ground floor column

Sl	Structural elements and locations	Column size	Design strength of concrete	Cylinder strength of concrete	RHT Rebound no R	Direction of Rebound	Concrete strength (f'_c) from chart	Remark (average strength, f_c)
		cm x cm	MPa	MPa	Nos		N/mm^2	MPa
1	B/1 C1	25x30			25		14	
2	B/2 C2	25x30			25		14	
3	E/1 C3	25x30			25		14	
4	E/2 C4	25x30			29		19	
5	H/1 C6	25x30	20		28		18	17.5
6	H/2 C7	25x30			29		19	
7	K/1 C9	25x30			32		23	
8	K/2 C8	25x30			29		19	

Table 4.2: Results of rebound test on selected building at Ground floor beam

Sl.	Structural elements and locations	Beam size	Design strength of concrete	Cylinder strength of concrete	RHT Rebound no R	Direction of Rebound	Concrete strength (f'_c) from chart	Remark (average strength, f_c)
		cm x cm	MPa	MPa	Nos		N/mm^2	MPa
1	B/1-2	25x45			34		20	
2	E/1-2	25x45	20		33		18	17
3	H/1-2	25x45			31		16	
4	K/1-2	25x45			29		14	

Table 4.3: Results of RHT test on selected building at 1st floor column

Sl.	Structural elements and locations	Column size	Design strength of concrete	Cylinder strength of concrete	RHT Rebound no R	Direction of Rebound	Concrete strength (f'_c) from chart	Remark (average strength, f_c)
		cm x cm	MPa	MPa	Nos		N/mm^2	MPa
1	B/1 C1	25x30			27		17	
2	B/2 C2	25x30			26		15	
3	E/1 C3	25x30			29		19	
4	E/2 C4	25x30			29		19	18.5
5	H/1 C6	25x30	20		32		22	
6	H/2 C7	25x30			30		20	
7	K/1 C9	25x30			27		17	
8	K/2 C8	25x30			29		19	

Table 4.4: Results of rebound test on selected building 1st floor beam

Sl.	Structural elements and locations	Beam size	Design strength of concrete	Cylinder strength of concrete	RHT Rebound no R	Direction of Rebound	Concrete strength (f'_c) from chart	Remark (average strength, f_c)
		cm x cm	MPa	MPa	Nos		N/mm^2	MPa
1	B/1-2	25x45	20		31	↑	16	17
2	E/1-2	25x45			29		14	
3	H/1-2	25x45			34		20	
4	K/1-2	25x45			33		18	

Table 4.5: Results of rebound test on selected building 2nd floor column

Sl.	Structural elements and locations	Column size	Design strength of concrete	Cylinder strength of concrete	RHT Rebound no R	Direction of Rebound	Concrete strength (f'_c) from chart	Remark (average strength, f_c)
		cm x cm	MPa	MPa	Nos		N/mm^2	MPa
1	B/1 C1	25x30	20		27	→	17	17.4
2	B/2 C2	25x30			28		18	
3	E/1 C3	25x30			28		18	
4	E/2 C4	25x30			23		12	
5	H/1 C6	25x30			29		19	
6	H/2 C7	25x30			27		17	
7	K/1 C9	25x30			26		15	
8	K/2 C8	25x30			32		23	

Table 4.6: Results of rebound test on selected building 2nd floor beam

Sl.	Structural elements and locations	Beam size	Design strength of concrete	Cylinder strength of concrete	RHT Rebound no R	Direction of Rebound	Concrete strength (f'_c) from chart	Remark (average strength, f_c)
		cm x cm	MPa	MPa	Nos		N/mm^2	MPa
1	B/1-2	25x45	20		31	↑	16	17
2	E/1-2	25x45			33		18	
3	H/1-2	25x45			31		16	
4	K/1-2	25x45			33		18	

Table 4.7: Results of rebound test on selected building 3rd floor column

Sl.	Structural elements and locations	Column size	Design strength of concrete	Cylinder strength of concrete	RHT Rebound no R	Direction of Rebound	Concrete strength (f'_c) from chart	Remark (average strength, f_c)
		cm x cm	MPa	MPa	Nos		N/mm^2	MPa
1	B/1 C1	25x30	20		34		26	18.1
2	B/2 C2	25x30			25		14	
3	E/1 C3	25x30			30		20	
4	E/2 C4	25x30			25		14	
5	H/1 C6	25x30			30		20	
6	H/2 C7	25x30			29		19	
7	K/1 C9	25x30			25		14	
8	K/2 C8	25x30			28		18	

Table 4.8: Results of rebound test on selected building 3rd floor beam

Sl.	Structural elements and locations	Beam size	Design strength of concrete	Cylinder strength of concrete	RHT Rebound no R	Direction of Rebound	Concrete strength (f'_c) from chart	Remark (average strength, f_c)
		cm x cm	MPa	MPa	Nos		N/mm^2	MPa
1	B/1-2	25x45	20		32		17	16.5
2	E/1-2	25x45			31		16	
3	H/1-2	25x45			31		16	
4	K/1-2	25x45			32		17	

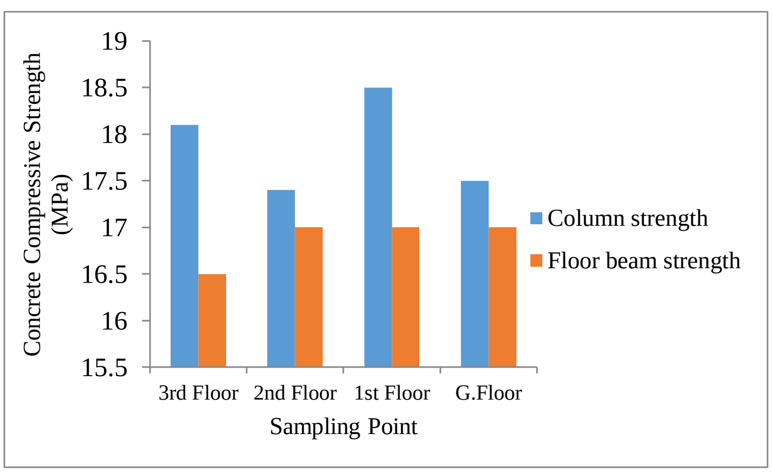

Figure 4.7: Average concrete strength of columns and beams of selected RC building

As determined from the calibration chart based on RHT test records, the selected 4-story hostel building of Halisahar Chattogram has variable strengths of concrete in different structural members. Since no baseline data was available for comparison, a baseline strength of 20 MPa is approximated as a benchmark strength of concrete in beams and columns considering design for static dead load and live load of the building. However, design considering wind force and earthquake forces would require a minimum of 25 MPa strength of RC members. Only a few concrete strength data are found to be nearly equal or above the baseline strength of concrete. However, the average concrete strength in many of the structural members (Figure 4.7) is not within the expected strengths of concrete and the results do not comply well according to time variation law of concrete strength.

The findings of RHT tests are also showing wide range of deterioration in concrete of columns, beams and slabs. Visual screening indicators of distress of concrete comply well with RHT results. Average concrete strength in different structural members of the selected aging structures was found to be well below (approximately 13% below) the baseline strength and the reduction of strength in an individual member is found to be even 35% less than the baseline strength. The results are generally indicative of the fact that the state of concrete of the aging RC structure has reached in a state where the building is no longer capable of sustaining extreme loading conditions or excessive overload situation such as those originating from earthquake or other extreme environmental loading conditions. The current state of the building is sustaining only the gravity loads as it would sustain with residual strength at the last zone of its capacity curve.

4.1.2.1 Evaluation of the Results of Concrete Strengths Determined by RHT Test

The visual screening of the selected building reveals numerous signs of concrete deterioration due to various types of cracks, spalling, and corrosion of reinforcement. These distress features in the aging RC structure are closely linked to the deterioration of steel strength, which can lead to further degradation of the concrete in addition to the natural deterioration of concrete strength due to its aging process. The results of concrete strengths determined by RHT tests represent an average loss up to 13% strength with respect to assumed design strength of concrete of 20 MPa. If the building was properly maintained for visually observed distress features of severe environmental or extreme loading conditions, its concrete strength would not have reduced within forty years of its life span. Since the aging reinforced concrete structure evaluated under the scope of the study has suffered several phenomena of distress in different structural members, it could have progressive degradation of the concrete strength due to secondary effects of distress other than natural aging process.

Consistent results of concrete strength at or near uncracked sections of different structural members has shown little or no degradation. Consistent results of concrete strengths determined by RHT test have been recorded at suitable points or locations of different structural members respectively for a typical beam and slab section as shown in Figures 4.8 and 4.9. For beam elements, the points of consistent results of strengths are mostly concentrated within the section of tied arch action of the beam (Figure 4.8). For a slab section, the points of consistent results are mostly found within *L*/4 (from slab periphery) section of the span as shown in Figure 4.9. It is observed that points having reinforcement inside a section behind them show anomalous results of strength. Therefore, it is important to do scanning by rebar scanning equipment to avoid those locations for an RHT test.

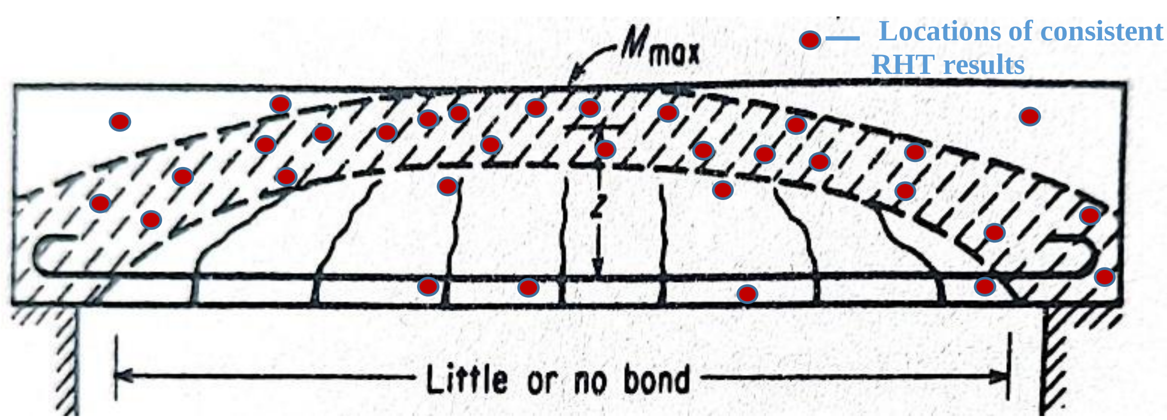

Figure 4.8: Points of consistent RHT results within tied-arch zone of beam

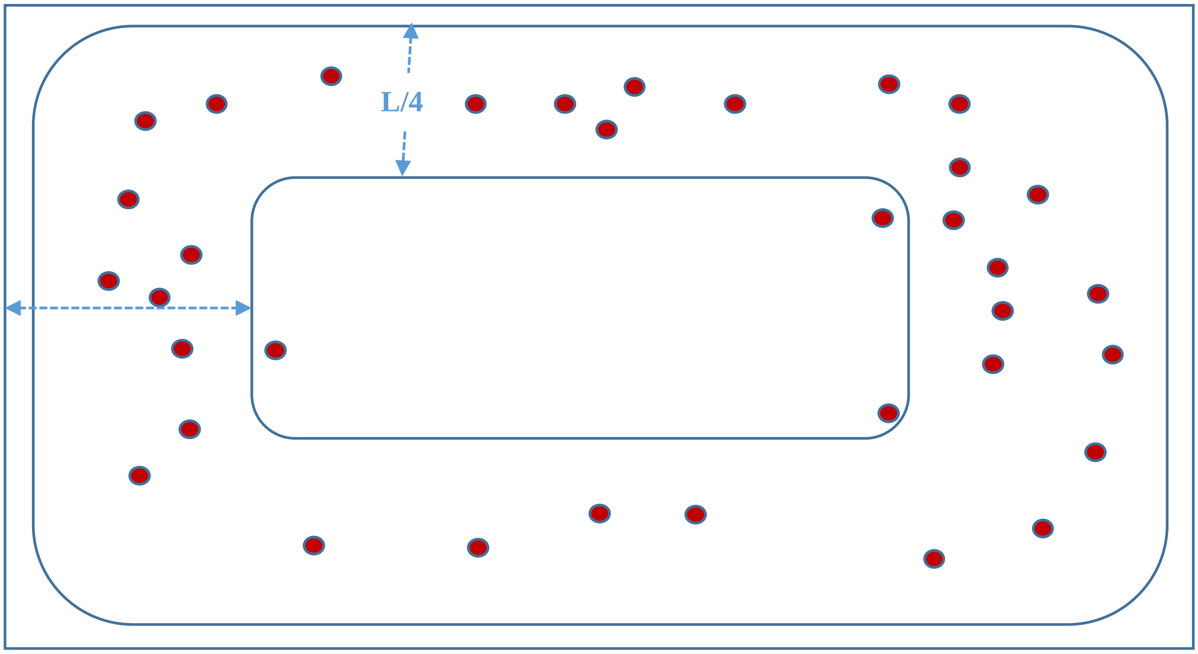

Figure 4.9: Points of consistent RHT results within a slab section

4.1.3 Calibration of RHT Result by Different Field and Laboratory Test of Concrete

The in-situ strength of RC structural elements are commonly determined by non-destructive RHT tests. Relevant RHT calibration charts are used to covert surface hardness data to a reference data of cylinder or cube strength of concrete. The Schmidt RHT equipment used for this study has a calibration chart using which the recorded RHT data can be converted to cube or cylinder strength of concrete. This method of indirect measurement of concrete strength is primarily developed based on comparative analysis of results of laboratory scale concrete elements and cylinder/cube strength. The conversion curves are valid for any test samples that are made from standard concrete using Portland or blast furnace slag cement with sand gravel (maximum particle size dia. ≤32mm) provided the tests are done on smooth, dry surface aged 14-56 days (Fewtrell, 1993). The reference RC samples used for developing the calibration chart may not also be representative of the field exposure conditions of practical RC structural elements and also for their variable aging conditions. Therefore, the strength of concrete converted from in-situ test of rebound data may not always be used as a reliable reference of in-situ strength of concrete.

In this regard, one of the major objective of this study was to perform a verification of RHT results through recalibration of RHT data. This component of the work is particularly aimed at developing a reliable basis of using Schmidt RHT test data for practical purposes of verifying in-situ strength of concrete in RC structural elements. In the process of recalibration, RHT tests were first conducted on randomly chosen structural members of two different RC structures for which reference strength of concrete could be compared with the audit records of strength of those structural members. RHT test results of several members were also verified with results of other destructive and non-destructive test results such as those of core cut tests, ultrasonic pulse velocity tests etc. In this connection, the following sequential steps were implemented in the study.

i) Conversion concrete cube strength to cylinder strength data (f'_c, characteristic compressive strength of concrete).
ii) Validation of RHT results of strength data in comparison with design strength data and with primary audit records of cylinder strength data during the time of casting.
iii) If baseline data is unavailable or unsatisfactory, conduct destructive test methods such as core cut tests or other alternatives such as ultrasonic pulse velocity tests.
iv) Further calibration of RHT results to develop a reliable basis of using them with reference to strength test results of laboratory scale RC beam specimens.

Three laboratory scale beam specimens are also cast, properly cured and left exposed to natural environmental conditions resembling that of practical field conditions of RC elements. A comparative analysis of time variable strengths of concrete is aimed for the beam specimens cast with concrete mixes of two reference strengths, 20 MPa and 22 MPa. Periodic measurements of RHT data are taken and respective records of time-variable strengths of cylinders are also determined by laboratory tests. A comparative analysis of two simultaneous records of strengths has been done for eight months duration after casting the beams.

4.1.3.1 Verification of RHT Test Data of a Building at Nasirabad I/A, Chattogram

One of the two buildings investigated for the recalibration procedure was a newly constructed 8-storied industrial building located Nasirabad Heavy Industrial Area Chattogram. The building was constructed 2 years ago, concrete strength data (cylinder and cube strength) were available for comparison. The building was designed considering average design strength of concrete of 30 MPa. However, primary audit records of design strength and in-situ strengths are used as references for comparison with RHT results of strengths. An effective calibration of the field test data is also aimed in relation to other secondary methods of evaluation that has been done for assessment of concrete strength. In addition to the RHT tests done on randomly selected structural elements of the building, further testing was conducted through core cut samples taken on selected elements. Two numbers core cut samples were taken from the 7th-floor roof and tested at laboratory. A comparative evaluation of RHT results and core cut strength results are presented in Tables 4.9-4.10 and Figure 4.10 below.

Table 4.9: Core cutting test data of an industrial building

Core cutting concrete test data									
Specimen age 2 years (as per age of the building)									
Sl.	Speci mens No.	Structural elements & locations	Diameter (d) of sample core	Height of sample	Weight of sample	Observe load (x)	Calibrated load (y)	Crushing strength (f_{cr})	Compressive strength (f'_c)
			cm	cm	gm	kN	kN	N/mm^2	N/mm^2
1	S1/7	Slab 7thfl.	6.50	12.9	940.0	85.0	87.69	25.9	20.9
2	S2/7	Slab 7thfl.	6.50	12.9	940.0	112.5	112.46	33.22	28.2

Table 4.10: Rebound test data of an industrial building on slab (near core cutting location)

Sl.	Structural elements and locations	Size or thickness (cm)	Design strength of concrete MPa	strength of concrete (audit record) MPa	RHT Rebound no, R	Direction of Rebound test	Compressive strength from RHT calibration chart (N/mm^2)
1	S1/7	20.00	28	35	36.00		33.0
2	S2/7	20.00	28	45	37.00		34.0

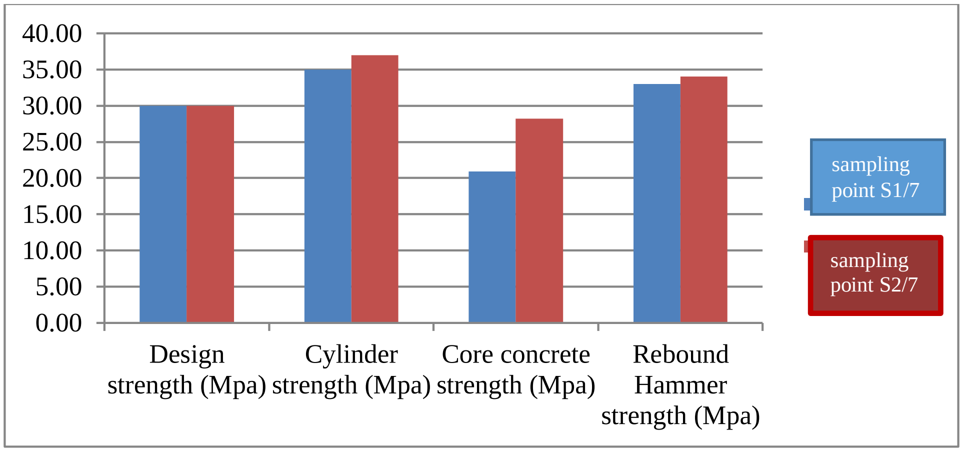

Figure 4.10: Comparison of compressive strength of concrete in an industrial building of Chattogram (Core cutting sample test results versus RHT results)

The respected compressive strength of the concrete test result of two core cut concrete samples were determined as 20.9 and 28.2 MPa from the laboratory test results. The Schmidt RHT test was conducted near the same location of the core cult points and the respective strengths were found as 33 MPa and 34 MPa. In this structure, concrete design strength, core cutting sample and rebound hammer test strengths show significant difference among them. The comparison of RHT and core cut results indicate that the core cut strength results is generally less than the indicative strength data of concrete found from the RHT results. This may be due to the fact that core cut samples are disturbed samples. This is indicative that the non-destructive RHT results may be taken as reliable indicator of concrete strength. The (cylinder) strength of concrete used at the test locations, as per audit records, is not an authentic basis of comparison with the RHT results because of significant variations between them. A considerably higher audit records of concrete strength in comparison to the lower strengths determined by RHT tests could be due to the several conditions of distress visible in the newly constructed structure. Defective construction practices, or malpractices during sampling of cylinder specimens of concrete and during mass concreting may be a few of the possible reasons of this discrepancy between audit records and in-situ RHT strength data.

4.1.3.2 Calibration of Test Data of a Building at Kumira, Chattogram

A two storied university cafeteria building located at Kumira, Chattogram was also investigated under the scope of the study. Although the building was constructed about 15 years ago, visual observations of the building conditions suggest poor quality of concrete due to unexplainable causes. No authentic reference data was also available to compare the RHT results with the in-situ strength data of concrete. Therefore, a few core cut samples were taken to validate measurements of RHT test results, comparison of results of tests are shown in Figure 4.11 and in Tables 4.11-4.12 below.

Table 4.11: Core cutting concrete test data of structural members of a two-storied RC building

Core cutting concrete test data									
Specimens' age as per age of building: 15 years.									
Sl.	Speci mens No.	Structural elements & locations	Diameter (d) of sample core	Height of sample	Weight of sample	Observe load (x)	Calibrated load (y)	Crushing strength (f_{cr}.)	Compressive strength (f'_c)
			cm	cm	gm	kN	kN	N/mm^2	N/mm^2
1	C1	Column GF	6.70	11.4	862.0	60.00	62.92	17.49	12.5
2	C2	Column 2nd floor	6.70	11.7	879.0	55.00	57.96	16.11	11.1
3	B1	Beam GF	6.70	12.6	969.0	40.00	43.10	11.98	7.0
4	S1	Slab 1st floor	4.50	4.63	146.0	20.00	23.29	14.64	9.6

Table 4.12: Rebound test data of a two storied RC building on slab (near core cutting location)

Sl.	Structural elements & locations	Size or thickness (cm)	Design strength of concrete MPa	strength of concrete (audit record) MPa	RHT Rebound no, R	Direction of Rebound test	Compressive strength from RHT calibration chart (N/mm^2)
1	Column GF	30x45			23.00	→	12.0
2	Column 1st floor	30x45			24.00		13.0
3	L/2 Beam	30x45			22.00		11.0
4	G/2 Slab	12.50			21.00	↓	14.0

There was no authentic design strength data or audit records available for comparative assessment of RHT results with reference strength of concrete. The RHT results of concrete strength comply well with the core cut results for only one of the four core cut sampling points. Core cut results of strength of concrete is generally much lower than the RHT tests which might due to the use of low grade aggregate in concrete.

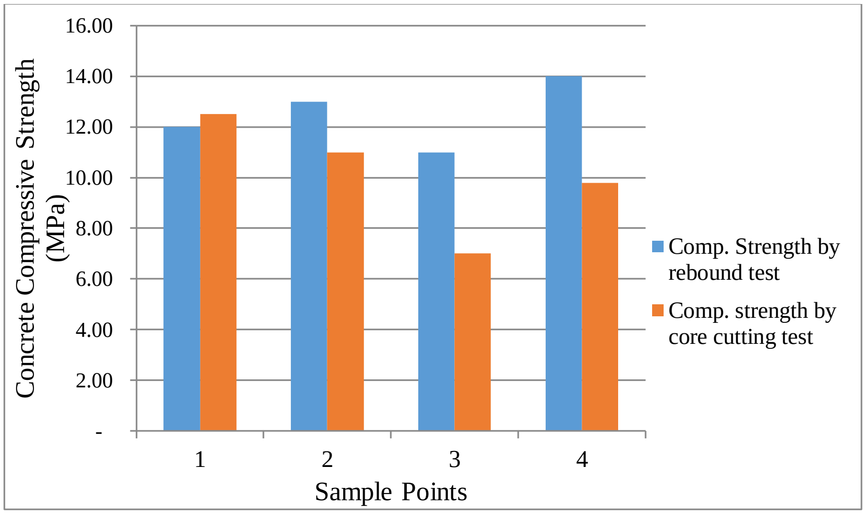

Figure 4.11: Compressive strength of concrete in the cafeteria building (Rebound hammer test vs. concrete core cutting test)

Figure 4.12: Core cut samples after crushing in CTM at laboratory

4.1.4 Laboratory Scale Beam Specimen Tests for Calibration of RHT Test Data

The RHT data of testing different structural members of the selected RC buildings do not comply well with audit records of concrete strengths or even with the results of the strength determined from core cut samples. In general, calibrating RHT data with respect to the field test results would require a conservative estimate of 15% to 20% less concrete strengths as determined from indirect measurements based on RHT data. Therefore, the RHT results of three laboratory scale beam specimens were taken for a comparative analysis of cylinder strength of concrete. Three laboratory scale RC beam specimens were constructed at laboratory conditions conforming to concrete mix design procedure in order to achieve target strengths of 22 MPa and 25 MPa. Depending on the scope of the study, the range of time variation in this case is limited to eight months and concrete mixes of the samples were done to achieve only two target strengths. Each beam was cast in two separate segments where concrete of two target strengths were poured (Figures 3.2-3.4). The beams were cast according to laboratory standards to control quality of casting as well as to avoid detrimental effects of environmental factors such as sulphate attack, temperature effect, carbonization etc. that may adversely affect concrete strength development at early ages.

The beams were cast at different times. However, the tests were performed on the beams and reference specimens at selected time intervals over a period of eight months. Standard cylinder samples of concrete were taken for testing at 7 days, 14 days, 28 days, 45 days, 3 months, 5 months and 8 months for comparison among three beam specimens. The experimental results were compiled with an average strengths calculated from the three identical test specimens. The development of strength in the concrete (cylinder) specimens are shown in Table 4.13 for the 22 MPa and 25 MPa target strengths.

Table 4.13: Variation of concrete strength of sample test cylinders with time

Concrete age Days/months (years)	Test cylinder strength (MPa) for target strength 22 MPa					Test cylinder strength (MPa) for target strength 25 MPa				
	sample 1	sample 2	sample 3	average strength	normalized strength	sample 1	sample 2	sample 3	average strength	normalized strength
7 days	15.2	15.7	15.6	15.50	0.82	15.9	16.5	15.6	16.0	0.65
14 days	19.0	18.5	18.9	18.80	0.87	23.2	21.7	21.1	21.4	0.87
28 days (0.077)	22.0	21.5	21.0	21.50	1.0	25.5	24.7	24.2	24.8	1.0
45 days (0.123)	23.0	22.0	20.4	21.80	1.01	25.9	25.0	24.4	25.1	1.01
3 months (0.25)	23.0	22.7	21.2	22.30	1.04	26.3	25.2	25.0	25.7	1.04
5 months (0.42)	23.7	23.0	21.55	22.75	1.06	26.8	26.0	25.8	26.2	1.06
8 months (0.70)	24.0	23.0	22.0	23.00	1.07	27.2	26.1	25.9	26.4	1.06

Table 4.13 shows that the compressive strengths of concrete after 8 months achieve 106% and 107% of the 28-day target strengths respectively for 22 MPa and 25 MPa specimens. Figure 4.13 and Figure 4.14 respectively show the variation of concrete strength of sample cylinders with time for two different target strength variations. The trend of variation in concrete strength indicates that the concrete strength steadily continues to increase over the period of eight months with nearly consistent variation of normalized strengths between the two concrete types. A logarithmic function fits well the variation of concrete strengths within up to 8 months age of the samples as shown in the figures, where f_1 and f_2 denotes best fit empirical equation developed based on experimental data of test results of strengths of cylinders taken for samples of target strengths 22 MPa and 25 MPa respectively. The logarithmic function of concrete strength is a time variable empirical function where t is age of concrete in years, as typically expressed in empirical functions proposed by Withey (Withey, 1961). Since, the data collected in this research are limited in regards to time or concrete strength variations, the logarithmic functions are not based on data of normalized compressive strengths. The equations for time variable strength are empirical equations and the equations differ depending on the target strengths of a concrete mix at a particular water-cement ratio and also due to the range of time variations of collecting the data.

$f_1 = 0.71\, ln\,(t) + 23.32$ .... Eq. 4.1

$f_2 = 0.78\, ln\,(t) + 26.78$ .... Eq. 4.2

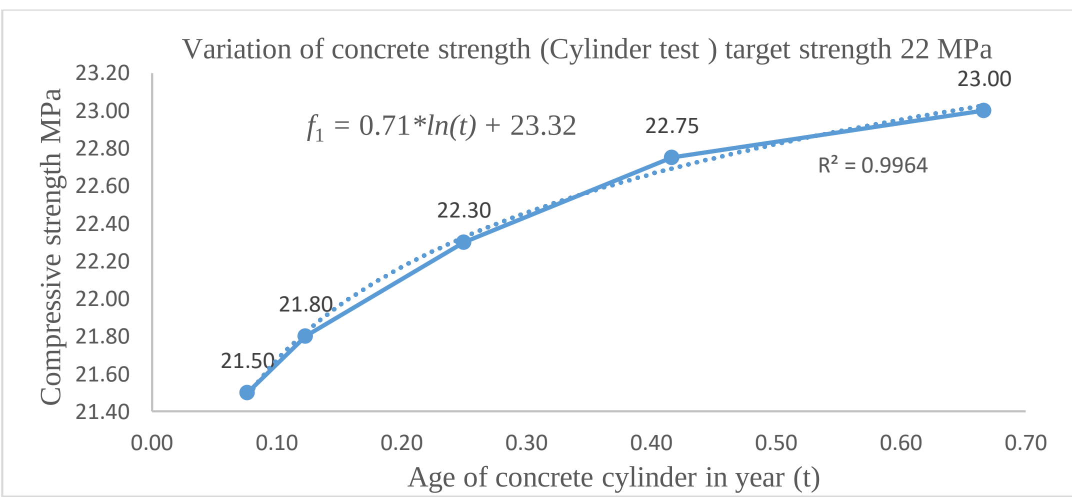

Figure 4.13: Variation of concrete strength of cylinder samples within 8 months of casting (target strength 22 MPa)

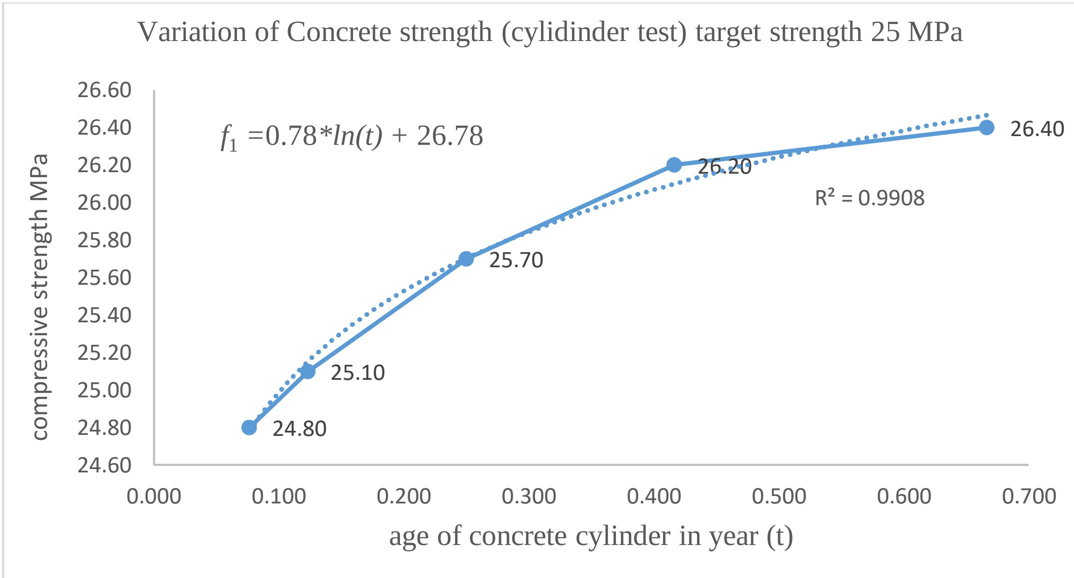

Figure 4.14: Variation of concrete strength of cylinder samples within 8 months of casting (target strength 25 MPa)

Non-destructive RHT tests were also conducted on three beam specimens at different time intervals and results are analyzed within a selected time range of eight months. The RHT test was conducted on beam samples at 28 days, 45 days, 3 months, 5 months, 6 months, 7 months and 8 months. The development of strength in the beam specimens (RHT) are shown in Table 4.14 for both 22 MPa and 25 MPa target strength. The variation RHT results of concrete strengths within eight months age of casting of beams are found to increase by about 7% and 9% respectively for beams cast for target strengths of 22 MPa and 25 MPa.

A logarithmic function fits well the variation of in-situ concrete strengths in the beams with up to eight months age of the samples as mathematically expressed by Eq. 4.3 and Eq. 4.4, where f_3 andf_4 denotes best fit empirical equations developed based on test results of strengths taken by RHT on sample beams. The logarithmic function of concrete strength is a time variable empirical function where *t* is age of concrete in years, as typically expressed in empirical functions proposed by Withey (Withey 1961).

$$f_3 = 0.74*ln\,(t) + 22.78 \quad \text{Eq. 4.3}$$

$$f_4 = 0.82*ln\,(t) + 26.33 \quad \text{Eq. 4.4}$$

Table 4.14: variation of concrete strength of sample beams with time

Concrete age Days/months (years)	RHT results of concrete strength (MPa) for target strength 22 MPa				RHT results of concrete strength (MPa) for target strength 25 MPa			
	sample 1	sample 2	sample 3	average strength	sample 1	sample 2	sample 3	average strength
28 days (0.077)	21.3	21.0	20.1	20.80	24.0	22.0	21.5	22.50
45 days (0.123)	21.5	21.4	21.0	21.30	24.5	23.0	21.5	23.00
3 months (0.25)	22.5	21.4	21.3	21.75	24.5	23.5	22.5	23.50
4 months (0.34)	22.5	22.0	21.5	22.00	25.0	24.0	23.00	24.00
5 months (0.42)	23.0	22.0	21.6	22.20	26.0	23.4	23.2	24.20
6 months (0.50)	23.3	22.0	21.6	22.30	26.2	23.5	23.5	24.40
7 months (0.58)	23.5	22.5	21.0	22.35	26.5	23.5	23.5	24.50
8 months (0.70)	23.5	22.5	21.2	22.40	26.8	23.5	23.5	24.60

Figure 4.15 and Figure 4.16 show respectively the comparison of variation of concrete strengths of sample cylinders versus the respective strengths in beams determined by RHT tests. The comparative figures of experimental data and empirical expressions (Eq. 4.1-4.4) show that the strength of concrete determined by RHT tests can be taken approximately 3% to 4% lower than the characteristic compressive strengths of concrete (f'_c) determined by cylinder tests. A prediction of probabilistic strengths by using empirical formulas of RHT results can also be made for long-term variation of concrete strength. For the two different target strengths data of this study, an indicative prediction of concrete strengths with time variation is shown in Table 4.15. Hence, the measurements of strength done by RHT can be used as a conservative estimate of the concrete strength in practical conditions of a RC structural members or specimens. Such empirical equations can be usefully applied for quality control, audit inspection, problem detection purposes or damage prognosis of aging RC structures.

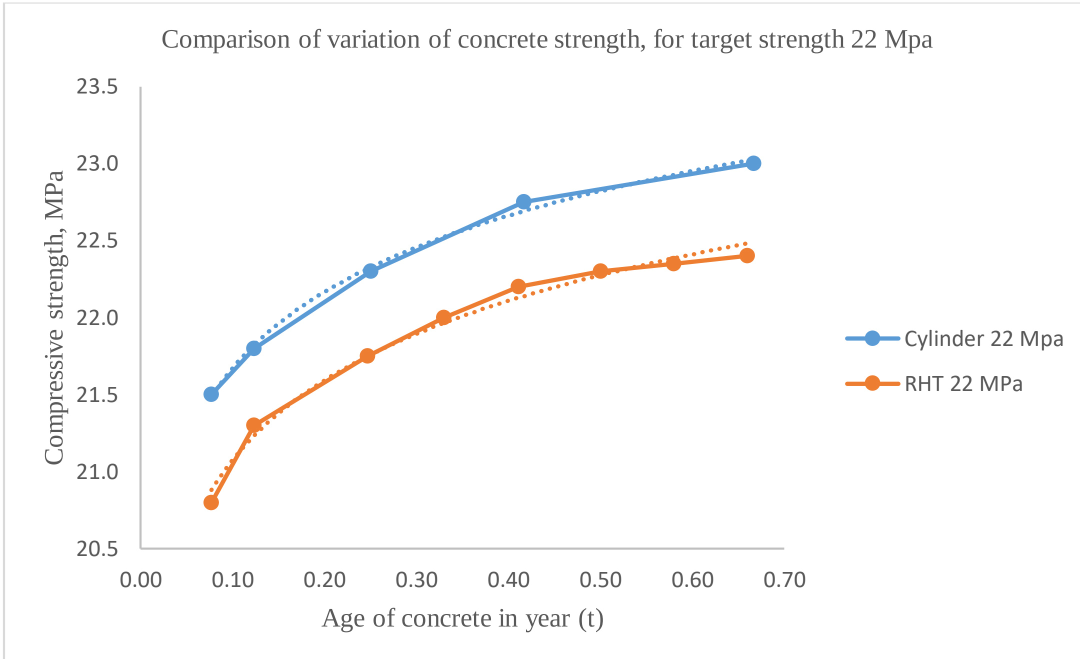

Figure 4.15: Comparison of variation of concrete strength (for target strength 22 MPa)

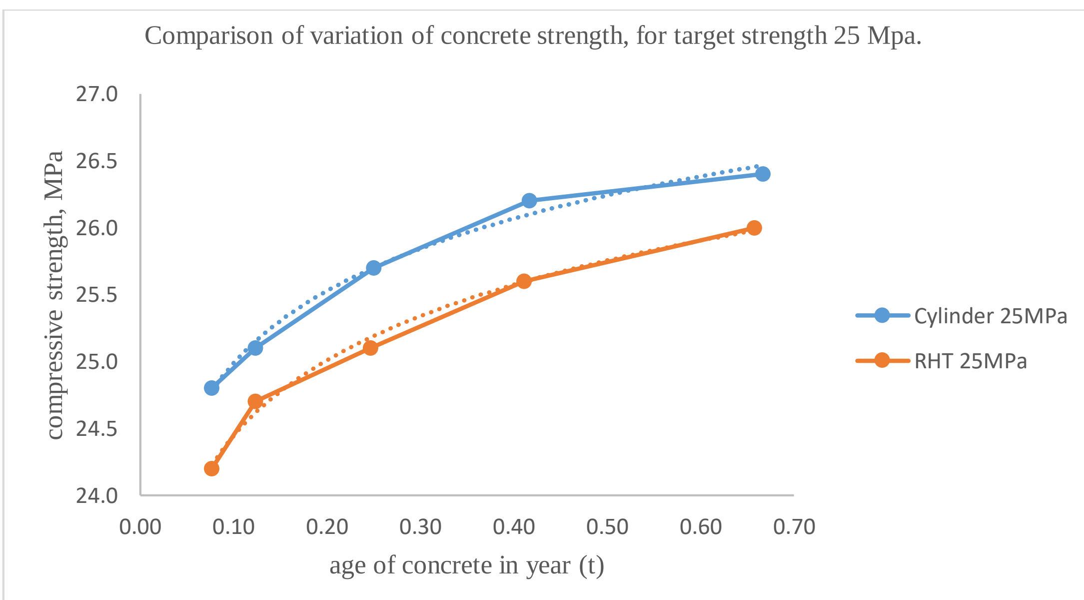

Figure 4.16: Comparison of variation of concrete strength (for target strength 25 MPa)

Table: 4.15: Prediction of concrete strengths using empirical formulas developed by RHT results

Concrete age in years (t)	RHT results of concrete strength (MPa) for target strength 22 MPa of 28 days	RHT results of concrete strength (MPa) for target strength 25 MPa of 28 days
	f_c predicted by Eq. 4.3 $f_3 = 0.74*ln\ (t) + 22.06$	f_c predicted by Eq. 4.4 $f_4 = 0.82*ln\ (t) + 26.33$
5	23.3	27.7
15	24.1	28.6
25	24.4	29.0
35	24.7	29.2
45	24.9	29.5

4.2 Evaluation of the Effects of Concrete Strength by Numerical Model Simulation

4.2.1 Structural Performance Evaluation by 3-D Pushover Analysis

4.2.1.1 Physical Modelling of an Aging RC Building Structure

The current state of strength of concrete in the selected aging RC structure of Halishahar is not good enough for modeling the structure for pushover analysis. In order to demonstrate the effect of concrete strength on the global capacity of the structure, a typical RC building was selected (plan, elevation and 3-D model views shown in Figures 4.17-4.19). The chosen building is a six-storied structure with a typical floor height of 10 feet. The beams, columns and slabs of the RC structure are modeled according to the dimensions of the structural drawings collected from the owner of the building. According to the structural drawings and design specifications, the compressive strength, modulus of elasticity, and Poisson ratio of concrete are respectively 40 MPa, 29900 MPa, and 0.2 respectively. The tensile strength and modulus of elasticity of steel are 415 MPa and 200000 MPa respectively. For structural analysis, structural modeling and analysis software ETABS (ETABS 2016) has been used. Beam and column elements of the building are modeled as frame elements; floor, roof, mat foundation, and shear wall are modeled as shell elements. The structure is modeled with concrete of two different strength variations, f'_c= 4 ksi as design strength of the structure and f'_c = 2.5 ksi, chosen random reduction of strength by 35% of the design strength.

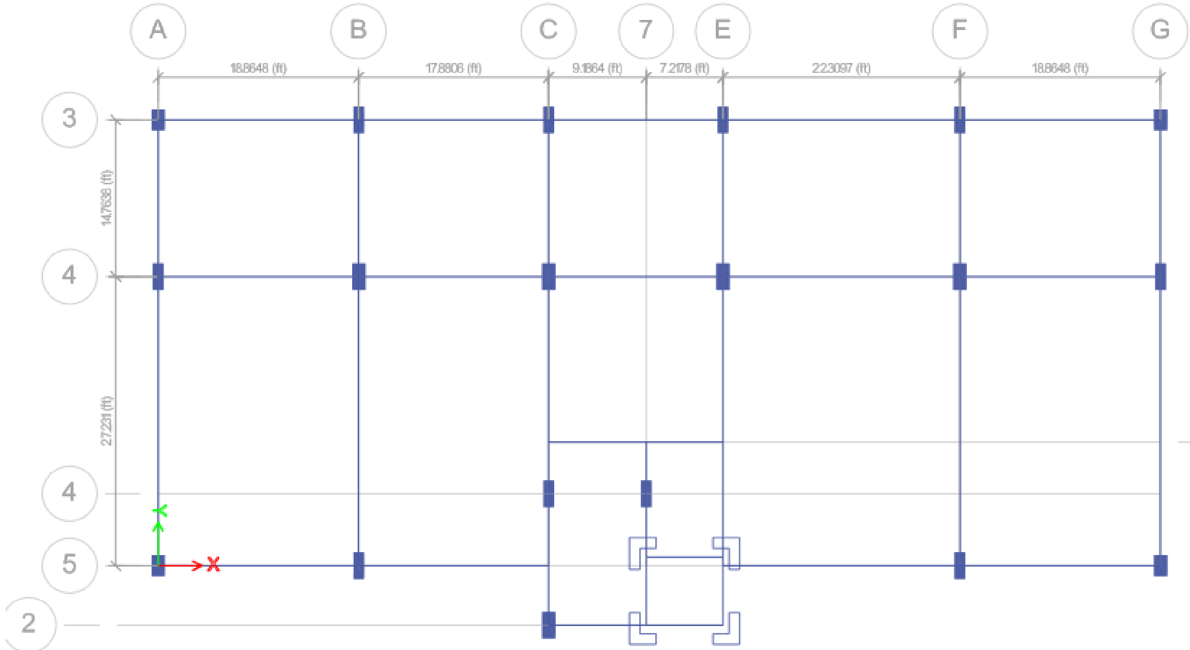

Figure 4.17: 2-D plan view of a selected RC building numerical analysis

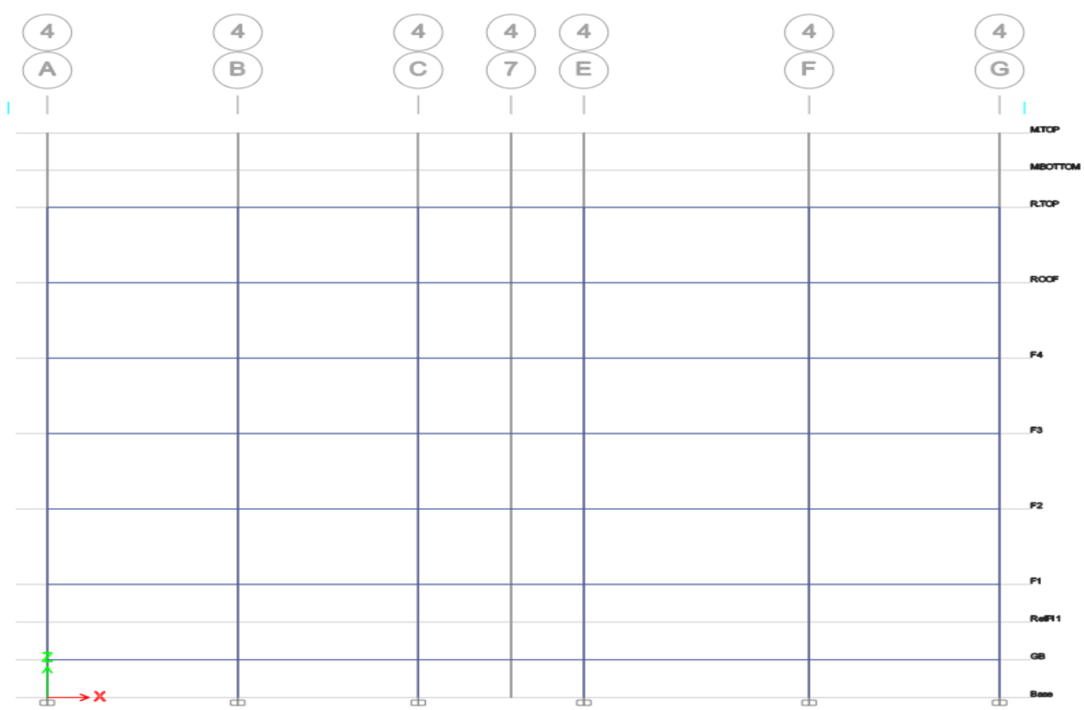

Figure 4.18: 2-D vertical elevation of the selected RC building numerical analysis

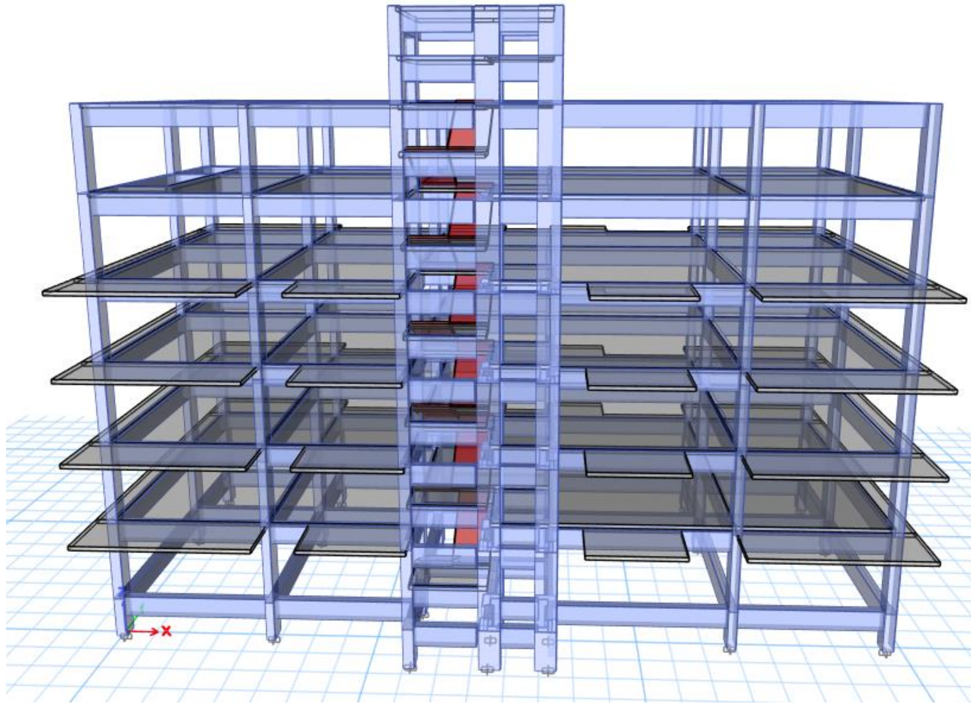

Figure 4.19: 3-D ETABS model of analyzed structure

4.2.1.2 Effect of Concrete Compressive Strength on Global Capacity of RC Structure

Figures 4.20 and 4.21 illustrate the force-deflection relationship of the chosen RC structure in X and Y-direction for randomly chosen concrete compressive strength variations of 4 ksi and 2.5 ksi. As shown in Figure 4.20 and Figure 4.21 depicting results of pushover analysis, the initial stiffness for both cases is identical which indicates that concrete compressive strength does not affect the initial stiffness and load-deflection relation. A comparative evaluation of the capacity curves in the figure for its progression up to bilinear range shows that the maximum capacity of RC structure with concrete compressive strength of 4 ksi is substantially high as compared to the same structure modeled with concrete strength 2.5 ksi. Similar behavior was observed in the Y-direction as shown in Figure 4.21. The results are generally indicative of the fact that the degradation of concrete strength of RC structures significantly affects the global capacity of structures.

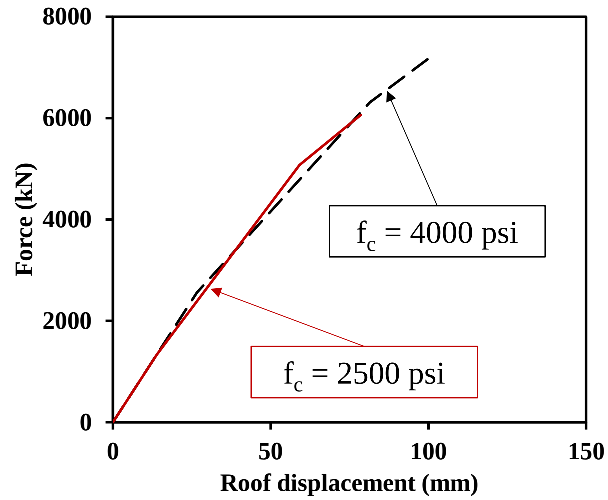

Figure 4.20: Force displacement relationship of the RC structure for pushover analysis in X-direction

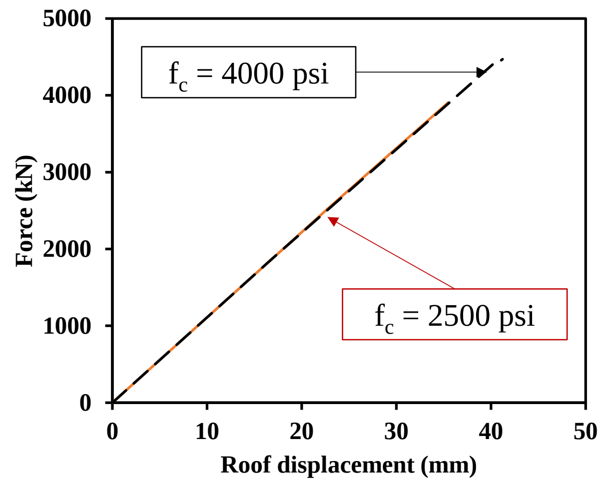

Figure 4.21**:** Force displacement relationship of the RC structure for pushover analysis in Y-direction

4.2.1.3 Effect of Concrete Strength on Formation of Plastic Hinges in Structural Elements

The force deflection relationship under application of pushover loads on a structure may be idealized with a linear representation as shown in Figure 4.22. The global structural behavior nearly remains in an elastic state when a hinge is formed in between A and B. When plastic hinges are formed between B and IO (Immediate Occupancy) with the next level of increase of pushover loads, structural elements do not fail and the structure can be reoccupied immediately with minor non-structural (element) repair works. After that, when the hinge is formed in between IO and LS (Life Safety) points, the structure is safe but repair works are to be done and rehabilitation methods to be applied. If the hinges are formed in between LS and CP (Collapse Prevention) then the structural elements are damaged, but the structure will not collapse. In this state, the building needs major rehabilitation works and sometimes retrofitting methods should be implemented based on the level of failure. If the hinges are formed in between CP to C (ultimate capacity) then the structure crosses its ultimate strength level; yielding starts and structure enters into a non-linear range of structural behavior. If a hinge is formed in between C (ultimate capacity) and D (residual strength), it is corresponding to a reduction in global load-carrying capacity. The load-carrying capacity of the structure suddenly drops to point D. If hinges are formed corresponding to a drop to point D or beyond D of the capacity curve, there will be no increase in load-carrying capacity but it will still continue to deform. If hinges are formed beyond the last point E, the structure will collapse (Santosh, 2014; Srinivasu and Panduranga, 2013; Mrugesh and Patel, 2011; Chopra, 2007).

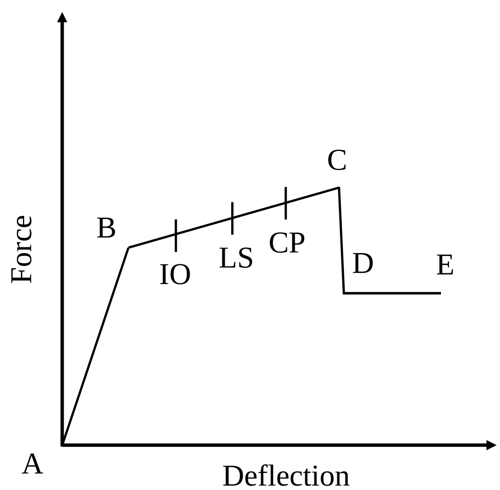

Figure 4.22: Linearized capacity curve as force deflection curve

There occurred a significant reduction of load carrying capacity of the structure with a random reduction of concrete strength by 35% of the original design strength (f'_c = 4 ksi). A further effect of reduction of strength of concrete is also evident from the results of formation of plastic hinges. Different points (A to E) of the capacity curve, as presented in Figure 4.22, explain consecutive shifts of various states of damages in the structure with progressive increase of pushover loads. The model simulation results of formations of plastic hinges at different stages of the capacity curve is reported in Tables 4.16 to 4.19.

As shown in Tables 4.16 to 4.19, the formation of hinges at different states also varied with the deterioration of concrete strength. There is increased numbers of plastic hinges formed in the structure modeled with concrete strength of 2.5 ksi, particularly beyond the final state of CP of the capacity curve. According to results observed for the application of pushover loads in the X-direction, the formation of hinges at the state of CP of the capacity curve is six for the structural model of concrete strength of 2.5 ksi while it is only two for concrete strength of 4 ksi. These results are generally indicating that with deterioration of concrete strength to a lower level, the formation of hinges in inelastic regions will be faster.

Table 4.16: Formation of plastic hinge in X-direction (f'_c = 4 ksi).

Step	Monitored Displ. (mm)	Base Force (kN)	A-B	B-C	C-D	D-E	>E	A-IO	IO-LS	LS-CP	>CP	Total
0	0	0	1700	0	0	0	0	1700	0	0	0	1700
1	-26.605	2558.0876	1698	2	0	0	0	1700	0	0	0	1700
2	-81.619	6320.7212	1338	360	0	0	2	1698	0	0	2	1700
3	-81.62	6319.5656	1338	360	0	0	2	1698	0	0	2	1700
4	-100.436	7193.5928	1241	457	0	0	2	1698	0	0	2	1700

Table 4.17: Formation of plastic hinge in X-direction (f'_c = 2.5 ksi).

Step	Monitored Displ. (mm)	Base Force (kN)	A-B	B-C	C-D	D-E	>E	A-IO	IO-LS	LS-CP	>CP	Total
0	0	0	1700	0	0	0	0	1700	0	0	0	1700
1	-26.078	2507.3847	1698	2	0	0	0	1700	0	0	0	1700
2	-73.999	5841.6261	1368	330	0	0	2	1694	0	0	6	1700
3	-76.464	5947.53	1348	342	0	0	10	1686	0	0	14	1700

Table 4.18: Formation of plastic hinge in Y-direction (f'_c = 4 ksi).

Step	Monitored Displ. (mm)	Base Force (kN)	A-B	B-C	C-D	D-E	>E	A-IO	IO-LS	LS-CP	>CP	Total
0	0	0	1700	0	0	0	0	1700	0	0	0	1700
1	-22.726	2520.5051	1698	2	0	0	0	1700	0	0	0	1700
2	-35.341	3889.8893	1684	16	0	0	0	1694	2	0	4	1700
3	-35.342	3889.9086	1684	16	0	0	0	1694	2	0	4	1700
4	-35.512	3907.3682	1684	16	0	0	0	1694	2	0	4	1700

Table 4.19: Formation of plastic hinge in Y-direction (f'_c = 2.5 ksi).

Step	Monitored Displ. **(mm)**	Base Force **(kN)**	A-B	B-C	C-D	D-E	>E	A-IO	IO-LS	LS-CP	>CP	Total
0	0	0	1700	0	0	0	0	1700	0	0	0	1700
1	-22.427	2487.3951	1698	2	0	0	0	1700	0	0	0	1700
2	-34.905	3841.3212	1684	16	0	0	0	1696	2	0	2	1700
3	-34.905	3841.317	1684	16	0	0	0	1696	2	0	2	1700
4	-34.997	3850.8435	1684	16	0	0	0	1696	2	0	2	1700

4.2.2 Numerical Modelling for Performance Evaluation of a RC Beam Element

4.2.2.1 Physical Modelling of the RC Beam Element

A simply supported RC beam is modelled using ATENA-GiD software to demonstrate a few of the major effects of changes of concrete strength on load deflection characteristics and also to investigate its associated effects on formation and propagation of cracks. ATENA-GiD is a finite element based software system commonly used for nonlinear analysis of RC structures (ATENA-GiD, 2019). The numerical modelling and simulation done at a structural element level is particularly aimed at investigating the possible interrelation among the following parameters

- maximum deflection of the RC beam
- development/propagation of cracks, crack widths etc. and
- Magnitude, propagation and development trend of fracture strains.

The geometrical setup and material properties of the beam materials according to Euro Code 2004 (CEN, 2004) correspond to the experimental setup by Leonhard in 1962 details of which can be obtained from the manual (ATENA-GiD, 2019).

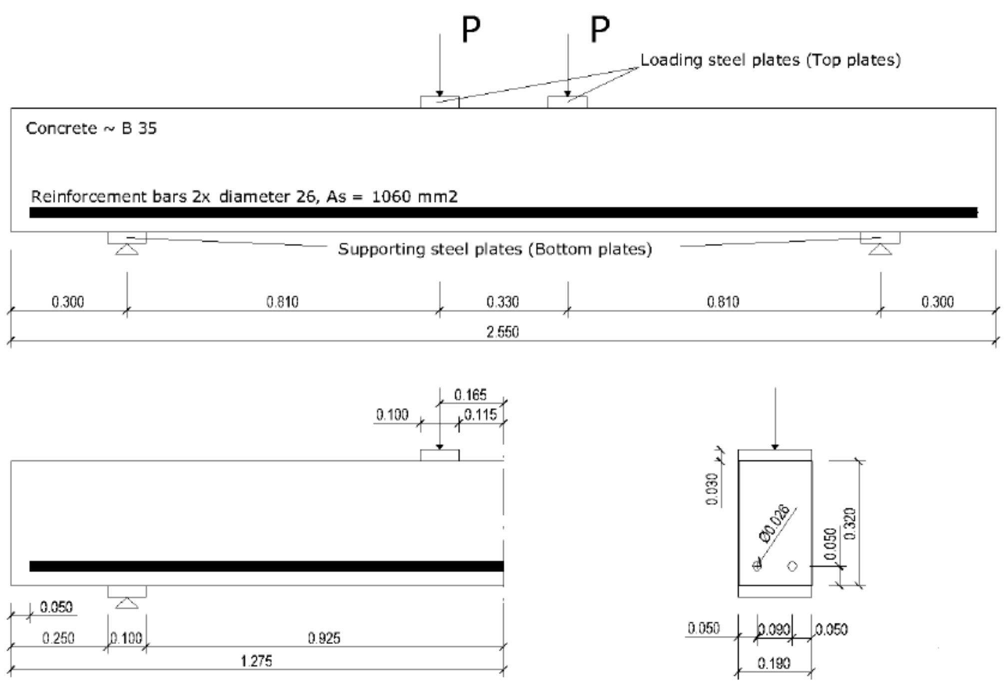

Figure 4.23: Geometry of the selected RC beam structure for numerical analysis

The RC beam has two concentric loads applied at points located at equal distance from the supports of the beam. Therefore, only half the geometric FE model of the beam is created considering symmetric load and support conditions. The FE model composed of three 3D regions of volume elements for concrete beam, loading and supporting steel plates. The geometry of the beam model is shown in Figure 24(a) within which the reinforcement (steel) bars are modelled with two straight lines [Figure 24(b)]. No shear reinforcement is provided in the beam in order to account for a greater share of the effects of concrete in overall load bearing capacity of the beam. The mode of shear failure near the supports would be same in both the variations of the beam models since the flexural steel bars is likely to have no effects on concrete within the shear zone near the supports. Randomly chosen variations of material parameters are implemented in 4 variants of the FE models of the RC beam, which correspond to two randomly chosen grades of steel and concrete strengths according to Euro Code 2004 (Table 4.20).

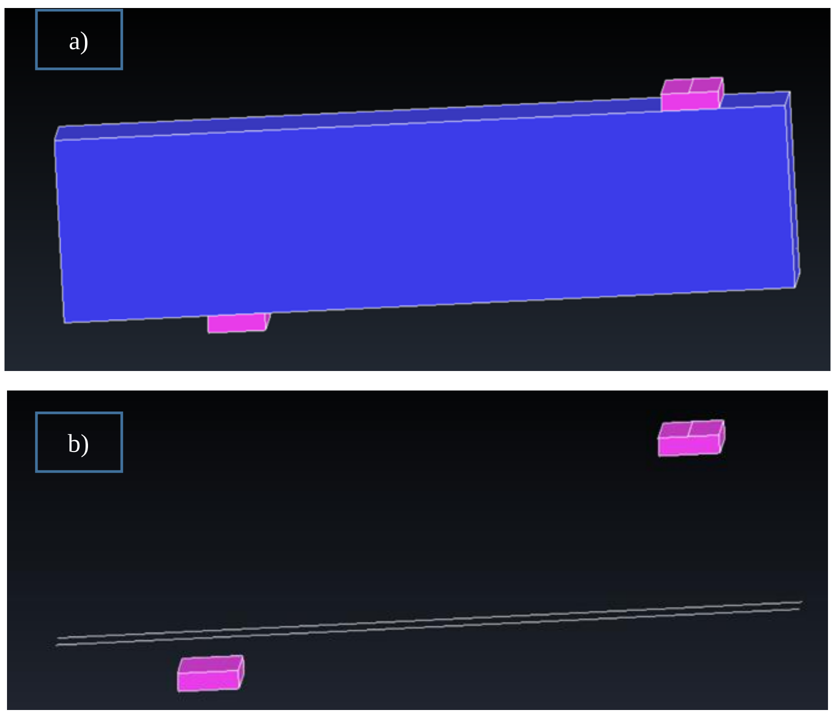

Figure 4.24: geometric FE model of volume elements and steel bars

A total of four identical geometry of FE beam models are simulated in the software system. Two variations of strengths of concrete are considered within identical geometry of the beam model and each beam variations is modelled incorporating two further variations of steel (diameters) in the model. MCR-1 and MCR-2 beams modeled with steel bar diameter d_b = 26 mm to compare between them the effects of changes of concrete strengths, f'_c = -24 MPa in MCR-1 and f'_c = -28 MPa. Each of these two variants of the beam models were changed for model simulations respectively as MCR-3 and MCR-4 only by changing steel bar diameters d_b = 32 mm in the models. The variation of steel strengths in MCR-3 and MCR-4 model simulations is considered to examine the likely effects of concrete strengths' variation in beams where the larger bar diameters have increased the overall load carrying capacity of the beam. Table 4.20 shows the material parameters for four FE beam models.

Table 4.20: Chosen material parameters of FE beam models

RC Beam FE models	Major parameters of strengths (class of concrete, according to *EC*2 2004)	Remarks
MCR-1 and MCR-3	Young modulus E_c= 29000 Fracture energy G_F= 4.75e-05 MN/m Poisson's ratio μ= 0.2 Compression strength f'_c= -24 MPa Tension strength f_t= 1.9 MPa Plastic strain ε_{cp}= -0.0010473 Onset of crushing F_{co} = -3.99 MPa (concrete class 16-20 according to *EC*2)	MCR-1 and MCR-2 beam modeled with steel bar diameter d_b= 26 mm MCR-3 and MCR-4 beam modeled with steel bar diameter d_b= 32 mm Young's modulus E_c= 200 GPa Characteristic yield strength f_{sk}= 500 MPa (modulus and yield strength chosen according to *EC*)
MCR-2 and MCR-4	Young modulus E_c= 30000 Fracture energy G_F= 5.5e-05 MN/m Poisson's ratio μ= 0.2 Compression strength f'_c= -28 MPa Tension strength f_t= 2.2 MPa Plastic strain ε_{cp}= -0.001033 Onset of crushing F_{co} = -4.62 MPa (concrete class 20-25 according to *EC*2)	

The values of other material parameters are chosen as default values calculated by the software program according to the respective classification in Euro Code 2004 (CEN, 2004). Since the concrete's tensile strength is typically much lower than the numeric value of the compressive strength of concrete, the input value of the tensile strength ($0.7f'_c$) is chosen that would be mainly responsible for controlling the behavior the beam in terms of crack generation (propagation and growth of cracks) and fracture strain etc.

4.2.2.2 Discussion on Results of FE Model Simulation

Load deflection characteristics: One of the major findings derived from the model simulation results is that the load carrying capacity of the RC beam is generally increased with the increase of the concrete strength. It is evident from the comparative diagram shown in Figure 4.25 that the increase of concrete compressive strength from 24 MPa (in model MCR-1) to 28 MPa (in model MCR-2) has increased its load capacity from 63.4 kN to 64.6 kN. The concrete strength is likely to provide relative higher contribution to overall load carrying capacity of the beams which are modeled with smaller size of steel bars (d_b= 26 mm). It is seen that the increased load capacity in MCR-2 is achieved with the same magnitude of maximum deflection for both beams (2.43 mm).

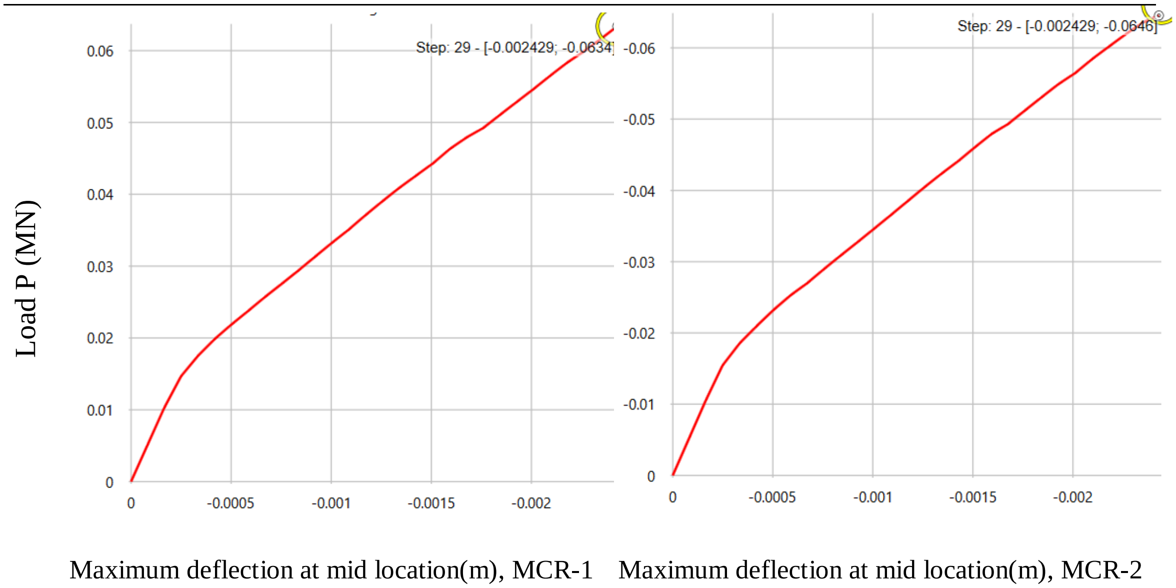

Figure 4.25: Comparison of the effects of concrete strength on load-deflection of RC beam, (modeled with steel d_b=26 mm)

The effect of change of concrete strength does not significantly affect the load capacity in model beam variations of MCR-3 and MCR-4 where an increased size of steel bars (d_b= 32 mm) are used. The increase of concrete strength has very insignificant effects on the increase of the load capacity of the beam models, from 75.1 kN to only 75.4 kN in MCR-3 and MCR-4 respectively (shown in Figure 4.26). The increased bar diameter (d_b= 32 mm) in these beams is likely to have dominated the overall load capacity as compared to the strengths of concrete. However, the beam modeled with lower strength of concrete has undergone more deflection (2.26 mm) at its maximum load capacity as compared to that (2.17 mm) of MCR-4 beam model.

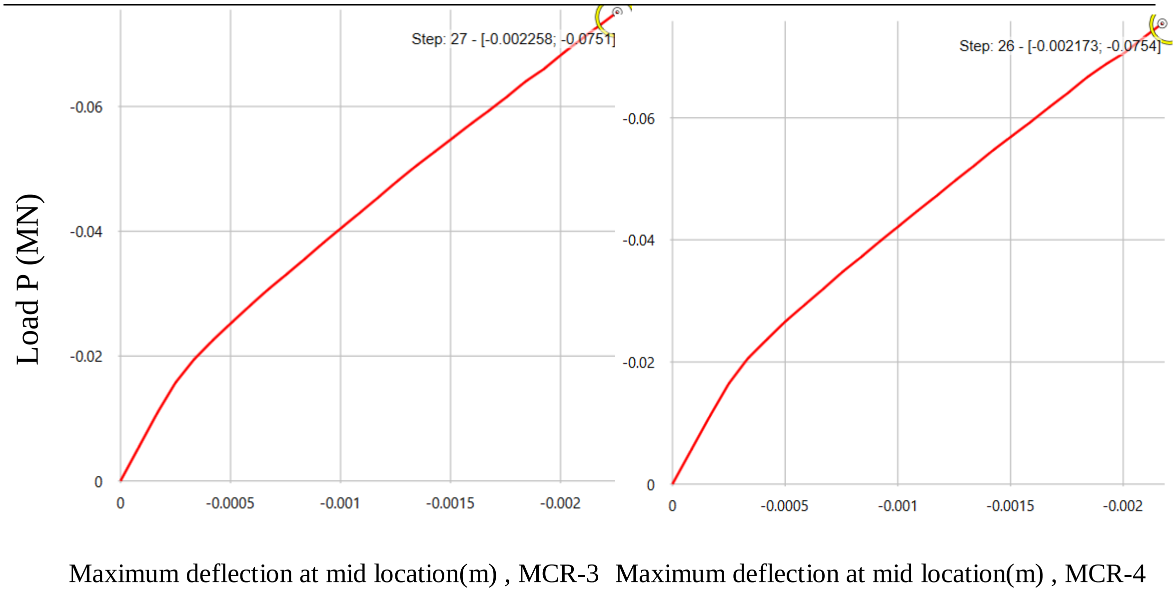

Figure 4.26: Comparison of the effects of concrete strength on load-deflection of RC beam, (modeled with steel d_b=32 mm)

Crack formation and propagation characteristics: The effect of reduced strength of concrete in the RC beam models generally has increased the deflection of the beams, as seen in observed load versus deflection characteristics for their maximum load cases (shown in Figures 4.25-4.26). This general aspect of increased deflection with reduced concrete strength may be further verified and discussed through observations of crack formation characteristics and its propagation throughout the beams.

The beam models MCR-3 (f'_c= -24 MPa) and MCR-4 (f'_c= -28 MPa) have nearly same load capacity (75.1 kN and 75.4 kN). However, MCR-3 beam modeled with reduced strength of concrete has undergone higher deflection at a relative lower magnitude of load. Figure 4.27 and Figure 4.28 respectively show comparison of development of cracks and contours of fracture strains at maximum load capacities of the beams. It is seen that the number of cracks and contours of fracture strain have progressed more towards the failure (shear) zone near the support of the beam model MCR-3.

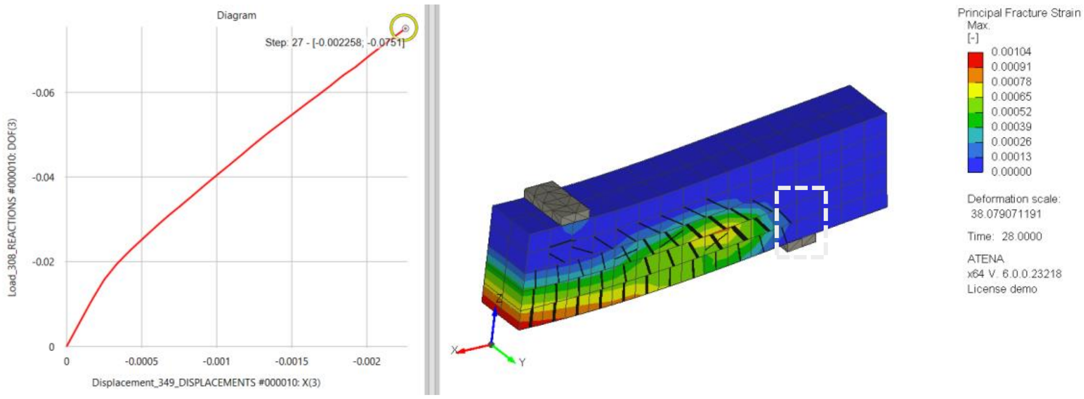

a) Development of cracks and contours of fracture strain at maximum load, MCR-3

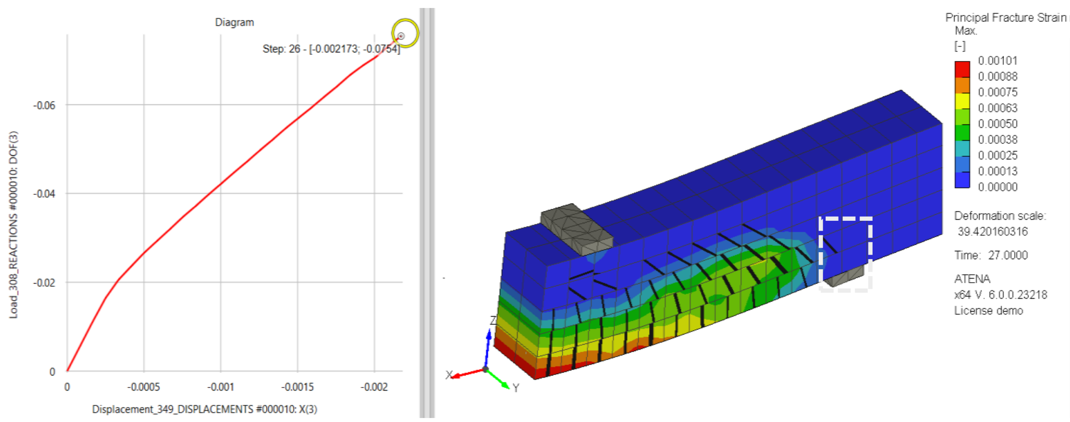

b) Development of cracks and contours of fracture strain at maximum load, MCR-4

Figure 4.27: Comparison of development of cracks and fracture strains in model beams

Figure 4.28 shows comparative figures of MCR-3 and MCR-4 beam models in their undeformed shapes with contours of fracture stains developed at their maximum load capacity. In this figure, the spread of contours in the beams is compared with an application of same load magnitude (of 75 kN) nearing the maximum load capacity of the beams. The comparative diagram shown in Figure 4.28(c) shows that the contour of fracture strain of beam model MCR-3 is spread over a relative larger area (185000 mm^2) than that (181000 mm^2) in MCR-4 beam model.

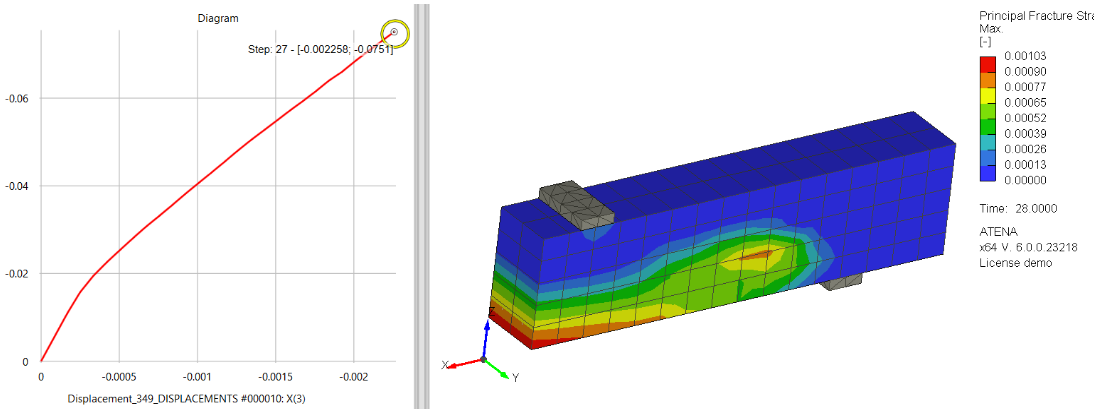

a) Contours of fracture strain in an under formed shape of MCR-3 beam model

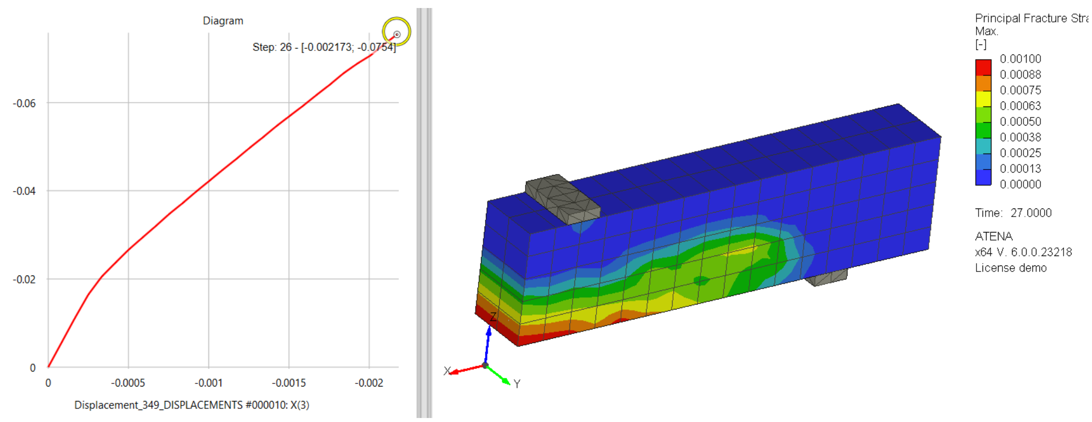

b) Contours of fracture strain in an under formed shape of MCR-4 beam model

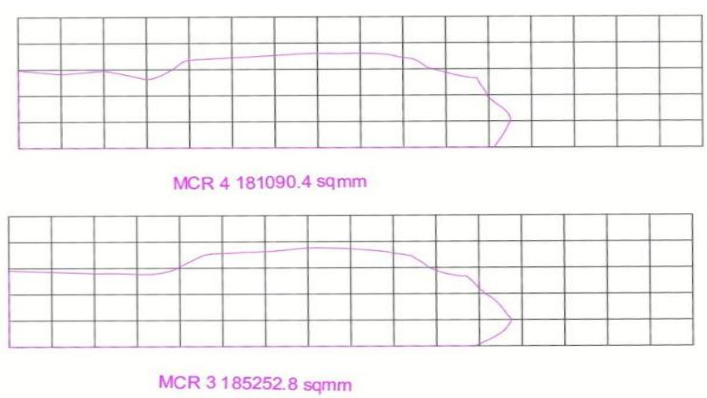

c) Comparison of area of fracture strain accumulation in under formed beam models

Figure 4.28: Comparison of development of cracks and fracture strains in FE model beams

Chapter 5
Conclusions and Recommendations

5.1 Conclusions

There can be many different causes of concrete strength degradation over time. It is, therefore, very important to monitor the state of concrete qualities of Reinforced Concrete (RC) structures not only during the initial time of construction of a building but also at different stages of its service life. The monitoring is especially important for aging RC structures since several visual signs of damages and concrete strength deterioration may become evident as any RC building ages with time. Some of the signs of damages such as cracks and spalling of concrete are linked to corrosion of reinforcement which cause further deterioration of concrete.

This work was intended for collecting data of concrete strengths of a selected aging RC structure through visual screening and also by conducting non-destructive rebound hammer test (RHT). A selected RC structure of Bangladesh Railway infrastructural zone at Halishahar region of Chattogram city was studied under the scope of the work. The results of concrete strengths determined by RHT test is indicative of significant strength degradation over time as many structural members of the building showed visual signs of damages or conditions of distress. Average concrete strength in different structural members of the selected aging structures was found to be well below (approximately 13% below) the baseline strength and the reduction of strength in an individual member is found to be even 35% less than the baseline strength. Only a few of the structural elements showed very little or no degradation of strength which is acceptable considering time variation law of concrete compressive strength. An assessment done by an ACI protocol for visual screening reveals that many of the damage conditions appeared due to poor maintenance of the building and also due to its exposure to environmental and other load extremities over its service life. Visual screening indicators of damage of RC structural elements comply well with RHT results. The results are generally indicative of the fact that the state of concrete of the aging RC structure has reached in a state where the building is no longer capable of sustaining extreme loading conditions or excessive overload situation such as those originating from earthquake or other extreme environmental loading conditions. The current state of the building is sustaining only the gravity load as it would sustain with residual strength at the last state of its capacity curve. However, the degradation of concrete strengths or visual signs of damages of the building could not be exclusively correlated with effects of natural aging of concrete.

In this connection, the calibration of RHT results was attempted to be done by comparing RHT data with audit records of cylinder strength tests of concrete that were collected from two selected RC buildings located at Bayezid and Kumira of Chattogram. Indirect measurements of concrete compressive strengths were made from calibration charts of a RHT instrument. No reliable correlation could be found between RHT results and design strength or audit records of strength based on which reliability of results of strengths could be established for the field level measurements. RHT data of those buildings could not be reliably verified from in-situ strength results of concrete core cut tests. In general, calibrating RHT data with respect to the field test results would require a conservative estimate of 15% to 20% less concrete strengths as determined from indirect measurements based on RHT data. Consistent results of concrete strengths determined by RHT tests have been recorded at suitable points or locations of different structural members. The points of consistent results of strengths are mostly concentrated within the section of tied arch action of a beam. For a slab section, the points of consistent results are mostly found within $L/4$ from the periphery of a slab.

However, a good correlation could be found between cylinder strengths and RHT measurements done on laboratory scale beam specimens. The concrete quality and exposure conditions of the beam specimens were well controlled to exclude the effects of other detrimental factors on degradation of strength. Sufficient numbers of cylinder or cube samples were taken for comparing time varying strength test results with RHT data taken on beam specimens. The time variation law of concrete compressive strength could be well correlated for both the strength records of the laboratory scale beam specimens. For the two different target strengths investigated under the scope of the study, the RHT test strength of the concrete can be estimated approximately 3 to 4% lower than the laboratory test results of characteristic compressive strength of concrete (f'_c). When normalized value of compressive strength is not used in mathematical formulations, the empirical expressions for time variation of concrete strength are different for variable target compressive strength of concrete. In general, the findings of the study suggest that a recalibration of RHT results is required to adjust for variability of concrete strengths of RC structures or specimens in practical exposure conditions.

When an aged building starts exposing its distress condition and corrosion of reinforcement, loss of compressive strength develops day by day. This may lead to conditions of structural instability, safety risks, decrease load bearing capacity and long term damage accumulation. In this stage, structural modeling approach can be suitably used to monitor damage status and serviceability compliance of any aging RC structure with a reliable input data of concrete strength derived from RHT. A structural model of a selected RC structure was numerically analyzed by software analysis using variable concrete strength data that could be indirectly derived from non-destructive testing methods such as the RHT test. The results of structural modeling and analysis of a selected RC structure for pushover analysis demonstrates that the deterioration of concrete strength substantially affects the global capacity of the structure. There is increased numbers of plastic hinges formed in the structure modeled with lower concrete strength, particularly beyond the final state of collapse prevention (CP) of the structure's capacity curve. These results of pushover analysis on the structure is generally indicative of faster rate of formation of hinges in inelastic regions of the capacity curve.

The degradation of concrete strength could not only have significant effects load-deflection characteristics of RC structural elements but also have considerable effects on crack development and its propagation characteristics. It is evident from the numerical model analysis of a RC beam element that the number of cracks and accumulation of fracture strain are more concentrated near the failure zone of a beam modeled with lower strength of concrete. The results of numerical modelling and analysis indicates that an undesired degradation of concrete strength may significantly reduce the service life of RC structures.

5.2 Recommendation for Future Works

This research presented results of damage prognosis of an aged RC structure using visual screening method and one of the non-destructive RHT test procedures. Numerical model analysis of performance of two RC structures were conducted using by ETABS and ATENA-GiD softwares. Significant information on the performance of the aged RC structures could be derived using analytical and numerical methodologies or approaches followed in this research. However, further research on the damage prognosis of aged RC structures should be carried out, and recommendations for future work in this regard are proposed as follows:

a) The spatial deterioration of concrete and rebar's strength of RC structure should be considered in predicting the performance of the aged structure.
b) Deterioration of concrete with time is to be established by collecting data of several years to several decades.
c) Structural modeling and analysis of aged RC structures of different ages should be done in correlation to data obtained from the rebound hammer test.
d) More works need to be done through non-destructive field testing methods to establish a reliable basis of using this approach for structural health monitoring.

References

Akashi, T. and Amasaki, S. (1984). Study of the stress waves in the plunger of a rebound hammer at the time of impact. SP 82-2, 17-34, American Concrete Institute ACI, Detroit. https://api.semanticscholar.org/CorpusID:114069919.

American Concrete Institute ACI (1992). Guide to Durable Concrete, ACI Report 201.2R-92, American Concrete Institute, Detroit, Michigan.

American Concrete Institute ACI (1993). Causes, Prevention, and Repair of Cracks in Concrete, ACI Report 224.1R-93, American Concrete Institute, Detroit, Michigan.

American Concrete Institute ACI (1993). Erosion of Concrete in Hydraulic Structures, ACI Report 210R-93, American Concrete Institute, Detroit, Michigan.

American Concrete Institute ACI (1998). ACI Manual on Nondestructive Test Methods for Evaluation of Concrete in Structure, ACI Report 228.2R-98, American Concrete Institute, Detroit, Michigan.

American Concrete Institute ACI (2001). Protection of Metals in Concrete against Corrosion, ACI Report 222R-01, American Concrete Institute, Detroit, Michigan.

American Concrete Institute ACI (2008). Guide for Conducting a Visual Inspection of Concrete in Service, ACI Report 201.1R-08, American Concrete Institute, Detroit, Michigan.

American Society for Testing and Materials ASTM (2019). Rebound Number of Hardened Concrete, ASTM C805, Philadelphia.

Applied Technology Council ATC-33 (1997). NEHRP Guidelines for the Seismic Rehabilitation of Buildings, FEMA Publication 273, Redwood City, California.

ATENA-GiD (2019). ATENA Program Documentation, ATENA Science-GiD Tutorial, Cervenka Consulting, Prague, Czech Republic.

Bagavathiappan, S.; Lahiri, B.B.; Saravanan, T.; Philip, J. and Jayakumar, T. (2013). Infrared thermography for condition monitoring - A review. Infrared Physics and Technology, 60, 35–55.

British Standards Institution BS (2001). Testing of Concrete in Structures: Non-destructive Testing: Determination of Rebound Number (British Standard), BS EN 12504-2:2001, British Standards Institution, London.

British Standards Institution BS (2010). Guide to Assessment of Concrete Strength in Existing Structures, BS 6089:1981, British Standards Institution, London.

Bungey, J.H. and Grantham, M.G. (2018). Testing of Concrete in Structures, 4th Edition, Routledge Taylor and Francis Group, UK.

Bungey, J.H. and Madandoust, R. (1994). Evaluation of non-destructive strength testing of lightweight concrete, Structural and Building Board Structural Panel, 10433, 275-283.

CEN, 2004. Eurocode 2: Design of Concrete Structures, Part 1-1: General Rules and Rules for Buildings, EN 1992-1-1:2004, CEN, Brussels.

Chaplin, R.G. (1980). Abrasion resistant concrete floors, In Advances in Concrete Slab Technology, Pergamon, Oxford, 532–543.

Chidiac, S.E.; Moutassem, F.; Mahmoodzadeh, F. (2013). Compressive strength model for concrete, Magazine of Concrete Research, 65, 557–572.

Chopra, A.K. (2007). Dynamics of structure: theory and application to earthquake engineering, Pearson Education, India.

Comite Euro-International Du Beton (1993). CEB-FIP Model Code 1990, Thomas Telford Services Ltd.: London, UK. https://vdocument.in/ceb-fip-model-code-1990pdf.html?page=1 (accessed on 23 March 2023).

Concrete Society CS (1992). Non-structural Cracks in Concrete, Concrete Society Technical Report No. 22, Concrete Society, Sandhurst, UK.

Datta, T.K. (2010). Seismic Analysis of Structures. John Wiley & Sons (Asia) Pte Ltd., Singapore.

Department of Disaster Management (2009). Earthquake risk assessment of Dhaka, Chittagong & Sylhet city corporation area. CDMP Report 2009, Ministry of Disaster Management and Relief, Government of Bangladesh.

Doebling, S.W.; Farrar, C.R. and Prime M.B (1998). A summary review of vibration-based damage identification methods. Shock and Vibration Digest, 30(2), 91-105.

ETABS 2016 v 16.2.1 (2016). Integrated Building Design Software, User's Guide, Computer's & Structures Inc., ISO ETA122815M2 Rev. 0, USA.

Fajfar, P. and Fischinger, M. (1988). N2-A method for non-linear seismic analysis of regular buildings, Proceedings of 9th World Conference on Earthquake Engineering, Tokyo, 5.

Fajfar, P. and Gasperisic, P. (1996).The N2 Method for the seismic damage analysis of RC buildings, Journal of Earthquake Engineering and Structural Dynamics, 25, 31-46.

Fewtrell, A. (1993). A special access techniques for inspection works, Proceedings of Structural Faults and Repairs, Eng. Technics Press, Edinburgh, 2, 19–24.

Gao, X.L.; Li, J.; Ren, X.D. (2018). Probabilistic model for long-term time-dependent compressive strength of concrete in existing buildings. Journal of Performance of Constructed Facilities, 32. https://api.semanticscholar.org/CorpusID:115157619.

Gehlot, T.; Sankhla, S.S. and Gupta, A. (2016), Study of concrete quality assessment of structural elements using rebound hammer test, American Journal of Engineering Research (AJER), 5(8), 192-198.

Higgins, D.D. (1981). Diagnosing the causes of defects or deterioration in concrete structures: Current Practice Sheet: Concrete (London), 15(10), 33–34.

Housing and Building Research Institute HBRI (2006). Bangladesh National Building Code (BNBC) 2006, Ministry of Housing and Public Works, Government of Bangladesh.

Housing and Building Research Institute HBRI (2021). Bangladesh National Building Code (BNBC) 2020, Ministry of Housing and Public Works, Government of Bangladesh.

Institution of Engineers, Bangladesh IEB (2007). Institute of engineers Bangladesh (IEB) investigation report on under construction Spectrum Garments Building Collapse, IEB Investigation Report: Part I.

International Labour Office ILO (2018). Bangladesh move towards employment injury insurance: The legacy of Rana Plaza, ILO Report. https://www.ilo.org/wcmsp5/groups/public/---ed_emp/documents/ publication/wcms_632364.pdf.

Khan M. A. (2013). Earthquake-Resistant Structures: Design, Build, and Retrofit, Elsevier Science, London.

Kolek, J. (1970). Non-destructive testing of concrete by hardness methods, In Non-destructive Testing of Concrete and Timber, Institution of Civil Engineers, London, 19-22.

Lawson, R.S.; Vance, V. and Krawinkler, H. (1994). Nonlinear static pushover analysis why, when and how?, Proceedings of 5th U.S. National Conference on Earthquake Engineering, Chicago, Illinois, 1, 283-292.

Malhotra, V.M. (1976). Testing hardened concrete: Non-destructive methods. Monograph 9, American Concrete Institute. Detroit.

MAPEI SpA (2021), Manual: The Deterioration of Concrete, Via Cafiero, 22, 20158 Milan-Italy.

Moghadam, A.S. and Tso, W.K. (2000). 3-D pushover analysis for damage assessment of buildings, Journal of Seismology and Earthquake Engineering, 2, 23-31, https://api.semanticscholar.org/CorpusID:61846323.

Mondal, D.R.; Mchugh, C.M.G.; Mortlock, R.; Steckler, M.S.; Mustaque S.; Akhtere S.H. (2018). Microatolls document the 1762 and prior earthquake along the southeast coast of Bangladesh, Tectonophysics. https://api.semanticscholar.org/CorpusID:53578945.

Moutassem, F. and Chidiac, S.E. (2015). Assessment of concrete compressive strength prediction models, KSCE Journal of Civil Engineering, 20, 343–358.

Mrugesh D.S. and Patel, S.B. (2011). Nonlinear static analysis of RCC frames (software implementation ETABS 9.7), Proceedings of National Conference on Recent Trends in Engineering & Technology, B.V.M Engineering College, Gujarat, India.

Niu, D.T.; Wang, Q.L. (1995). Models of concrete strength changing with time in general air environment. Ind. Constr., 25, 36–38. (In Chinese)

Plankias, A. (2012). Structural health monitoring Mems sensors using elasticity-based beam vibrations, Master thesis, Colorado State University, USA.

Pollock, D.J., Kay, E.A. and Fookes, P.G. (1981). Crack mapping for investigation of Middle East concrete. Concrete, 15(5), 12-18.

Proceq, (RHT Manufacturer Manual) - Concrete test Hammer Manual, Proceq SA, Schwerzenbach, Swizerland.

Qi, X. and Moehle, J.P. (1991). Displacement design approach for reinforced concrete structures subjected to earthquakes, Report UCB/EERC-91/02, Earthquake Engineering Research Center, University of California-Berkeley.

Saidii, M. and Sozen, M.A. (1981). Simple Nonlinear Seismic Analysis of R/C Structures, Journal of the Structural Division, 107, 937-952.

Santosh, D. (2014). Pushover analysis of RC frame structure using ETABS 9.7.1, IOSR Journal of Mechanical and Civil Engineering (IOSR-JMCE), 11(1), 8-16.

Shariati, M. Ramli-Sulong, M. H., Arabnejad, K- R., Shafigh, P. and Sinaei, H. (2011). Assessing the strength of reinforced concrete structures through ultrasonic pulse velocity and Schmidt rebound hammer tests, Scientific Research and Essays, 6(l), 213- 220.

Smith, J.R. (1991). Assessment of concrete buildings. Concrete International, 13(12), 48-49.

Srinivasu, A. and Panduranga Rao, B. (2013). Non-linear static analysis of multi-storied building, International Journal of Engineering Trends and Technology (ILETT), 4(10), 4629-4633.

Storchak, D.A.; Giacomo, D. Di.; Bondár, I.; Engdahl, E.R.; Harris, J.; Lee, W.H.K.; Villaseñor, A. and Bormann, P. (2013). Public Release of the ISC-GEM Global Instrumental Earthquake Catalogue (1900-2009). Seismoligical Research Letters, 84, 5, 810-815, doi: 10.1785/0220130034.

Vision 2000 Committee (1995). Performance based seismic engineering of buildings: pt. 1. interim recommendations. pt. 2. conceptual framework, Structural Engineers Association of California.

Wang, R.I. and Yue, Q. (2023). The time variation law of concrete compressive strength: A review. Applied Sciences, 13, Article 4947. https:// doi.org/10.3390/app13084947.

Wang, R.I.; Zhang, Q.J. and Li, Y. (2022). Deterioration of concrete under the coupling effects of freeze–thaw cycles and other actions: A review. Construction and Building Materials, 319, Article 126045.

Wang, W.N. (2022). Research and prediction of time variation model on the compressive strength of concrete in existing buildings, Master’s Thesis, School of Civil Engineering, Shandong Jianzhu University, Jinan, China.

Washa, G.W. and Wendt, K.F. (1975). Fifty year properties of concrete. ACI Materials Journal, 72, 20–28.

Washa, G.W.; Saemann, J.C. and Cramer, S.M. (1989). Fifty-year properties of concrete made in 1937. ACI Materials Journal, 86, 367–371.

Withey, M.O. (1961). Fifty year compression test of concrete. ACI Materials Journal, 58, 695–712.

Wood, S.L. (1992). Evaluation of the long-term properties of concrete, ACI Materials Journal, 88, 630–643.

Appendix-1

Selected Building Information

1. Present view of the selected Aging RC building:

2. 3-D ETABS model of the selected Aging RC building:

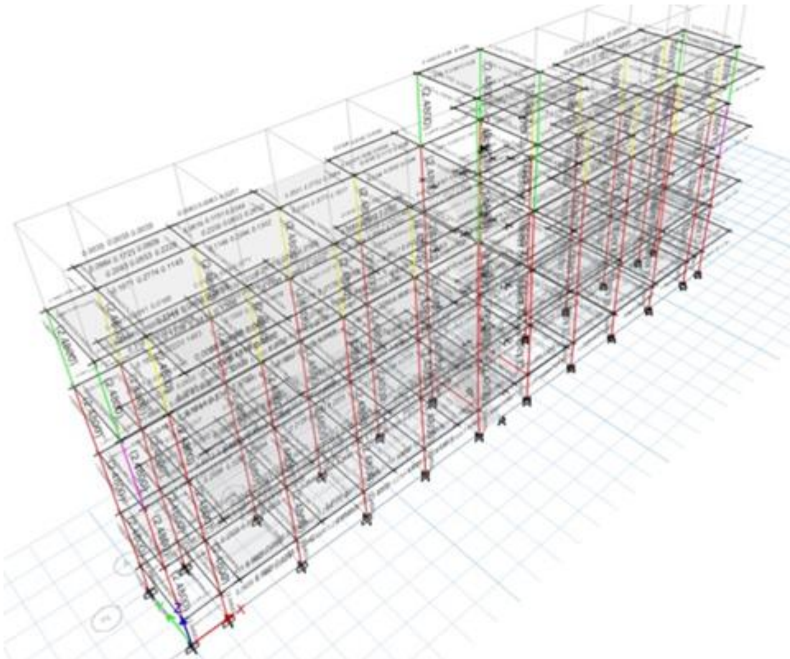

3. Selected RC structure location in the earthquake zone map of Bangladesh:

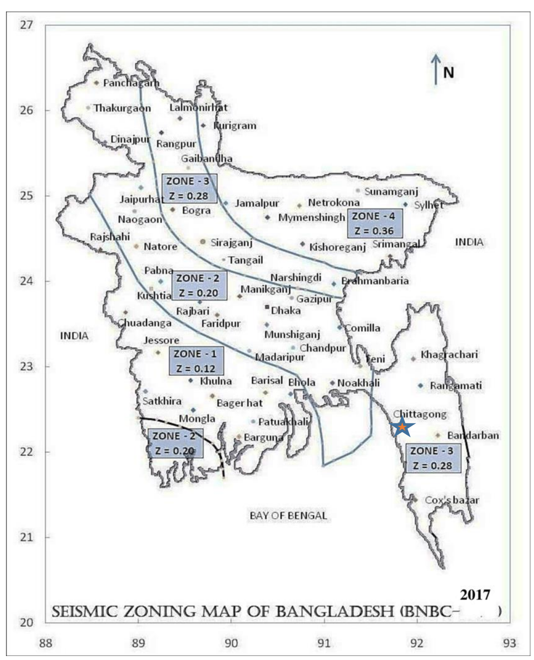

Appendix-2

Visual inspection Report on selected RC building

Inspection PART-1

Visual Screening Form (ACI 201.01-8R)				
1. General	Report number			RTA HOST. 12, 08.08.2023
	Purpose of inspection			MSc. Engineering Thesis
	Inspector’s name(s)			M. Mahmudur Rahman Patwary
1A. Description of the Structure	Name			RTA Hostel ….
	Location			Halishahar Chattogram
	Type			I -shape 4 storied building.
	Size			59.00mX8.97m
	Owner			Bangladesh Railway
	Project engineer			Divisional Engineer-…. Bangladesh Railway.
	Contractor			……. Construction
	Date(s) of construction			1983
	Photographs	General view		Attached
		Detailed close-up of the condition of the area		Attached
	Sketch map orientation indicating sunny and shady areas and well and poorly-drained regions			Attached
1B. Materials Used (if known)	Concrete	Normal weight aggregate type		1450 kg/cum
		Aggregate size		20 mm down
		Admixture type		N/A
		Mixture proportion		Column 1:1.5:3, Beam & Slab 1:2:4 (from drawing)
		Compressive strength		
		Modulus of elasticity		

Inspection PART-2

Visual Screening Form (ACI 201.01-8R)				
2. Nature of Environmental and Loading Conditions	Exposure	Environment (arid, subtropical, marine, freshwater, industrial, etc.)		Coastal Area, Tropic of cancer
		Weather (July and Jan. mean temperatures, mean annual rainfall, and months in which 60% of rainfall occurs)		Mean temp. July 32° C, January 22, mean annual rainfall 200mm, 60% rainfall Jun-July. Source
		Freezing and thawing		N/A
		Wetting and drying		Wetting
		Drying under dry atmosphere		Yes
		Chemical corrosion and attack (sulfates, acids, bases, chloride, gases)		Chloride corrosion. (Assumed)
		Abrasion, erosion, cavitation, impact		Yes
		Electric conductivity		
		Deicing chemicals that contain chloride ions		
		Heat from adjacent sources		

Inspection PART-2

Visual Screening Form (ACI 201.01-8R)				
2. Nature of Environmental and Loading Condition	Drainage	Flashing		Yes
		Joint sealants		
		Weep holes		
		Contour		
		Elevation of drains		
	Loading conditions	Dead		Yes
		Live		Yes
		Impact		
		Vibration		
		Traffic		
		Seismic		Yes
		Other		wind
	Soils (foundation conditions)	Expansive soil		
		Compressible soil (settlement)		wooden pile with isolated footing foundation
		Evidence of pumping		

Inspection PART-3

Visual Screening Form (ACI 201.01-8R)				
3. Distress Indicators	Cracking			Slab & beam 5 nos. beam and slab small cracked, two numbers column cracked seen.
	Staining			Staining seen at the rooftop stair column.
	Surface deposits and exudations			
	Leaking			Roof leaking top slab.

Inspection PART-4

Visual Screening Form (ACI 201.01-8R)				
4. Present Condition of Structure	Overall apparent alignment of structure	Settlement		No
		Deflection		No
		Expansion		No
		Contraction		No
4. Present Condition of Structure	Surface condition of concrete	General condition: good, satisfactory, poor		Poor
		Formed and finished surfaces	Smoothness	Not smooth
			Bug holes (surface air voids)	Yes
			Cold joints	
			Staining	Yes

Inspection PART-4

Visual Screening Form (ACI 201.01-8R)				
4. Present Condition of Structure	Surface condition of concrete	Exposed reinforcement: corrosion		Slab-Beam Every Floor, Column 2 nos.
		Curling and warping		
		Erosion	Abrasion	Yes
			Cavitation	Yes
		Previous patching or other repair		
		Surface coatings, protective systems, linings, toppings	Type and thickness	12mm plaster and painting
			Bond to concrete	Cement bond.